Quantum Mechanics/Molecular Mechanics Studies of Triosephosphate Isomerase-Catalyzed Reactions: Effect of Geometry and Tunneling on Proton-Transfer Rate Constants

Qiang Cui[†] and Martin Karplus[*,†,‡]

Contribution from the Department of Chemistry and Chemical Biology, Harvard University, Cambridge, Massachusetts 02138, and Laboratoire de Chimie Biophysique, ISIS Universitè Loius Pasteur, 67000 Strasbourg, France

Abstract: The role of tunneling for two proton-transfer steps in the reactions catalyzed by triosephosphate isomerase (TIM) has been studied. One step is the rate-limiting proton transfer from Cα in the substrate to Glu 165, and the other is an intrasubstrate proton transfer proposed for the isomerization of the enediolate intermediate. The latter, which is not important in the wild-type enzyme but is a useful model system because of its simplicity, has also been examined in the gas phase and in solution. Variational transition-state theory with semiclassical ground-state tunneling was used for the calculation with potential energy surface determined by an AM1 method specifically parametrized for the TIM system. The effect of tunneling on the reaction rate was found to be less than a factor of 10 at room temperature; the tunneling becomes more important at lower temperature, as expected. The imaginary frequency (barrier) mode and modes that have large contributions to the reaction path curvature are localized on the atoms in the active site, within 4 Å of the substrate. This suggests that only a small number of atoms that are close to the substrate and their motions (e.g., donor−acceptor vibration) directly determine the magnitude of tunneling. Atoms that are farther away influence the effect of tunneling indirectly by modulating the energetics of the proton transfer. For the intramolecular proton transfer, tunneling was found to be most important in the gas phase, to be similar in the enzyme, and to be the smallest in water. The major reason for this trend is that the barrier frequency is substantially lower in solution than in the gas phase and enzyme; the broader solution barrier is caused by the strong electrostatic interaction between the highly charged solute and the polar solvent molecules. Analysis of isotope effects showed that the conventional Arrhenius parameters are more useful as experimental criteria for determining the magnitude of tunneling than the widely used Swain−Schaad exponent (SSE). For the primary SSE, although values larger than the transition-state theory limit (3.3) occur when tunneling is included, there is no clear relationship between the calculated magnitudes of tunneling and the SSE. Also, the temperature dependence of the primary SSE is rather complex; the value of SSE tends to decrease as the temperature is lowered (i.e., when tunneling becomes more significant). For the secondary SSE, the results suggest that it is more relevant for evaluating the "coupled motion" between the secondary hydrogen and the reaction coordinate than the magnitude of tunneling. Although tunneling makes a significant contribution to the rate of proton transfer, it appears not to be a major aspect of the catalysis by TIM at room temperature; i.e., the tunneling factor of 10 is "small" relative to the overall rate acceleration by 10^9. For the intramolecular proton transfer, the tunneling in the enzyme is larger by a factor of 5 than in solution.

I. Introduction

An understanding of the rate constants for proton- and hydride-transfer reactions is of fundamental interest.[1] It is of particular importance for living system, where such transfers are of widespread occurrence.[2] As in other reactions, an evaluation of the free energy of activation and of the dynamical pre-exponential factors is required. The possibility that tunneling makes a significant contribution to the rate, even at room temperature, has to be considered for such reactions. A number of experimental studies point to the importance of proton and hydride tunneling in enzymes.[3] Klinman and co-workers have measured kinetic isotope effects (KIEs) and their temperature dependences for several systems, such as alcohol dehydrogenases,[4] amine oxidases,[5] glucose oxidases,[6] and lipoxygenase.[7] Factors that have been used as evidence for tunneling include large primary/secondary KIEs, isotope effects on the Arrhenius prefactor deviating significantly from unity,[3] and, most commonly, the value of the Swain−Schaad exponent,[8] $\ln(k_H/k_T)/\ln(k_D/k_T)$ (where k_I is the rate for isotope I). Specifically, if the exponent is larger than 3.3, the value predicted by a classical vibrational model, then it has been concluded that tunneling is important. Corresponding effects have been observed in other enzymes, such as triosephosphate isomerase (TIM)[9] and

---

† Harvard University.
‡ ISIS Universitè Loius Pasteur.
(1) See, for example: Bell, R. P. *The proton in chemistry*; Chapman and Hall: London, 1973.
(2) Fersht, A. *Structure and mechanism in protein science*; W. H. Freeman and Co.: New York, 1999.

(3) For a recent review, see: Kohen, A.; Klinman, J. P. *Acc. Chem. Res.* **1998**, *31*, 397.

NAD-malic-enzyme.[10] Further, these experimental results have been instrumental in focusing attention[11] on the possible role of protein dynamics in determining the extent of tunneling in enzyme catalysis.

Although accurate approaches for calculating quantum reaction rates for small systems (three or four atoms in the gas phase) are available,[12] more approximate methods have to be used for treating proton-transfer reactions in solution[13,14] and in enzymes. For the latter, which are of primary interest here, most of the analysis of quantum corrections has been based on simplified models.[15,16] The widely used variational transition-state theory with semiclassical ground-state multidimensional tunneling (VTST−SAG)[17,18] has been recently applied by Alhambra et al.[19] to yeast enolase with an AM1/MM description of the potential energy surface for proton-transfer reaction, making use of a new interface between the POLYRATE program[20] (for doing the rate constant calculations) and the CHARMM program[21] (for determining the potential energy surface). They found that the quantum-mechanical treatment of the vibrational partition functions in the VTST calculations was more important than tunneling; i.e., compared with a purely classical transition-state treatment, the computed rate constant at 300 K increased by a factor of about 40 from the former and only 1.7 from the latter, respectively. Similar results were obtained by Alhambra et al. for LADH with the same method.[22] Hwang and Warshel have studied the effect of proton tunneling in lactate dehydrogenase and carbonic anhydrase using a path integral formulation with an empirical valence bond potential energy surface.[23] They found that tunneling is substantial (on the order of a factor of 10−20 at 300 K) in these enzymes but that a similar tunneling contribution occurs for the corresponding solution reactions. The present study of TIM complements these calculations on other enzyme systems.

Because of the sensitivity of the tunneling contribution to the shape of the barrier for the proton transfer, meaningful calculations are limited by the accuracy of the potential energy surface. Recently, we have made a detailed study[24] of the potential energy surface and kinetics in the classical limit of the proton-transfer reactions catalyzed by the enzyme triosephosphate isomerase. TIM catalyzes the interconversion of dihydroxyacetone phosphate (DHAP) and (*R*)-glyceraldehyde 3-phosphate (GAP), which is an important step in the glycolytic pathway. Three different mechanisms had been proposed (see Scheme 1), which involve both Glu 165 and His 95 (path A) or Glu 165 alone (paths B and C). To examine which of these is most important, we used the quantum mechanics/molecular mechanics (QM/MM) method[25] to determine the potential energy surface for the reactions involved at a sufficiently high QM level of B3LYP[26]/6-31+G(d,p).[27] The substrate and the catalytic residues, Glu 165 and/or His 95, were treated with QM, and the rest of the enzyme was described by MM with the all-atom CHARMM22 force field.[28] It was found that path A and path C have similar rate-limiting barriers and yield rates in reasonable agreement with experiment; path B was found to be much higher in energy and could be excluded as a contribution to the reaction in the wild-type enzyme.

The detailed and relatively high-level QM/MM potential energy surface obtained for the TIM-catalyzed reactions sets the stage for an analysis of the effect of tunneling on the various proton-transfer steps involved and of its relative contribution to the different proposed mechanisms. In both paths A and C, the elementary step that has the largest barrier is the first proton transfer from Cα of the substrate DHAP to Glu 165, a step common to all three paths. Consequently, we examine the contribution of tunneling to this step. For path B, the intramolecular proton transfer in the enediolate species has the highest barrier. If tunneling is significant in this step, it might increase the rate sufficiently so that it could contribute to the overall reaction. We therefore also determine the role of tunneling for this step. In addition, we made comparison calculations for the intramolecular proton process of a model enediolate in the gas phase and in aqueous solution.

Alston et al.[9] were able to make the proton-transfer steps rate-limiting by using [1(*R*)-2H]-labeled substrate in D$_2$O to slow the chemical steps relative to the product release, which is normally rate limiting.[29] The secondary H/T KIE was found to be rather large in magnitude (∼1.27 for the deuterated substrate in D$_2$O), and the secondary Swain−Schaad exponent was determined to be 4.4 ± 1.3. These results were interpreted by Alston et al.[9] as indicating that proton tunneling is important in the transfer of the proton from DHAP to Glu 165. In the current work, variational transition-state theory with the semiclassical adiabatic vibrational ground-state tunneling (VTST−SAG)[17] method was used for the rate constant calculations. Corresponding calculations were performed in the gas phase and in solution for the intramolecular proton transfer (see above) to compare with the results obtained for the enzyme. The potential energy

(4) (a) Kohen, A.; Cannio, R.; Bartolucci, S.; Klinman, J. P. *Nature* **1999**, *399*, 496. (b) Cha, Y.; Murray, C. J.; Klinman, J. P. *Science* **1989**, *243*, 1325.
(5) Grant, K. L.; Klinman, J. P. *Biochemistry* **1989**, *28*, 6597.
(6) Kohen, A.; Jonsson, T.; Klinman, J. P. *Biochemistry* **1997**, *36*, 2603.
(7) Glickman, M. H.; Klinman, J. P. *J. Am. Chem. Soc.* **1994**, *116*, 793.
(8) Swain, C. G.; Stivers, E. C.; Reuwer, J. F., Jr.; Schaad, L. J. *J. Am. Chem. Soc.* **1958**, *80*, 5885.
(9) Alston, W. C.; Manska, M.; Murray, C. J. *Biochemistry* **1996**, *35*, 12873.
(10) Karsten, W. E.; Hwang, C. C.; Cook, P. F. *Biochemistry* **1999**, *38*, 4398.
(11) Wilson, E. K. *Chem. Eng. News* **2000**, *78*, 42.
(12) See, for example: Bowman, J. M.; Schatz, G. C. *Annu. Rev. Phys. Chem.* **1995**, *46*, 169.
(13) (a) Borgis, D.; Hynes, J. T. *J. Chem. Phys.* **1991**, *94*, 3619. (b) Borgis, D.; Hynes, J. T. *J. Chem. Phys.* **1993**, *170*, 315.
(14) Staib, A.; Borgis, D.; Hynes, J. T. *J. Chem. Phys.* **1995**, *102*, 2487.
(15) Antoniou, D.; Schwartz, S. D. *Proc. Natl. Acad. Sci. U.S.A.* **1997**, *94*, 12360.
(16) Antoniou, D.; Schwartz, S. D. *J. Phys. Chem. B* **2001**, *105*, 5553.
(17) (a) For a recent review, see: Truhlar, D. G.; Garrett, B. C.; Klippenstein, S. J. *J. Phys. Chem.* **1996**, *100*, 12771. (b) Truhlar, D. G.; Isaacson, A. D.; Garrett, B. C. In *Theory of Chemical Reaction Dynamics*; Bear, M., Ed.; CRC Press: Boca Raton, FL, 1985; Vol. 4, p 65.
(18) Truhlar, D. G.; Garrett, B. C. *Annu. Rev. Phys. Chem.* **1984**, *35*, 159.
(19) Alhambra, C.; Gao, J.; Corchado, J. C.; Villà, J.; Truhlar, D. G. *J. Am. Chem. Soc.* **1999**, *121*, 2253.
(20) Chuang, Y.; Corchado, J. C.; Fast, P. L.; Villa, J.; Coitino, E. L.; Hu, W.; Liu, Y.; Lynch, G. C.; Nguyen, K.; Jackels, C. F.; Gu, M. Z.; Rossi, I.; Clayton, S.; Melissas, V.; Steckler, R.; Garrett, B. C.; Isaacson, A. D.; Truhlar, D. G. POLYRATE version 8.0 (August 1998); Department of Chemistry and Supercomputer Institute, University of Minnesota, Minneapolis, MN.
(21) Brooks, B. R.; Bruccoleri, R. E.; Olafson, B. D.; States, D. J.; Swaminathan, S.; Karplus, M. *J. Comput. Chem.* **1983**, *4*, 187.
(22) Alhambra, C.; Corchado, J. C.; Sánchez, M. L.; Gao, J.; Truhlar, D. G. *J. Am. Chem. Soc.* **2000**, *122*, 8197.
(23) Hwang, J. K.; Warshel, A. *J. Am. Chem. Soc.* **1996**, *118*, 11745.

(24) (a) Cui, Q.; Karplus, M. *J. Am. Chem. Soc.* **2001**, *123*, 2284. (b) Cui, Q.; Karplus, M. *J. Phys. Chem. B*, in press.
(25) (a) Field, M. J.; Bash, P. A.; Karplus, M. *J. Comput. Chem.* **1990**, *11*, 700. (b) Gao, J. In *Reviews in Computational Chemistry*; Lipkowitza, K. B., Boyd, D. B., Eds.; VCH: New York, 1996; Vol. 7, p 119.
(26) (a) Becke, A. D. *Phys. Rev. A* **1988**, *38*, 3098. (b) Lee, C.; Yang, W.; Parr, R. G. *Phys. Rev. B* **1988**, *37*, 785. (c) Becke, A. D. *J. Chem. Phys.* **1993**, *98*, 5648.
(27) (a) Ditchfield, R.; Hehre, W. J.; Pople, J. A. *J. Chem. Phys.* **1971**, *54*, 724. (b) Hehre, W. J.; Ditchfield, R.; Pople, J. A. *J. Chem. Phys.* **1972**, *56*, 2257. (c) Hariharan, P. C.; Pople, J. A. *Theor. Chim. Acta* **1973**, *28*, 213.
(28) MacKerell, A. D.; et al. *J. Phys. Chem.* **1998**, *102*, 3586.
(29) Knowles, J. R.; Albery, W. J. *Acc. Chem. Res.* **1977**, *10*, 105.

Scheme 1. Proposed Catalytic Mechanisms for TIM-Catalyzed Reactions
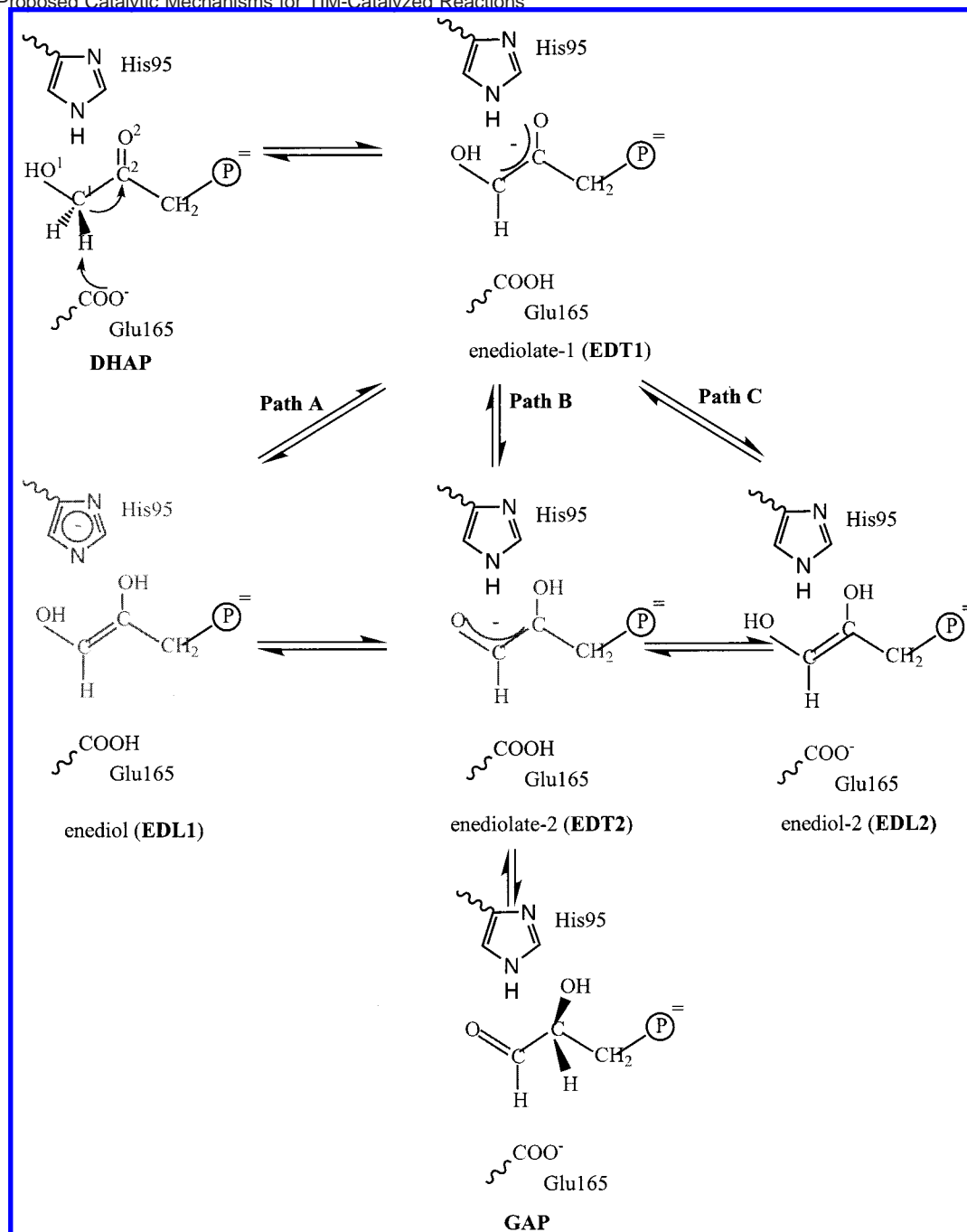
surfaces for the proton transfers were calculated with the AM1-SRP/MM[24] approach for the reactions in the enzyme and in solution; the gas-phase system was described by both AM1-SRP and B3LYP/6-31+G(d,p) as a verification of the validity of the former. In a complementary study,[30] we consider the intramolecular reaction in the gas phase and the intermolecular reaction in the enzyme, as well as some model reactions, to identity vibrational modes that are important in determining the proton-transfer rate ("promoting modes").[15,16] Here, we focus on a comparison of the magnitude of tunneling in different media (gas phase, solution, and enzyme) and the effect of tunneling on experimentally measurable quantities, such as the

Swain−Schaad exponents. Where appropriate, we relate the present results to the analysis of the promoting modes.

In section II, we briefly review the variational transition-state method and its implementation in the CHARMM program, which is somewhat different from that of Alhambra et al.[19] The results and discussion are presented in sections III and IV, respectively, and the conclusions are in section V.

II. Computational Methods

II.1. Rate Constant Calculation. We briefly review the variational transition-state theory with semiclassical adiabatic ground-state tunneling (VTST−SAG)[18] employed in the rate constant calculations to define the notation and to provide a framework for analysis of the results. In this approach, several corrections to classical TST are made. By "classical" TST, we mean that neither quantization of vibrations

(30) (a) Cui, Q.; Karplus, M., to be submitted. (b) Cui, Q.; Brumer, Y.; Reichman, D. R.; Karplus, M., work in progress.

nor tunneling was included; the term TST is employed to describe calculations with quantized vibrations without tunneling. A major assumption of TST is that classical trajectories do not recross the dividing surface, which is usually chosen as the hyperplane orthogonal to the reaction coordinate and containing the saddle point. Accordingly, the TST rate constant is an upper bound to the exact classical result.[31] The ratio of the actual classical rate constant and that from the TST limit is defined as the transmission coefficient; the calculated value of the transmission coefficient[32] for the first proton-transfer step in TIM is 0.4.[33] In VTST without tunneling, the effect of recrossing is reduced by letting the transition state deviate from the saddle point *along* the reaction coordinate and optimizing its position by variationally minimizing the reaction flux.[17] This corresponds to searching for the free energy maximum along the reaction coordinate in the canonical ensemble (CVTST) or allowing the position of the transition state to be vibrational-state-dependent in the microcanonical ensemble (μVTST).[34]

To introduce quantum corrections, the energy-dependent transmission coefficient, $P_{1d}^{SAG}(E)$, is computed semiclassically using the one-dimensional WKB integral along a given path (see below). The result includes both tunneling *through* the barrier and nonclassical reflection *above* the barrier. The expressions are[18]

$$P_{1d}^{SAG}(E) = \{1 + \exp[2\hbar^{-1}\int_{s_<}^{s_>}\{2\mu_{eff}(s)[V_A^G(s) - E]\}^{1/2}\,ds]\}^{-1},$$
$$E \le V_A^{\ddagger G} \quad (1a)$$

$$P_{1d}^{SAG}(E) = 1 - P_{1d}^{SAG}(2V_A^{\ddagger G} - E), \qquad V_A^{\ddagger G} < E \le 2V_A^{\ddagger G} \quad (1b)$$

$$P_{1d}^{SAG}(E) = 1 \qquad E > 2V_A^{\ddagger G} \quad (1c)$$

where $s_<$ and $s_>$ are the values of the path coordinate at the left and right turning points, respectively, corresponding to the energy E of the system. The quantity $V_A^G(s)$ is the vibrational ground adiabatic potential energy along the tunneling path, and $V_A^{\ddagger G}$ is the value at the saddle point; $\mu_{eff}(s)$ is the reduced mass associated with the tunneling degree of freedom.

The optimal tunneling path is the one that maximizes $P_{1d}^{SAG}(E)$, which is rather expensive to compute and has so far been done only for small molecules.[35,36] An approximate approach is to evaluate $P_{1d}^{SAG}(E)$ along the intrinsic reaction path (IRP),[37] which can be readily obtained for polyatomic systems from knowledge of the potential energy surface.[38] Such an approximation is also known as the zero-curvature theory (ZCT),[39] since the effect of reaction path curvature on the tunneling is neglected. As pointed out by a number of authors,[40] the curvature of the reaction path has a negative centrifugal effect that makes the optimal tunneling path deviate from the IRP; this is the so-called "corner-cutting" effect. A practical, alternative implementation for polyatomic system is to compute the tunneling probability along the IRP but with a modified effective mass, $\mu_{eff}(s)$, which depends on the curvature of the reaction path;[41] this is known as the small-curvature theory (SCT). The effective mass is found by using the centrifugal-

dominant small-curvature adiabatic approximation,[42] which expresses the effective mass in terms of vibrational frequencies and reaction path curvature along the reaction path; the latter is evaluated by the reaction path Hamiltonian method of Miller and co-workers.[43] After a canonical transformation from Cartesian to curvilinear coordinates, the Hamiltonian of a polyatomic molecule (with zero total angular momentum) along the reaction coordinate s, which is taken to be the Fth coordinate, ($F = 3N - 6$, where N is the number of atoms), is given by[43]

$$H(p_s,s,\{P_k,Q_k\}) = \sum_{i=1}^{F-1}\left[\frac{P_k^2}{2} + \frac{\omega_k^2(s)Q_k^2}{2}\right] + V_0(s) + \frac{1}{2}[p_s - \sum_{k,l=1}^{F-1}Q_kP_lB_{k,l}(s)]^2/[1 + \sum_{k=1}^{F-1}Q_kB_{k,F}(s)]^2 \quad (2)$$

where p_s and P_k are the momenta conjugate to the reaction coordinate s and the kth orthogonal degrees of freedom Q_k, respectively. The $\{Q_k(s)\}$ are obtained by normal-mode analysis along the reaction coordinate s (the IRP in the current implementation) by diagonalizing the Hessian with the reaction coordinate direction projected out. The first term in eq 2 represents the Hamiltonian for the harmonic degrees of freedom orthogonal (transverse) to the reaction path; the second term is the potential energy along the path; the third term is the kinetic energy term of the motion along the reaction path; the denominator and the extra term in the numerator arise from the coupling between the transverse modes and the reaction path motion, and the Coriolis-like coupling among the transverse modes, respectively. The reaction path curvature component, $B_{k,F}$, is given by

$$B_{k,F}(s) = L_k^T\cdot\frac{d\vec{v}}{ds} = -|g|^{-1}L_k^T\cdot\frac{d\vec{g}}{ds} = |g|^{-1}L_k^T\cdot[H\cdot\vec{v}] \quad (3)$$

In eq 3, L_k is the kth eigenvector of the Hessian H, and $\vec{v}$ is the vector along the direction of the reaction coordinate, which by definition[37] is antiparallel to the normalized gradient in the mass-weighted coordinate, $-\vec{g}/|g|$. Note that in eq 3, the second equality holds because L_k is orthogonal to $\vec{v}$ and therefore annihilates another term that also contributes to $d\vec{v}/ds$.[44] The $B_{k,F}$ values represent the change in the direction of the kth eigenvector induced by the variation of the reaction coordinate. The curvature of the reaction path induces a negative centrifugal effect due to the imaginary value of the momenta conjugate to the reaction coordinate; it is this which produces the corner-cutting.[35,40] The norm of the reaction path curvature $\{B_{k,F}\}$, $(\sum_{k=1}^{F-1}B_{k,F}^2)^{1/2}$, is referred to as Γ in sections III and IV and contributes to the effective one-dimensional reduced mass $\mu_{eff}(s)$.[41,42]

In VTST−SAG, the tunneling transmission coefficients for the vibrational excited states are assumed to be related to that for the vibrational *adiabatic ground* state (eq 1) by a simple energy shift approximation,

$$P_{1d}^{\{n\}}(E) = P_{1d}^{SAG}[E - (V_A^{\ddagger\{n\}} - V_A^{\ddagger G})] \quad (4)$$

where $V_A^{\ddagger\{n\}}$ is the vibrational adiabatic energy at the transition state of the state characterized by the vibrational quantum numbers $\{n\}$. A similar approximation was employed by Bowman and Wang in the development of a reduced dimensionality theory for quantum scattering.[45]

The VTST−SAG temperature-dependent transmission coefficient, $\kappa^{CVT-SCT}(T)$, (i.e., the correction factor to the TST rate constant in the

(31) Pechukas, P. In *Dynamics of Molecular Collisions*, Part B; Miller, W. H., Ed.; Plenum Press: New York, 1976.
(32) Rosenberg, R. O.; Berne, B. J.; Chandler, D. *Chem. Phys. Lett.* **1980**, 75, 162.
(33) Neria, E.; Karplus, M. *Chem. Phys. Lett.* **1997**, 267, 23.
(34) Isaacson, A. D.; Sun, M. T.; Rai, S. N.; Truhlar, D. G. *J. Chem. Phys.* **1985**, 82, 1338.
(35) (a) Truhlar, D. G.; Gordon, M. S. *Science* **1990**, 249, 491. (b) Garrett, B. C.; Truhlar, D. G. *J. Chem. Phys.* **1983**, 79, 4931.
(36) Carrington, T., Jr.; Miller, W. H. *J. Chem. Phys.* **1986**, 84, 4364.
(37) (a) Fukui, K. *J. Phys. Chem.* **1970**, 74, 4161. (b) Shavitt, I. *J. Chem. Phys.* **1968**, 49, 4048. (c) Marcus, R. A. *J. Chem. Phys.* **1968**, 49, 2610. (d) Truhlar, D. G.; Kupperman, A. *J. Am. Chem. Soc.* **1971**, 93, 1840.
(38) See, for example: Gonzales, C.; Schlegel, H. B. *J. Chem. Phys.* **1989**, 90, 2154.
(39) Truhlar, D. G.; Kupperman, A. *J. Am. Chem. Soc.* **1971**, 93, 1840.
(40) See, for example: Marcus, R. A.; Coltrin, M. E. *J. Chem. Phys.* **1977**, 67, 2609.
(41) Skodje, R. T.; Truhlar, D. G.; Garrett, B. C. *J. Phys. Chem.* **1981**, 85, 3019.

(42) Liu, Y.; Lynch, G. C.; Truong, T. N.; Lu, D.; Truhlar, D. G.; Garrett, B. C. *J. Am. Chem. Soc.* **1993**, 115, 2408.
(43) Miller, W. H.; Handy, N. C.; Adams, J. E. *J. Chem. Phys.* **1980**, 72, 99.
(44) Page, M.; McIver, J. W., Jr. *J. Chem. Phys.* **1988**, 88, 922.
(45) Bowman, J. M.; Wang, D. *Advances in Molecular Vibrations and Collision Dynamics*; JAI Press Inc.: Greenwich, CT, 1994; Vol. 2B, p 187.

canonical ensemble with quantized vibrations) is given by the expression,

$$\kappa^{\text{CVT-SCT}}(T) = \kappa^{\text{CVT}} \times \frac{\int P_{1d}^{\text{SAG}}(E) \, e^{-K/k_B T} \, dE}{\int h\{E - V_A^G[S_*^{\text{CVT}}(T)]\} \, e^{-K/k_B T} \, dE} \quad (5)$$

where $h(E)$ is the Heaviside function. In eq 5, κ^{CVT} is the correction factor relative to TST due to the change in the position of the transition state (S_*^{CVT}) in canonical VTST, and the other factor corresponds to the tunneling correction to CVT.

From the above, the required quantities in the VTST–SAG calculations include the frequencies and the generalized normal modes (i.e., the normal modes obtained by diagonalizing the Hessian matrix with the reaction path component projected out) at a set of points along the reaction coordinate. For large systems (more than 100 atoms that are allowed to move relative to a fixed environment) as considered here, saving the eigenvectors at many points is very memory intensive. We have therefore implemented the algorithm to evaluate the reaction path curvature components, $B_{k,F}$ (eq 3), in the TRAVEL module of CHARMM.[21] This allows us to use the conjugate peak refinement (CPR) algorithm[46] to optimize the IRP (i.e., the steepest descent path in mass-weighted coordinate) for large systems and reduces the memory requirement of the computation dramatically. Only the frequencies and the curvature components along the IRP have to be saved in disk or memory (rather than keeping the entire Hessian and eigenvectors along the reaction path, as in the standard implementation with POLYRATE); they form two arrays that are linear in the size of the system. The required information (geometries, energies, frequencies, and curvature components along the IRP) is then used as input for a modified version of POLYRATE8.0[20] to calculate the effective reduced mass along the IRP, the tunneling integrals (eq 1), and the rate constants. In this way, large systems with hundreds of movable atoms can be studied on normal workstations. The present approach differs from that of Alhambra et al.,[19] who created a very convenient interface between POLYRATE[20] and CHARMM. Their implementation is more memory intensive because all the eigenvectors along the reaction path have to be saved. This has so far limited the number of movable atoms (to about 30 in the context of enzyme systems[19,22] and 57 for gas–surface reactions[47]) that can be included in the calculations.

II.2. Details of the Calculations. As mentioned in the Introduction and in the earlier paper on TIM,[24] the potential energy surface for the TIM-catalyzed proton-transfer reactions was determined with the QM/MM methodology, where the QM part was at the B3LYP/6-31+G-(d,p) level and the MM part was given by the CHARMM22 force field. Although, in principle, the tunneling calculations could be done with B3LYP (e.g., a DFT/MM approach has been developed for normal-mode analysis[48]), the computational cost is too high. Consequently, we used a semiempirical QM method of AM1 type, reparametrized[49] (AM1-SRP) relative to the B3LYP results for the TIM-catalyzed reactions; details of the parametrization are given in ref 24. The AM1-SRP/CHARMM results overall are in satisfactory agreement with the B3LYP/6-31+G(d,p) calculations for the reactions studied here; the differences at the stationary points correspond to an RMS error of 4.5 kcal/mol. This is to be compared with the standard AM1/CHARMM, which has an RMS error of 8.4 kcal/mol compared to the B3LYP/6-31+G(d,p) results.

For reactions in the enzyme, the same system as that used in the calculation of the potential energy surface was employed; for details, see ref 24. The active site structures for the two steps in the TIM reactions that are studied here are shown in Figure 1. To reduce the cost of the calculations, atoms that are relatively far from the active site were fixed in the reaction path and normal-mode calculations. In the "small" model, all atoms beyond 4 Å of Cγ in the substrate (see Figure 1) were fixed; this results in a system consisting of 106 movable atoms, including six residues (K12, H95, E165, I170, G210, G231) and one water molecule. In the "larger" model, atoms beyond 8 Å of Cγ were kept fixed; this results in 445 movable atoms, including 16 water molecules. In addition, 2235 atoms in the small model and 1895 atoms in the larger model provided a fixed environment to complete the sphere used in ref 24. By comparison, Alhambra et al. included 25 movable atoms in their pioneering study of yeast enolase[19] and 21 movable atoms in LADH.[22]

For the gas-phase calculations of the intramolecular proton transfer, an enediolate model without the phosphate group was used (Figure 3a) because, as we showed in earlier work,[24] inclusion of the latter leads to unphysical results for the potential energy surface. Calculations with both the AM1-SRP and B3LYP/6-31+G(d,p) methods were carried out for this small system; the latter result provides a check on the former. For the intramolecular transfer in water, the full substrate (including the phosphate group) was used (Figure 2). It was solvated by a 16 Å water sphere, with a stochastic boundary potential;[50] a total of 549 water molecules were included. The solute was described with AM1-SRP, and the water was treated with a flexible modified TIP3P model to simplify the normal-mode analysis.[51] The optimized structures of reactant, saddle point, and product, each with a small number of solvent molecules, are shown in Figure 2. During the reaction path and normal-mode analyses, water molecules beyond 8 Å from Cγ of the substrate were fixed, leaving 308 movable atoms, of which 98 were water molecules. A smaller model with water molecules fixed beyond 4 Å from Cγ was also used; it includes 65 movable atoms, of which 17 were water molecules.

To determine the effect of fluctuation in the environment, molecular dynamics simulations were carried out for the intramolecular proton-transfer reaction in the enzyme and in solution. The motions of the system with the EDT1 intermediate (see Scheme 1) were calculated by use of the mixed MD/LD stochastic boundary algorithm, with atoms in the reaction region treated with MD and those in the buffer region with Langevian dynamics;[52] the reaction region had a radius of 12 Å and the buffer region 2 Å. The simulations were carried out for 50 ps of equilibration and 100 ps of production at 300 K with a time step of 2 fs; all the bonds involving hydrogen were fixed by using SHAKE.[53] Ten configurations were selected from the trajectory at 10 ps intervals. Using these as starting structures, reaction path optimizations with the small model were carried out.

After the reaction paths were optimized for each of the systems by use of the TRAVEL module in CHARMM, normal modes and reaction path curvatures along the reaction coordinate were calculated and used in a modified version of POLYRATE to compute the rate constants, as described in section II.1. Between 70 and 110 points along the reaction coordinate were used in the VTST–SAG calculations. Of these, at least 50 points were in the critical region, with the mass-weighted reaction coordinate in the range of $(-3.0, +3.0)$ amu$^{1/2}$·bohr. Test calculations with 320 points gave transmission coefficients within a factor of 1.2 at 300 K, indicating that the results with 50 points are sufficiently accurate for the present semiquantitative analysis.

The vibrational degrees of freedom were treated as quantized in the rate constant calculations, unless stated otherwise; i.e., the vibrational partition function was evaluated with the quantum-mechanical rather than the classical formula. The correction factor of CVT–SCT relative to CVT is designated as $\kappa^{\text{CVT-SCT}}$ (see eq 5) and referred to loosely as

(46) Fischer, S.; Karplus, M. *Chem. Phys. Lett.* **1992**, *194*, 252.
(47) Wonchoba, S. E.; Truhlar, D. G. *J. Chem. Phys.* **1993**, *99*, 9637.
(48) Cui, Q.; Karplus, M. *J. Chem. Phys.* **2000**, *112*, 1133.
(49) Rossi, I.; Truhlar, D. G. *Chem. Phys. Lett.* **1995**, *233*, 231.

(50) Brooks, C. L., III; Karplus, M. *J. Chem. Phys.* **1983**, *79*, 6312.
(51) (a) Jorgensen, W. L.; Chandrasekhar, J.; Madura, J. P. *J. Chem. Phys.* **1983**, *79*, 926. (b) Neria, E.; Fischer, S.; Karplus, M. *J. Chem. Phys.* **1996**, *105*, 1902.
(52) (a) Brooks, C. L., III; Karplus, M. *J. Mol. Biol.* **1989**, *208*, 159. (b) Brooks, C. L., III; Brünger, A.; Karplus, M. *Biopolymers* **1985**, *24*, 843.
(53) Ryckaert, J.-P.; Ciccotti, G.; Berendsen, H. J. C. *J. Comput. Phys.* **1977**, *23*, 327.
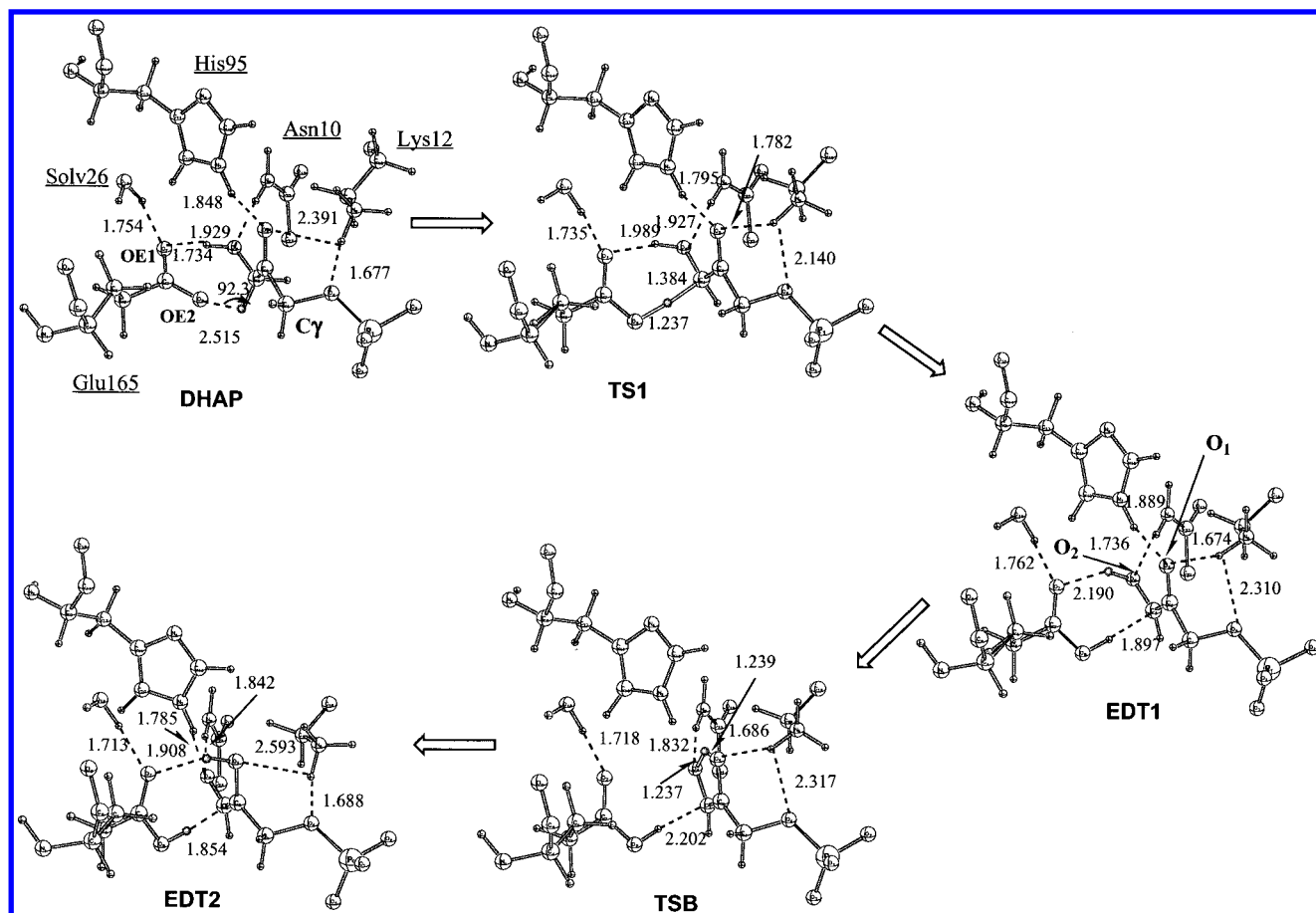
Figure 1. Active site structures of species involved in the two proton-transfer reactions in TIM obtained with the "large" model, which includes 445 movable atoms out of a total of 2340 atoms.

the "tunneling coefficient", although it includes the nonclassical reflection effects, which can be important for low-barrier cases for energies larger than the barrier (see eq 1b).[54]

For computing the rate constants, the most expensive part is the determination of the reaction path properties. This is dominated by the normal-mode analysis along the reaction path. For the large model with about 400 atoms, the whole reaction path calculation (including normal-mode and path curvature evaluations) requires about a week on a single R10000 processor of an Origin 2000. The VTST calculation itself (i.e., the calculation of the tunneling integrals and rate constants) takes only a few hours on the same machine. For the small model with about 100 atoms, the reaction path calculations required about 2 days and the VTST part about an hour.

Several quantities frequently used in experimental analyses of tunneling were calculated to compare the conclusions normally drawn from the measured values with the calculated tunneling contribution. They are all isotope-dependent ratios defined as follows:

Kinetic isotope effects (KIEs): k_H/k_D and k_H/k_T (6a)

Swain–Schaad exponent: $\alpha_{SS} = \ln(k_H/k_T)/\ln(k_D/k_T)$ (6b)

Arrhenius parameters: A_H/A_T and $E_a(T) - E_a(H)$ (6c)

where k_I is the rate constant for isotope I (I = H, D, or T); $E_a(I)$ and A_I are the apparent activation energy and intercept from an Arrhenius plot for isotope I. For the KIEs and the Swain–Schaad exponent, secondary as well as primary quantities were computed for the intermolecular proton transfer (there is no secondary hydrogen in the

intramolecular proton transfer). For the Arrhenius parameters, only the primary effect was studied. In the VTST calculations, the reaction path and generalized normal modes and finally the rate constants were determined for appropriate isotope substitutions.

To interpret and compare the reaction paths and rate constants in different media (gas, solution, and enzyme), curvature components for selected configurations along the reaction paths were examined. The inverse participation ratios, which have been used to characterize the degree of delocalization of the normal modes in liquid[55] and protein systems,[56] were also determined. Two quantities, R_i^I and R_i^{II}, are defined for each (generalized) normal-mode k; they are

$$R_k^I = \sum_j^{3N} L_{jk}^4 \tag{7a}$$

$$R_k^{II} = \sum_i^{M_{res}} [\sum_j^{3N_i} L_{jk}^2]^2 \tag{7b}$$

where N and N_i are the numbers of atoms in the whole system and in the ith residue, respectively; M_{res} is the number of residues in the system. R_k^I indicates the number of atoms involved in the kth (generalized) normal mode, and R_i^{II} corresponds approximately to the number of residues involved.

To determine the effect of geometry relaxation on the proton transfer, potentials of mean force (PMF) were calculated with the umbrella sampling technique[57] for the intramolecular proton transfer in water and in TIM, and for the intermolecular proton transfer in TIM. In the

(54) See, for example: Hu, W.; Rossi, I.; Corchado, J. C.; Truhlar, D. G. *J. Phys. Chem. A* **1997**, *101*, 6911.

(55) See, for example: Cho, M.; Fleming, G.; Saito, S.; Ohmine, I.; Stratt, R. M. *J. Chem. Phys.* **1994**, *100*, 6672.

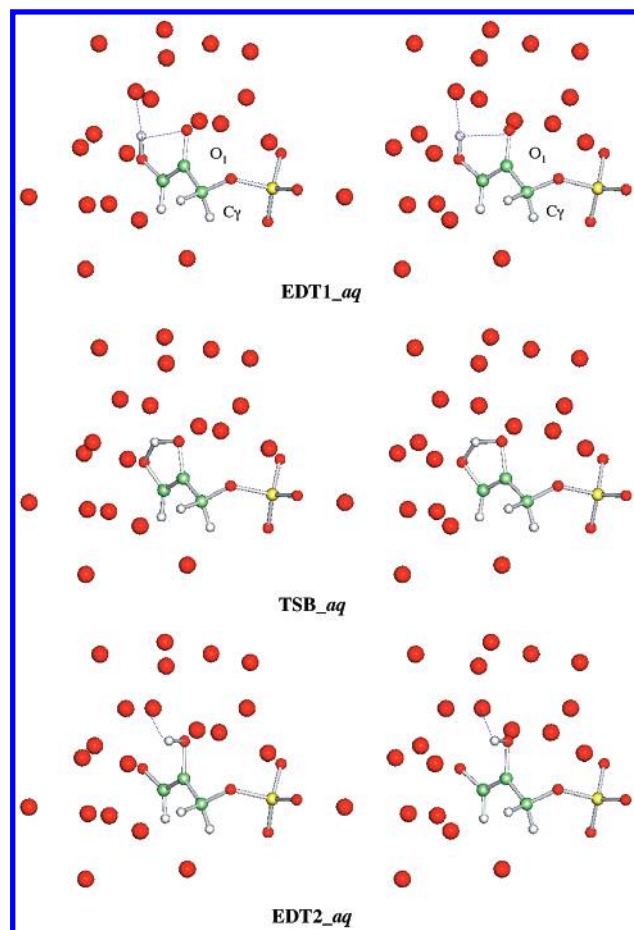(56) Sagnella, D. E.; Straub, J. E. *Biophys. J.* **1999**, *77*, 70.

Figure 2. Stereo plots (cross-eyed) of the solute structure for the species involved in the proton-transfer reactions in solution obtained with the "large" model, which includes 308 movable atoms in a 16 Å water sphere.

PMF calculations, the antisymmetric stretch coordinate involving the donor, proton, and acceptor, $\delta = r_{\text{D−H}} - r_{\text{A−H}}$, was used as the approximate reaction coordinate, which was found to sufficiently describe the proton-transfer process in the previous study.[24] Twenty windows were used for the intramolecular proton transfer in water and the intermolecular proton transfer in TIM, with the center of the umbrella potential ranging from −1.2 to 1.2 Å. For the intramolecular proton transfer in TIM, 25 windows were used, with the center of the umbrella potential in the range of −1.2 and 2.2 Å. For each window, 25 ps molecular dynamics was carried out with an integration step of 0.5 fs; the first 5 ps was discarded in the analysis. The distributions of δ from the different windows were combined using the Weighted Histogram method (WHAM)[58] to obtain the final PMF.

III. Results

In this section, we focus on the calculated rate constants, tunneling coefficients, and isotope effects at 300 K. Because the intramolecular proton transfer in the enediolate intermediate is the simpler problem, in part due to the intrinsic symmetry of the gas-phase model, we begin by describing the results obtained for that reaction (see section III.1). Moreover, we were able to study this reaction in the gas phase, in solution, and in the enzyme. The results for the intermolecular proton transfer between the DHAP substrate and Glu 165 in the enzyme are

(57) (a) Torrie, G. M.; Valleau, J. P. *J. Chem. Phys*. **1974**, *66*, 1402. (b) Allen, M. P.; Tildesley, D. J. *Computer simulation of liquids*; Oxford University Press: New York, 1987.
(58) Kumar, S.; Bouzida, D.; Swendsen, R. H.; Kollman, P. A.; Rosenberg, J. M. *J. Comput. Chem.* **1992**, *13*, 1011.

presented in section III.2. A more detailed discussion of their temperature dependence and interpretations is given in section IV.

III.1. Intramolecular Proton Transfer. III.1a. Rate Constants in the Gas Phase. Figure 3a shows the optimized (adiabatic) potential energy profile along the minimum energy path obtained with AM1-SRP and B3LYP. The energy is symmetric with respect to the saddle point because the phosphate group has been replaced by a hydrogen atom (see Computational Methods). The results obtained from the two methods are very similar: the potential energy barrier for the proton transfer is 9.5 kcal/mol at the AM1-SRP level and 8.6 kcal/mol at the B3LYP/6-31+G(d,p) level, both without zero-point energy (ZPE) corrections. The imaginary frequency at the saddle point is $1365i$ cm^{-1} at the AM1-SRP level and $1379i$ cm^{-1} at the B3LYP/I level. Therefore, the AM1-SRP method used in the present work is satisfactory for studying the kinetics of the intramolecular proton-transfer reaction.

The essential geometrical parameters vary along the reaction path in a manner typical for proton-transfer reactions.[59] As shown in Figure 3b, the initial stage of the reaction ($-2.5 < s < -0.5$) involves mainly the decrease of the donor−acceptor (O^D−O^A) and acceptor−proton (O^A−H) distances, while the donor−proton (O^D−H) distance increases only slightly to 1.08 Å from the equilibrium value (0.966 Å). Starting from s equal to about −0.5, the O^D−H distance increases rapidly to about 1.25 Å at the saddle point. Several bond angles (such as ∠H−O^A−C^A, ∠H−O^D−C^D, and ∠O^D−H−O^A in Figure 3c) change significantly in the region $-0.7 < s < 0.7$; i.e., ∠O^D−H−O^A becomes more linear in the region of the saddle point. The magnitude of the reaction path curvature (Γ) reaches a maximum of 2.3 amu$^{-1/2}$·bohr^{-1} at s equals to −0.5, as shown in Figure 3d. This is consistent with the fact that the direction of the reaction path (i.e., the rate of change of the significant degree of freedoms) varies in this region. The symmetric behavior on the product side ($s \geq 0$) mirrors that of the potential energy surface, as expected.

The proton-transfer rate constants obtained with canonical variational TST (CVT), canonical variation TST with the zero reaction path curvature (CVT−ZCT, i.e., $\mu_{\text{eff}} = \mu_H$), and the small-curvature approximation (CVT−SCT, i.e., μ_{eff} modified by the reaction path curvature, at both the AM1-SRP and B3LYP levels) are shown in Figure 3e. The values at 300 K are summarized in Table 1. As a consequence of the symmetric character of the reaction, the CVT rate constant is identical to the TST value because the position of the transition state is only allowed to move *along* the reaction path in the current formulation of VTST.[18] The AM1-SRP and B3LYP/I results are very close in all cases, which is expected since the barrier height and the imaginary frequency are nearly identical (see above). Tunneling as obtained from the ratio of $k^{\text{CVT−SCT}}$ and k^{CVT} (eq 5) is significant, particularly at 100 K. It is about a factor of 7.7 at 300 K and 10^7 at 100 K with the CVT−SCT method. At the CVT−ZCT level, the tunneling is about 3.3 at 300 K and 10^5 at 100 K. Thus, the effect of reaction path curvature is about a factor of 2 at room temperature and a factor of 10^2 at 100 K.

The isotope effects on the reaction path properties and rate constants at different levels of rate theory are shown in Figure

(59) Garrett, B. C.; Truhlar, D. G. *J. Phys. Chem.* **1991**, *95*, 10374.
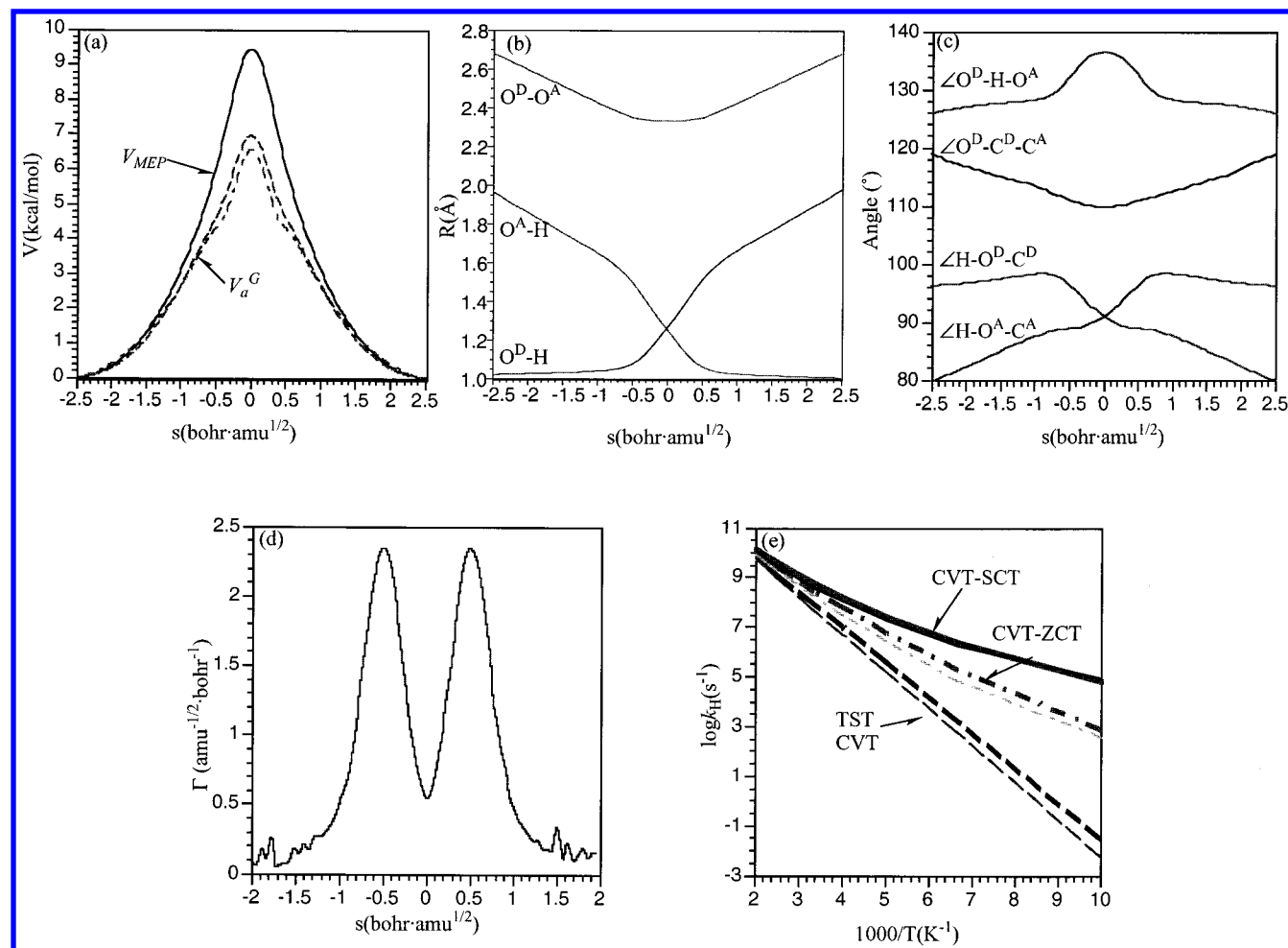
Figure 3. Reaction path properties along reaction coordinate s and rate constants for the intramolecular proton transfer in the gas phase as a function of temperature. (a) Minimum energy profile at the AM1-SRP (solid), and the adiabatic vibrational ground state at the AM1-SRP (dash) and B3LYP/6-31+G-(d,p) levels (dot−dash). (b) Important distances: donor−proton (O^D···H), acceptor−proton (O^A···H), and donor−acceptor (O^D···O^A) distances. (c) Important angles. (d) Reaction path curvature. (e) Rate constants obtained with TST (dash), CVT−ZCT (dash−dot), and CVT−SCT (solid). Due to the symmetry of the system, TST is equivalent to CVT. The set of bold lines was obtained with the B3LYP/6-31+G(d,p) parameters, and the other set was calculated with AM1-SRP.

4; all calculations were carried out with AM1-SRP. As the mass of the transferred nucleus increases, the minimum energy profile as a function of the mass-weighted reaction path becomes wider (Figure 4a), and the maximum of the reaction path curvature decreases from 2.3 for H and 1.5 for D to 1.0 for T (Figure 4b). The imaginary vibrational frequency at the saddle point decreases from $1365i$ cm^{-1} for H and $1009i$ cm^{-1} for D to $848i$ cm^{-1} for T. The H/D KIE at 300 K is 4.56 at the CVT (TST) level, 6.57 at the CVT−ZCT level, and 8.99 at the CVT−SCT level. The H/T KIE at 300 K is 8.88, 15.3, and 20.8 at the CVT (TST), CVT−ZCT, and CVT−SCT levels, respectively. The Swain−Schaad exponent, α_{SS}, is close to 3.3 at the CVT level at temperatures ranging from 100 to 500 K, as expected from the differences in barrier heights for different isotopes including ZPE; the values of the adiabatic barrier height are 6.6 kcal/mol for H, 7.5 kcal/mol for D, and 7.9 kcal/mol for T. The value of 3.3[8] for α_{SS} is obtained if the donor−H stretch is assumed to be 3000 cm^{-1} in the reactant; this frequency scales according to the square root of the mass and is assumed to be lost at the barrier top. With the CVT−SCT model, which includes tunneling, the value is about 3.6 at 300 K (i.e., only very slightly different from that without tunneling), and it *decreases* to 2.8 at 100 K, even though tunneling is calculated to be orders of

Table 1. Rate Constants, Kinetic Isotope Effects (KIE), and Tunneling Factors for the Intramolecular Proton-Transfer Reaction in the Gas Phase at 300 K[a]

	classical TST[b]	CVT[c]	CVT−ZCT	CVT−SCT
$V^{\ddagger}/\omega^d$	9.5/1365 (8.6/1379)			
$\log(k_H)$	6.18	7.72 (7.90)	8.25 (8.48)	8.61 (8.76)
$\kappa_H^{\mathrm{CVT-SCT}}$ [e]			3.30 (3.72)	7.71 (7.23)
KIE (H/D)	1.35	4.56	6.57	8.99
KIE (H/T)	1.61	8.88	15.3	20.8
α_{SS}^f	2.76	3.27	3.22	3.63
$\Delta E_a(H,T)^g$		1.16	1.77	2.05
A_H/A_T^h		1.27	0.80	0.66

[a] The numbers without parentheses are AM1-SRP results, and those in parentheses are B3LYP/6-31+G(d,p) values. [b] The bound vibrational modes were treated classically, and the vibrational adiabatic energy does not include the zero-point energies. For the other calculations (i.e., CVT, CVT−ZCT, and CVT−SCT), the quantum mechanical vibrational partition functions were used. In the other tables, unless specified, the quantum mechanical partition functions were used. [c] Due to the symmetry of the reaction, CVT is equivalent to TST. [d] $V^{\ddagger}$ is the barrier height, in kcal/mol, without zero-point energy (ZPE) correction; ω is the imaginary frequency (in cm^{-1}) at the saddle point. [e] The SCT correction factor defined as $k^{\mathrm{CVT-SCT}}/k^{\mathrm{CVT}}$ (eq 5 in text). This applies to all the tables. [f] The Swain−Schaad exponent is defined as $\ln(k_H/k_T)/\ln(k_D/k_T)$. [g] The difference in the apparent activation energy for H and T at 300 K obtained by fitting the logarithm of the rate constants computed at 250, 300, and 350 K to a linear function with respect to $1/T$. [h] The ratio of Arrhenius prefactor for H and T at 300 K obtained as the intercept from (g).
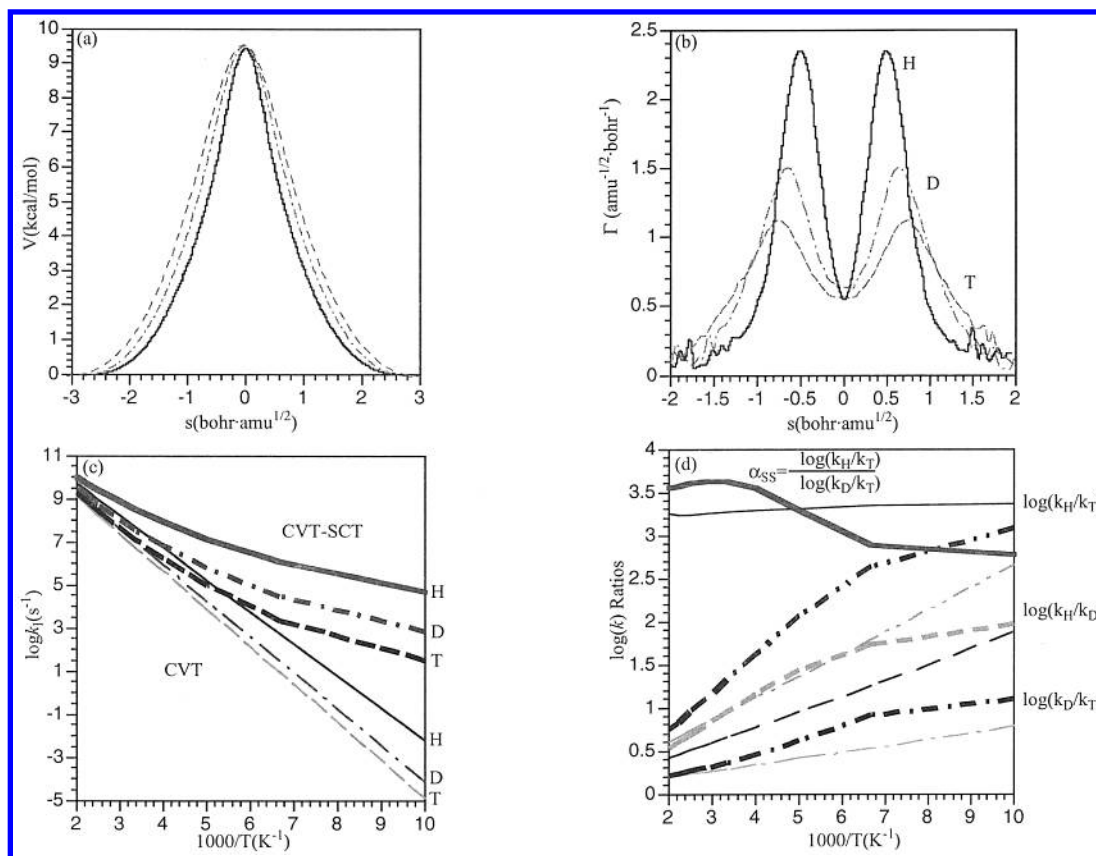
Figure 4. Reaction path properties along reaction coordinate s and rate constants for the intramolecular proton transfer in the gas phase with H, D, and T as a function of temperature. (a) Minimum energy profile. (b) Reaction path curvature. (c) CVT and CVT−SCT (bold) rate constants. (d) Kinetic isotope effects. In (a)−(c), the solid, dash−dot, and dashed lines represent results for H, D, and T, respectively. In (d), the dashed lines represent $\log(k_H/k_D)$; the dash−dot lines represent $\log(k_D/k_T)$; the dash−dot−dot lines give $\log(k_H/k_T)$; and the solid lines give the Swain−Schaad exponent, α_{SS}. The bold lines in (c) and (d) represent CVT−SCT results, and the thin lines represent CVT results.

magnitude larger at low temperature (see above). It should be noted that CVT−SCT substantially underestimates the degree of tunneling at low temperature in some cases.[60] For the present case, good agreement for the temperature dependence of the Swain−Schaad exponent was observed between the CVT−SCT results and path-integral simulations (to be published). As discussed in more detail in section IV, the Swain−Schaad exponent does not have to be larger than 3.3 in systems where tunneling is important, although this has been assumed in the analysis of many experiments.[3] The Arrhenius parameters, A_H/A_T and $E_a(T) - E_a(H)$, are influenced by tunneling even at 300 K, as indicated by the differences between CVT and CVT−SCT results (Table 1). For example, A_H/A_T is 1.27, 0.80, and 0.66 at the CVT, CVT−ZCT, and CVT−SCT levels, respectively. The value of $E_a(T) - E_a(H)$ is 1.16, 1.77, and 2.05 kcal/mol, respectively; the "quasi-classical" limit[61] (i.e., the difference arising from zero-point energy) is 1.8 kcal/mol. From the slopes of the CVT−SCT results in Figure 4c, one can estimate the "crossover" temperature (i.e., the temperature at which the proton transfer changes character from a thermally activated process to one that is tunneling dominated) for different isotopes. The values are approximately 222, 180, and 154 K for H, D, and T, respectively, and close to estimations based on one-dimensional semiclassical theories.[62,63]

At room temperature, the quantization of the bound vibrational degrees of freedom has a more significant effect on the rate constant than tunneling along the reaction coordinate; the effective barriers are 9.4 and 6.6 kcal/mol with and without zero-point energy, respectively. This behavior is in agreement with the study of proton transfer in the enzyme yeast enolase.[19] At 300 K, the fully classical TST gives a rate constant that is 32 times smaller than the quantized TST (CVT) value, which in turn is 1 order of magnitude smaller than the CVT−SCT rate constant. Classical TST also gives much too small isotope effects since the KIEs come from the classical vibrational partition functions; the H/T KIE is 1.61, 8.88, and 20.8 at the classical TST, CVT, and CVT−SCT levels, respectively. In what follows, we do not consider the purely classical TST values further.

III.1b. Rate Constants in Enzyme. For the intramolecular proton transfer in TIM, the barrier height is calculated to be 12.8 kcal/mol at the AM1-SRP/CHARMM level (Figure 5a). As shown in our previous work,[24] the increase of the barrier in the enzyme compared to the gas phase (9.5 kcal/mol) is due mainly to the unfavorable interaction with His 95 (see Figure 1). The potential energy along the reaction coordinate is approximately symmetric, even in the presence of the phosphate group and the enzyme environment. The imaginary frequency

(60) Garrett, B. C.; Joseph, T.; Truong, T. N.; Truhlar, D. G. *Chem. Phys.* **1989**, *136*, 271.
(61) Karplus, M.; Porter, R. N.; Sharma, R. D. *J. Chem. Phys.* **1965**, *43*, 3259.

(62) (a) Miller, W. H. *J. Chem. Phys.* **1975**, *62*, 1899. (b) Benderskii, V. A.; Markarov, D. E.; Wight, C. A. *Advances in Chemical Physics 88*; John Wiley & Sons: New York, 1994.
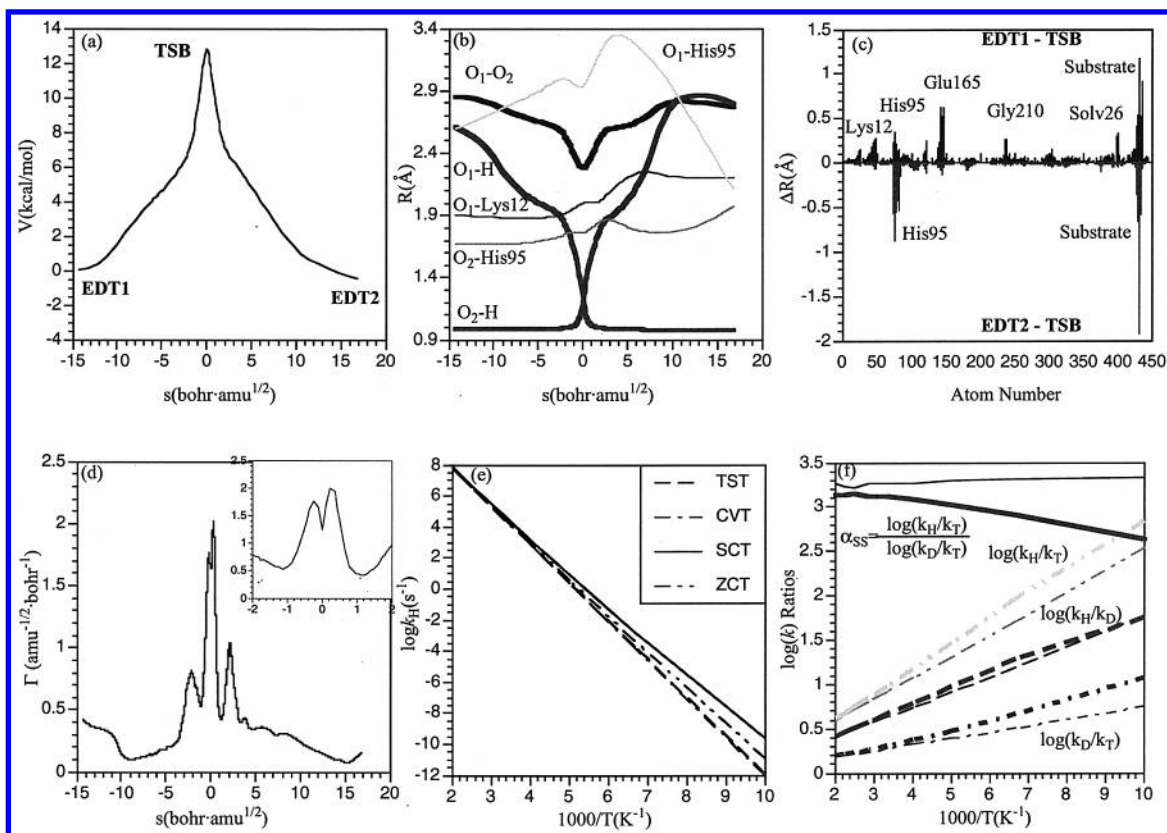(63) Häggi, P.; Grabert, H.; Ingold, G. L.; Weiss, U. *Phys. Rev. Lett.* **1985**, *55*, 761.

Figure 5. Reaction path properties along reaction coordinate *s* and rate constants for the intramolecular proton transfer in TIM with the "large" model as a function of temperature. (a) Minimum energy profile. (b) Important geometric parameters: donor−proton ($O_2 \cdots H$), acceptor−proton ($O_1 \cdots H$), and donor−acceptor ($O_1 \cdots O_2$) distances; see Figure 1 for atomic labels. Also shown in thin lines are other important geometrical parameters that vary significantly during the reaction, which involve the movement of His 95 and Lys 12. (c) Displacement of atoms in EDT1 and EDT2 measured from the saddle point; note that many residues move substantially during the reaction. (d) Reaction path curvature. (e) Rate constants obtained with TST (dash), CVT (dash−dot), CVT−ZCT (dash−dot−dot), and CVT−SCT (solid). (f) Kinetic isotope effects. See Figure 4 for symbols used for different isotope quantities.

at the saddle point is significantly smaller in the enzyme than in the gas phase; for hydrogen it equals $798i$ cm^{-1} as compared with $1365i$ cm^{-1} in the gas phase. However, the reaction path is much longer ($\sim$30 amu$^{1/2}\cdot$bohr) than that in the gas phase ($\sim$5 amu$^{1/2}\cdot$bohr); see Figure 5a. This is due to two factors. First, the proton moves a larger distance during the reaction in the enzyme because the proton starts farther from the acceptor due to the presence of a strong hydrogen bond with Glu 165 in EDT1 (see Figure 1); i.e., the proton, which is transferred from O_1 to O_2, is oriented away from O_2. Second, a larger number of atoms move during the reaction in the enzyme, and their displacements contribute to the length of the reaction path. For example, Lys 12, His 95, and Glu 165 and an active site water molecule (Solv 26) move significantly relative to the substrate during the reaction (Figure 5b,c). The displacements of these heavy atoms contribute substantially to the path length due to their heavy masses, as discussed already for the gas-phase reaction. The potential energy increase slowly as a function of the reaction coordinate far from the saddle point and becomes much more steep between (-2.5, $+2.5$). This trend correlates with the variation of the essential geometrical parameters along the reaction path; i.e., those related to the transferring proton itself and the donor and acceptor distances have their largest change in the same region (Figure 5b). Correspondingly, the reaction path curvature (Γ) peaks around $s \approx \pm 0.3$ (see inset in Figure 5d). There is an additional set of smaller peaks in Γ at $s \approx \pm 2.0$. These peaks are related to the motion of the environmental groups that are coupled to the substrate. In other

words, the initial stage of the reaction path involves mainly motions that reorganize the environment, including the donor−acceptor distance. This can be compared to the "solvation" coordinate in the electron-transfer reactions in the condensed phase,[64] or solvent motion in ion-pair dissociation[65] and isomerization reactions in solution. The effect of the secondary set of peaks in Γ on the rate constant is described below.

The CVT values of the rate constant are essentially identical to the TST results (with quantized vibrations) at all temperatures (Figure 5d); see also Table 2. This is due to the fact that the asymmetry of the potential along the reaction coordinate is small, as noted above (Figure 5a), so that the positions of the transition state in CVT and TST are essentially the same (see Table 2). The tunneling coefficient ($\kappa^{CVT-SCT}$) in the enzyme is much smaller than that in the gas phase. At the CVT−SCT level, $\kappa^{CVT-SCT}$ is around 1.66 at 300 K and 230 at 100 K. Correspondingly, the KIE values are smaller in the enzyme than those in the gas phase, as shown in Figure 5e and Table 2. The H/D KIE at 300 K is about 4.65 at the CVT−SCT level and 4.50 at the CVT level, compared to the value of 8.31 and 4.66 in the gas phase. The behavior of the Swain−Schaad exponent is similar to that in the gas phase, even though the tunneling contribution is much smaller in the enzyme; the TST value remains around 3.34 independent of temperature, while the CVT−SCT value is 3.13 at 300 K and decreases with temper-

(64) Marcus, R. A. *Annu. Rev. Phys. Chem.* **1964**, *15*, 155.
(65) Bolhuis, P. G.; Dellago, C.; Chandler, D. *Proc. Natl. Acad. Sci. U.S.A.* **2000**, *97*, 5877.

Table 2. Rate Constants, Kinetic Isotope Effects (KIE), and Tunneling Factors for the Intramolecular Proton-Transfer Reaction in TIM at 300 K Calculated with Two Different Models[a]

	classical TST	classical CVT	TST	CVT	CVT–ZCT	CVT–SCT
$V^{\ddagger}/\omega$	12.8/798 (9.7/795) [18.1/889]					
$s*^{\text{CVT}\,b}$	−0.03 (0.00)			−0.07(−0.07) [0.05]		
$\log(k_H)$	3.55 (6.09)	3.54 (6.09)	4.51 (7.33) [1.86]	4.49 (7.32) [1.77]	4.57 (7.40) [1.90]	4.71 (7.54) [2.10] {4.71}[c]
$\kappa_H^{\text{CVT}-\text{SCT}}$					1.23 (1.22) [1.36]	1.68 (1.64) [2.17] {1.68}[c]
KIE (H/D)	1.43 (1.43)	1.42 (1.43)	4.50 (4.56) [4.17]	4.31 (4.53) [3.78]	4.25 (4.46) [4.03]	4.65 (4.78) [5.16]
KIE (H/T)	1.68	1.67	8.56 [7.94]	8.21 [7.13]	8.35 [7.90]	9.57 [10.9]
α_{SS}	3.12	3.15	3.34 [3.22]	3.27 [3.10]	3.15 [3.07]	3.13 [3.21]
$\Delta E_a(H,T)$			1.12 [1.08]	1.01 [1.00]	1.11 [1.13]	1.28 [1.49]
A_H/A_T			1.31 [1.31]	1.33 [1.34]	1.31 [1.19]	1.12 [0.89]

[a] The values without parentheses were obtained with the large model including 445 movable atoms; those in parentheses or brackets were obtained with a smaller model including 106 movable atoms with the rest of the atoms fixed at the positions optimized for the saddle point and the reactant, respectively (see text). The definitions of other quantities are the same as in Table 1. [b] The optimized position of the transition state in CVT in amu$^{1/2}$·bohr. [c] The results were obtained by setting the reaction path curvature to zero beyond [−1.5, 1.5] amu$^{1/2}$·bohr.

ature to a value of 2.64 at 100 K. Due to the small tunneling contribution, the Arrhenius parameters at the CVT−SCT level are similar to the CVT results and close to the expected quasi-classical values (i.e., difference arises from zero-point energy). Thus, in the enzyme, even though the barrier is higher than that in the gas phase (12.8 vs 9.4 kcal/mol), the significantly broader barrier leads to a much smaller tunneling contribution; even at 100 K, $k^{\text{CVT}-\text{SCT}}$ is only 230 times k^{CVT}.

Despite the small tunneling contribution, the effect of reaction path curvature on tunneling is significant. The tunneling coefficient is smaller at the CVT−ZCT level relative to CVT−SCT by a factor of 1.36 at 300 K and 19.5 at 100 K. Calculations with the curvature components set to zero beyond (−1.5,+1.5) along the reaction path gave virtually identical CVT−SCT results. This indicates that only the path curvature close to the saddle point is important for tunneling. Such behavior is expected because the tunneling coefficient has an exponential distance dependence and the outer regions correspond to a larger tunneling distance.

Effect of Number of Movable Atoms. To determine the effect of limiting the size of the flexible region, we compare the reaction path and rate constants calculated in the enzyme with a model having 106 movable atoms, rather than 446 as in the treatment just described. Two small models were tested, one with the environment (the atoms not allowed to move) fixed at the coordinate set obtained from optimizing the large model with the substrate in the reactant geometry and the other from optimizing the large model with the substrate in the saddle point geometry. The RMS difference for the fixed atoms in the two limiting models is 0.03 Å (0.06 Å for atoms between 4 and 8 Å from the C_γ atom in the substrate). For the saddle-point-optimized configuration, the barrier height is, as expected, lower (9.7 vs 12.8 kcal/mol) and the exothermicity of the reaction is larger (−2.4 vs −0.5 kcal/mol), as compared with the large model. The barrier imaginary frequency (795i cm^{-1}) is quite similar to that in the large model (798i cm^{-1}). By contrast, when the environment is fixed at the reactant-optimized configuration, the barrier becomes significantly higher (18.1 vs 12.8 kcal/mol) and the reaction becomes slightly endothermic (2.3 kcal/mol) rather than nearly thermoneutral (−0.5 kcal/mol). The higher barrier is due to the fact that residues affected by the proton transfer are not allowed to move as freely (or not all) in the small model. For example, Glu 165 moves significantly in the large model so as to stabilize the negative charge developed on O^1 at the saddle point; the O^1···OE2 distance decreases from 3.46 Å in the reactant to 2.78 Å at the saddle point. In the small

model, however, Glu 165 cannot move as freely, and the O1···OE2 distance is reduced only to 3.30 Å at the saddle point. Also, the local geometry of the saddle point is altered; the proton−donor and proton−acceptor distances are 1.21 and 1.24 Å, respectively, in the large model and 1.27 and 1.19 Å, respectively, in the small model. As already pointed out, the transition-state configuration for the intramolecular proton transfer is not linear, although it is more linear near the saddle point than in the reactant configuration; see Figure 1 or Figure 3. The barrier frequency becomes substantially higher, 889i cm^{-1}, compared to the value of 798i cm^{-1} in the large model. Interestingly, the reaction path curvatures in the different models are rather similar, especially in the barrier region. Larger differences are observed in the regions close to the reactant or product.

Corresponding to the dependence of reaction path properties on the size and fixed coordinate geometry of the model, the calculated rate constants differ significantly. Compared to the results with the large model, the two smaller models give rate constants that are too small (reactant-optimized) and too large (saddle-point-optimized) by about 3 orders of magnitude, respectively, at the both the TST and CVT levels at 300 K (Figure 6c and Table 2). The difference in the TST rate constant corresponds to a *free energy barrier* difference of +3.9 (reactant-optimized) and −3.8 kcal/mol (saddle-point-optimized) compared to the large model. The difference in the *potential energy barrier* (including ZPE) for the reactant-optimized and the saddle-point-optimized model is +4.3 and −3.7 kcal/mol, respectively, compared to the large model. Therefore, the small models have a smaller entropic contribution to the free energy barrier than the large model; the difference is 1.5 cal/(mol·K) for the reactant-optimized and 0.3 cal/(mol·K) for the saddle-point-optimized small model, respectively. The absolute activation entropies can be evaluated from normal-mode calculations; they are −1.2, 0.3, and −0.9 cal/(mol·K) for the large model, reactant-optimized model, and saddle-point-optimized model, respectively. It is interesting to note that the reactant-optimized and the saddle-point-optimized small models have entropic contributions of different signs, with the overall effect small in all cases.

The effect of environmental geometry on the tunneling coefficients and isotope effects is less significant, especially at room temperature. With the saddle-point-optimized structures, the value of the tunneling factor, $\kappa^{\text{CVT}-\text{SCT}}$, is 1.64 at 300 K, which is close to the value of 1.68 from the large model. The H/D KIE at the CVT−SCT level is 4.78 at 300 K; the value
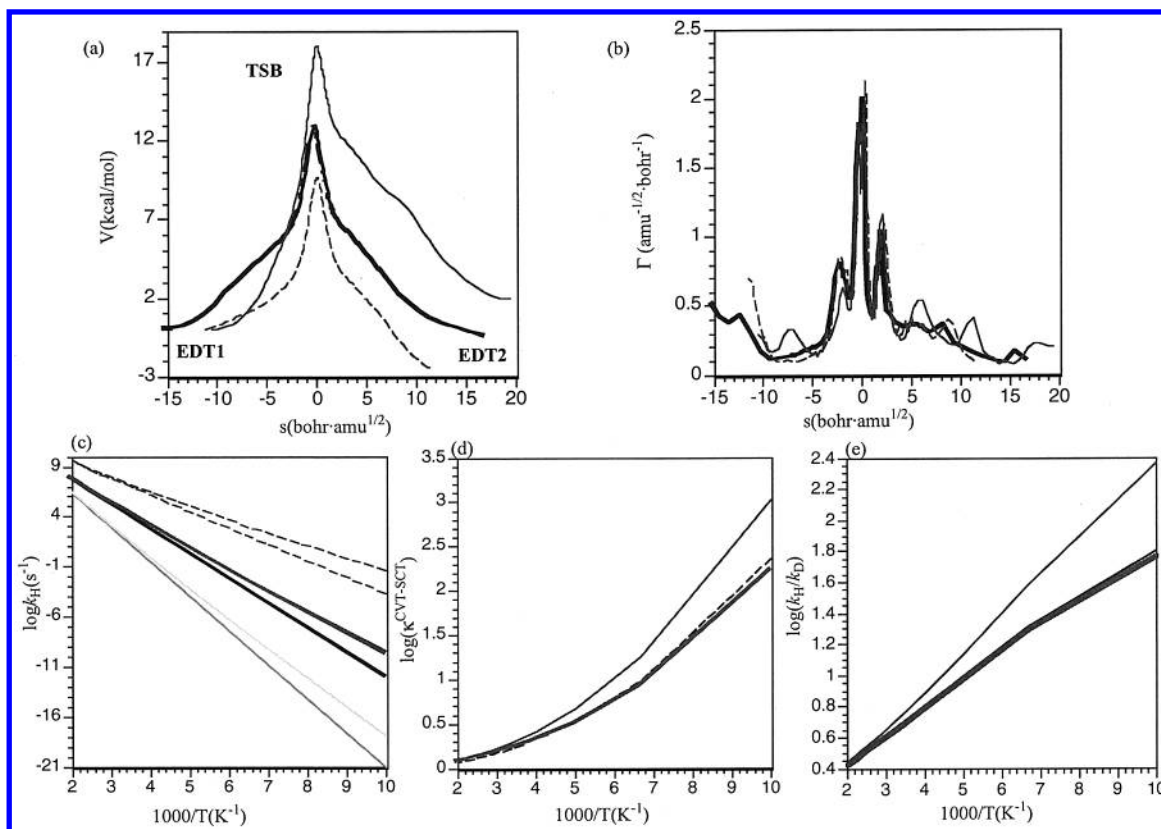
Figure 6. Comparison of reaction path properties obtained with the "large" (in bold, contains 445 movable atoms) and two "small" models (contain 106 movable atoms) for the intramolecular proton transfer in TIM. In one set (dash), the environment was fixed at the coordinates in the saddle point that was optimized with the large model; in the other (thin solid), the environment was fixed at those in the reactant optimized with the large model. (a) Minimum energy profile. (b) Reaction path curvature. (c) $\log(k_H^{CVT-SCT})$. (d) $\log(\kappa_H^{CVT-SCT})$. (e) Kinetic H/D effect.

from large model calculation is 4.65. Even at 100 K, the saddle-point-optimized model gives results similar to those obtained with the large model; i.e., the tunneling coefficient is 166 and the H/D KIE is 63, while the large model gives 230 and 58, respectively. The reactant-optimized small model gives results that are more different from the large model calculations; i.e., the tunneling coefficient is 2.17 and 1749 at 300 K and 100 K, respectively; the H/D KIE at the CVT−SCT level is 5.16 and 191 at the two temperatures (Figure 6d,e). One reason for the small dependence of $\kappa^{CVT-SCT}$ and KIE at room temperature on the size of the model, especially when the environment in the saddle-point region is allowed to relax, is that the barrier imaginary frequency and reaction path curvatures are not altered very much. As discussed in section IV, this is due to the fact that generalized normal modes that are important in calculating these quantities are fairly *localized*. The present results and their interpretation justify the use of the smaller model in investigating the qualitative effect of the geometry of the environmental on tunneling at room temperature. Since the isotope effect does not involve the classical barrier height, the dependence of KIE on the size of the system arises mainly from the effect on the bound vibrations, which is relatively small. By contrast, the variation in the tunneling depends on both the barrier and the bound generalized normal modes and so is more sensitive.

Effect of Geometry on Reaction Rate and Tunneling. As stated in Computational Methods (section II.2), 10 configurations were selected from a molecular dynamics trajectory at 10 ps intervals with the entire stochastic boundary system and the reactant (EDT1) in the binding site. Using these as starting

structures, reaction path optimizations, normal-mode analyses, and rate constant calculations were carried out with the small model; the environment configuration was fixed to that in the reactant EDT1. As shown in Figure 7 and Table 3, the reaction paths depend significantly on the environmental configuration. The barrier height ranges from 15.4 to 21.0 kcal/mol, with an average value of 19.1 kcal/mol and a standard deviation of 1.8 kcal/mol. The exothermicity of the reaction shows larger variations from −2.2 to 11.6 kcal/mol, with an average value of 6.8 kcal/mol and a standard deviation of 4.6 kcal/mol. The barrier imaginary frequencies vary from $855i$ to $1171i$ cm^{-1}. The lengths of the reaction path also differ significantly, ranging from 15.7 to 36.0 amu$^{1/2}$·bohr. As shown in Figure A1 in the Supporting Information, active site residues undergo substantial structural fluctuations, especially Lys 12, His 95, and Glu 165. In the two cases with the largest exothermicities (sets 5 and 6 in Table 3), the orientation of Glu 165 is such that the substrate proton has to move farther from the donor to form a hydrogen bond (Figure 7b); this also causes the reaction path to be considerably longer (Figure 7a) than in the other sets considered. The Hϵ proton in His 95 is closer to the transferred proton at the saddle point in set 1 (1.66 Å) than in set 6 (1.81 Å), and consequently the former has a higher barrier due to the unfavorable electrostatic interaction with the NH of His 95.

The rate constants vary by several orders of magnitude for systems with different environmental configurations, in correspondence with the variation in the barrier heights. The tunneling factors also show a rather significant dependence on the environmental configuration at the CVT−SCT level; they
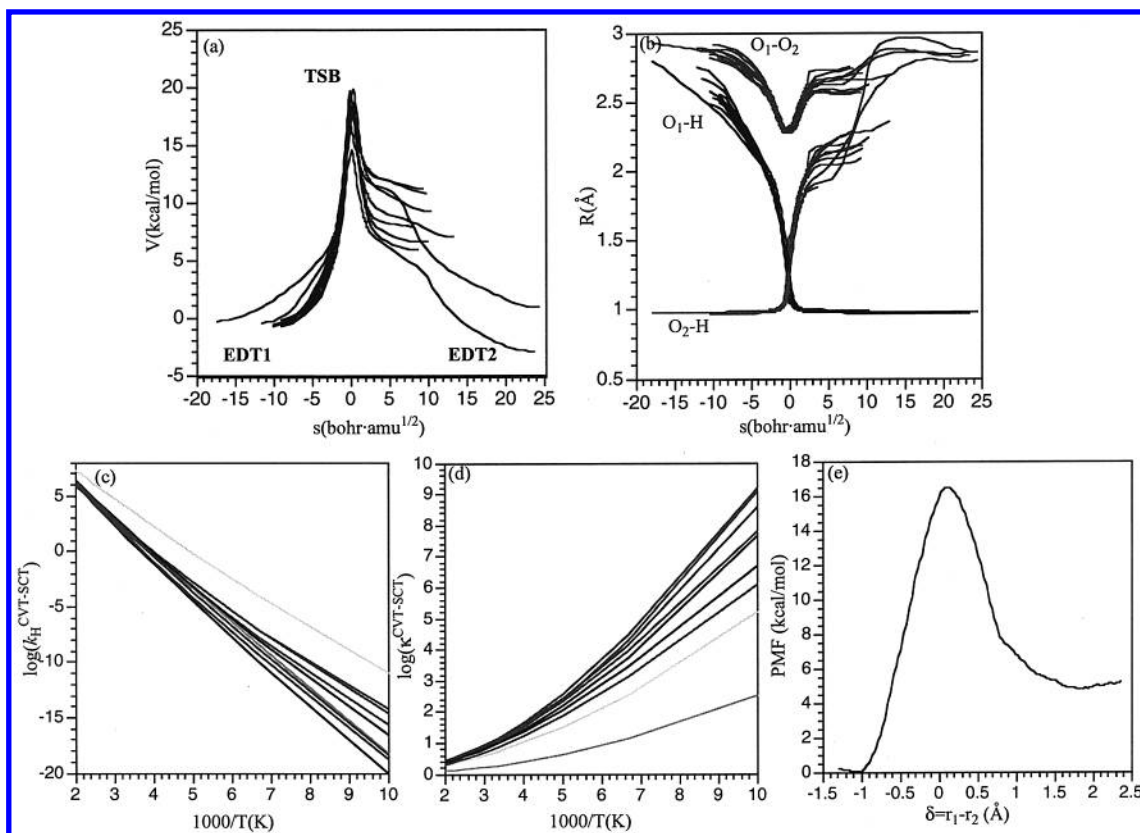
Figure 7. Reaction path and kinetic properties for the intramolecular proton-transfer reactions in TIM obtained with the "small model" as a function of temperature starting from 10 minimized configurations along a 100 ps trajectory. (a) Minimum energy profile (EDT1 was taken to be the zero of energy); as discussed in the text, the fluctuations of the barrier heights and exothermicities are exaggerated due to the limited number of atoms allowed to move in the reaction path calculations; see Table 3 for unconstrained results. (b) Important geometric parameters. (c) $\log(k_H^{CVT-SCT})$. (d) SCT correction factor for the CVT rate constant, $\kappa_H^{CVT-SCT}$. (e) Potential of mean force using the antisymmetric stretch involving the donor, the proton, and the acceptor as the reaction coordinate.

Table 3. Rate Constants and Tunneling Factors for the Intramolecular Proton-Transfer Reaction in TIM for Different Reactant Configurations[a]

set	ω (cm^{-1})	$V^{\ddagger}$ (kcal/mol)	E_x (kcal/mol)	s_*^{CVT}	$\log(k^{CVT-SCT})$	$\kappa_H^{CVT-ZCT}$	$\kappa_H^{CVT-SCT}$
1	1064	21.0 (16.5)	11.6 (4.3)	0.11	1.14	2.00	9.72
2	1155	19.0 (16.4)	6.8 (1.5)	0.06	1.89	2.41	11.0
3	1171	19.8 (14.8)	8.4 (2.3)	0.06	1.57	2.72	14.0
4	1084	18.5 (13.5)	6.2 (0.4)	0.01	1.89	2.51	14.5
5	855	17.4 (11.7)	1.3 (−3.3)	0.07	1.95	1.33	1.92
6	964	15.4 (11.6)	−2.3 (−5.5)	0.02	3.88	1.60	5.52
7	1050	19.7 (16.3)	7.5 (3.4)	0.01	1.95	2.01	10.3
8	1040	19.9 (16.1)	11.4 (6.5)	0.06	1.71	2.11	7.55
9	1083	20.9 (17.2)	9.9 (5.8)	0.02	1.28	2.37	13.2
avg	1052	19.1 (14.7)	6.8 (1.6)	0.05	1.92	2.11	9.75
std	96	1.8 (2.1)	4.6 (3.8)	0.03	0.79	0.44	4.16
PMF[b]	1251	16.5	4.8				

[a] The configurations were collected from a 100 ps (excluding equilibration) trajectory at 300 K. The definitions of quantities are the same as in Tables 1 and 2; E_x is the energy of reaction. The values without parentheses were obtained with the small model that allows 106 atoms to move in the reaction path and rate constant calculations; those in parentheses were obtained with all atoms allowed to move in the reaction path calculations. [b] Potential of mean force obtained using asymmetric stretch involving the donor, acceptor, and the transferred proton as the reaction coordinate. All atoms in the model (2340) were allowed to move.

range from 1.92 to 14.5 at 300 K. At the CVT−ZCT level, by contrast, the tunneling coefficient is around 2 for all sets of models at 300 K. This highlights once more the importance of reaction path curvature in determining the magnitude of proton tunneling. A more detailed analysis of the system properties that influence tunneling is given in section IV.

We note that since the intramolecular proton transfer, perhaps surprisingly, requires substantial structural reorganization of the active site, the constraint on the geometry in the small system has an important effect on the quantitative barrier height and exothermicity of the reaction. For instance (see Table 3), the average barrier is too high by 4.4 kcal/mol, and the reaction is more endothermic by 5.2 kcal/mol, compared to calculations without geometry constraints. The magnitudes of the variation in the barrier heights are similar with or without the geometry constraint. The average of the reaction path results is in a relatively good agreement with that from the potential of mean force calculations, which gives a barrier of 16.5 kcal/mol and an endothermicity of 4.8 kcal/mol. These are slightly larger than the averaged results from a limited number of reaction path results without the geometrical constraints, which are 14.7 and 1.6 kcal/mol, respectively. The barrier frequency of the potential of mean force is $1251i$ cm^{-1}, which is reasonably close to the average barrier frequency of $1052i$ cm^{-1} from minimizations.

III.1c. Rate Constants in Water. For the intramolecular proton transfer in a water sphere, the barrier height obtained with the large model is 6.3 kcal/mol, smaller than that in the gas phase (9.5 kcal/mol) or the enzyme (12.8 kcal/mol); the solvent water molecules stabilize the transition state over the reactant (and product) structures because the former has a larger dipole moment (2.49 and 1.99 D, respectively). The phosphate group in the substrate, which was included in the calculations, is stabilized by the solvent. Due to the presence of the phosphate

Table 4. Rate Constants and Tunneling Factors for the Intramolecular Proton-Transfer Reaction in a Water Sphere at 300 K Calculated with Two Different Models[a]

	TST	CVT	CVT–ZCT	CVT–SCT
$V^{\ddagger}/\omega$	6.3/591 (11.2/671)			
s_*^{CVT}		−0.04 (0.20)		
$\log(k_H)$	9.08 (6.58)	9.08 (6.35)	9.10 (6.48)	9.17 (6.61)
$\kappa_H^{CVT-SCT}$			1.05 (1.34)	1.23 (1.81)

[a] The values without parentheses were obtained with the large model including 308 movable atoms; those in parentheses were obtained with a smaller model including 65 movable atoms (see text). The definitions of other quantities are the same as in Table 1.

group and the anisotropic solvent environment, the reaction profile is no longer symmetric, in contrast to the gas-phase result without a phosphate group. The imaginary frequency associated with the barrier is significantly smaller in water; it is $591i$ cm^{-1} compared to $1365i$ cm^{-1} in the gas phase, and $798i$ cm^{-1} in the large enzyme model. The essential geometrical parameters (Figures 5b and 8b) and reaction path curvatures along the reaction coordinate (Figures 5c and 8c) are similar to those found in the enzyme. The tunneling coefficient, $\kappa^{CVT-SCT} = 1.23$ at 300 K, is slightly smaller than that in the enzyme (1.68) with CVT–SCT (see Table 4).

The size dependence is quite significant in solution (see Figure 9). The barrier height is 11.2 and 6.3 kcal/mol with the small (65 atoms; 14 solute atoms with 17 water molecules) and large (308 atoms which includes 98 water molecules) number of movable atoms, respectively. The reaction is *exothermic* by −1.5 kcal/mol with the large model and *endothermic* by 5.7 kcal/mol with the small model. The barrier frequency is 591 and $671i$ cm^{-1} for the large and small models, respectively. The reaction rate constants computed using the two models differ by a factor of 316 at the TST level and 536 at the CVT level at 300 K. The difference in TST rate constants corresponds to a difference of 3.5 kcal/mol in the activation free energy barrier, which is smaller than the difference in the potential energy barrier, 4.6 kcal/mol (including ZPE). This suggests that the activation entropy is less negative in the small model by about 3.7 cal/(mol·K); the values from normal-mode calculations are −0.3 and −4.0 cal/(mol·K) for the small and large model, respectively. This is in qualitative agreement with the consideration that a larger number of water molecules are involved in the proton transfer in the large model, and that this results in a larger entropic penalty. The tunneling factor is slightly larger with the small model; i.e., it is 1.81 at 300 K compared to the value of 1.23 obtained with the large model. This results in a smaller difference (by a factor of 360) between the CVT–SCT rate constants calculated with the two models at room temperature.

The reaction path properties and rate constants in solution vary significantly as a function of the environmental configurations (see Figure 10 and Table 5), even more so than in the enzyme. As shown in Figure A2 of the Supporting Information, the instantaneous solvent configuration around the reactant state of the solute determines the character (energetics, barrier frequencies, etc.) of the reaction. The barrier height ranges from 3.9 to 12.5 kcal/mol, and the heat of reaction varies from being exothermic by 13.4 kcal/mol to being endothermic by 2.8 kcal/mol. The averaged barrier and exothermicity are 7.5 and 6.1 kcal/mol, respectively. These are close to the values from PMF calculations, which are 10.0 and 3.6 kcal/mol, respectively. The

barrier frequency varies between 439 and $878i$ cm^{-1}, with an average value of $622i$ cm^{-1}; the latter is close to the PMF result of $769i$ cm^{-1}. At 300 K, $\log(k_H^{CVT-SCT})$ varies from 5.8 to 11.6, compared to the extreme values of 1.14 and 3.88 in the enzyme, as expected from the higher barrier due to the presence of His 95 in the latter. The correction to the TST rate constant resulting from the use of CVT, both with quantized vibrations, deviates more from unity than that in the enzyme; the average factor (averaged over all the configurations) at 300 K is 0.72 in solution and 0.95 in TIM. This suggests that the classical transmission coefficient is closer to unity in this reaction than for the intermolecular step, although only part of the recrossing effect is taken into account by CVT. As shown in Figure A3 of the Supporting Information, the deviation of the variational transition state from the saddle point is caused primarily by the variation of the zero-point energy (ZPE) along the reaction path; variation in the vibrational entropy makes a relatively small contribution in the present case. The tunneling factors in solution are consistently smaller than those in the enzyme. They are less than 2 at 300 K; even at 100 K, the largest tunneling factor in solution is 10^4, in contrast to the value of $10^{9.2}$ observed in the enzyme.

III.2. Intermolecular Proton Transfer. For the intermolecular proton-transfer reaction, from DHAP to EDT1 (see Scheme 1), the reaction is highly endothermic (>20 kcal/mol) in the gas phase such that the enediolate species does not exist as a stable minimum on the potential energy surface. In what follows, we consider only the reaction in the enzyme, where the enediolate species is stabilized compared to DHAP. This is due mainly to the charged Lys 12 at the active site, although some other groups and solvents contribute as well. EDT1 is about 11.2 kcal/mol higher than DHAP at the AM1-SRP/CHARMM level, and only 7.4 kcal/mol at the B3LYP/6-31+G-(d,p)/CHARMM level. Therefore, the forward barrier is significantly overestimated at the AM1-SRP/CHARMM level. However, as shown in previous work,[24] the major error in AM1-SRP/CHARMM arises for DHAP. Therefore, the reverse barrier (EDT1 → TS1) is better reproduced; it is 6.1 kcal/mol at the AM1-SRP/CHARMM level in comparison to the value of 4.4 kcal/mol at the B3LYP/6-31+G(d,p)/CHARMM level. Therefore, we report only the reverse rate constant in the present work. Since tunneling is determined mainly by the potential energy surfaces close to the saddle point in the VTST framework (in contrast to certain other semiclassical models[13]), the fact that the potential energy surface drops too much after the barrier is crossed has a small effect on the results. We discuss here the results with the large model in which the enzyme configuration is close to the X-ray structure; the effect of the size and active site configuration, which has a trend similar to that of the intramolecular proton transfer in TIM, is discussed in the Supporting Information.

As shown in Figure 11, the reaction path properties for the intermolecular proton transfer are rather similar to those for the intramolecular reaction in the enzyme, although the potential is very asymmetric far from the saddle point. The three distances that are involved directly (D−H, A−H, and D···A) only start to change rapidly close to the saddle point, in the range −1.0 to 2.0 amu$^{1/2}$·bohr. Both His 95 and Lys 12 are perturbed substantially by the reaction, as indicated in Figure 11b; that is, the O1−HNζ of Lys 12 and O2−Hε of His 95 increase by
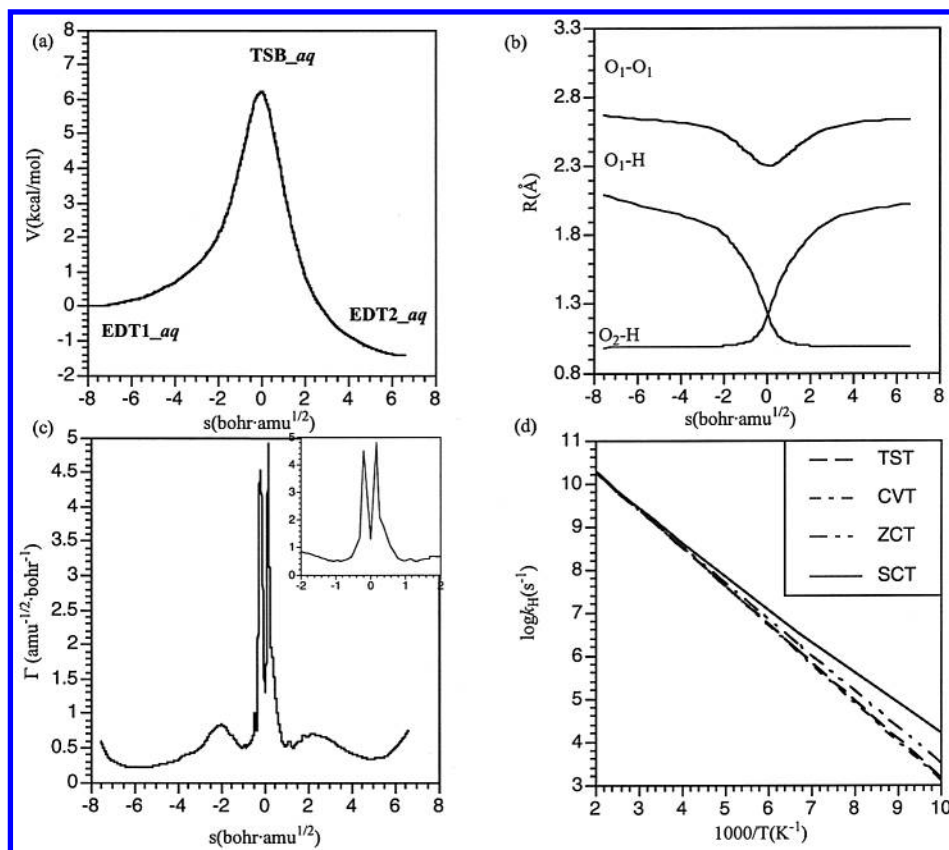
Figure 8. Reaction path properties along reaction coordinate s and rate constants for the intramolecular proton transfer in a water sphere with the "large" model as a function of temperature. (a) Minimum energy profile. (b) Important geometric parameters: donor−proton (O_2···H), acceptor−proton (O_1···H), and donor−acceptor (O_1···O_2) distances; see Figure 2 for atomic labels. (c) Reaction path curvature. (d) Rate constants obtained with TST (dash), CVT (dash−dot), CVT−ZCT (dash−dot−dot), and CVT−SCT (solid).
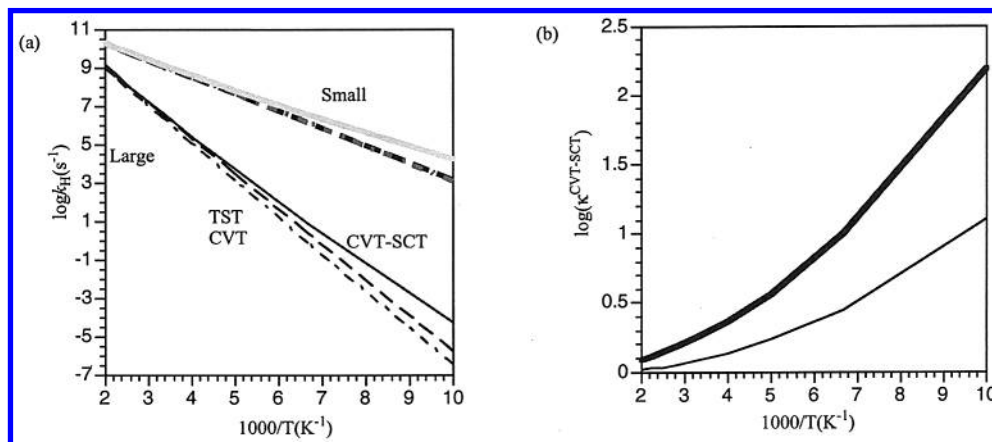

Figure 9. Comparison of kinetics obtained with the "large" (in thin lines, 308 movable atoms) and "small" (in bold, 65 movable atoms) models for the intramolecular proton transfer in water as a function of temperature. (a) Rate constants at different levels: TST (dash), CVT (dash−dot), CVT−ZCT (dash−dot−dot), and CVT−SCT (solid). (b) SCT correction factor $\kappa_H^{CVT-SCT}$.

nearly 0.2 Å during the critical part of the reaction. The reaction path curvature shows two sets of peak positions, one set with large curvature (>2.0 amu$^{-1/2}$·bohr^{-1}) at $s \approx \pm 0.5$ and another set with smaller peak values ($\sim$0.7 amu$^{-1/2}$·bohr^{-1}) at larger s values, -3.0 and $+2.0$ amu$^{1/2}$·bohr; this is similar to Figure 5 for the intramolecular reaction.

The CVT rate constants differ notably from the TST values, as shown in Figure 11 and Table 6. The s value for the free energy maximum at 300 K is $\sim$0.3 amu$^{1/2}$·bohr. This effect is not observed in pure classical CVT calculations (Table 6), which suggests that the variation of the zero-point energy along the

IRP is primarily responsible for the deviation of the transition state from the saddle point in this case. The reduction of the CVT rate constant relative to the TST value corresponds to a transmission coefficient of 0.69 at 300 K; this is qualitatively similar to the result ($\sim$0.43) from activated dynamics calculations based on an EVB potential. The value from the current calculation is larger partly because barrier recrossing induced by the environment (atoms other than the substrate and Glu 165) is already partially accounted for in the TST result by including the environment in the normal-mode analysis (i.e., the definition of the dividing surface). The CVT calculation reduces the
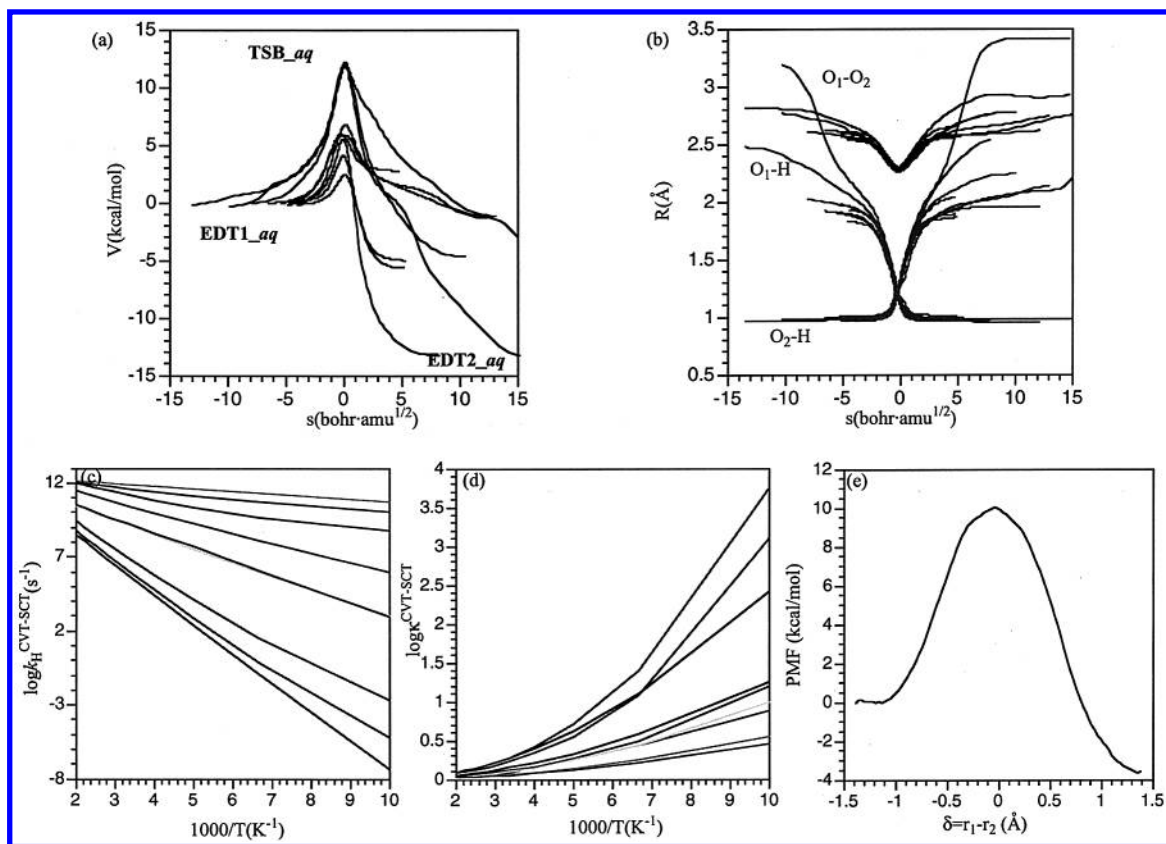
Figure 10. Reaction path properties and rate constants for the intramolecular proton-transfer reaction in solution as a function of temperature obtained with the "small" model starting from different configurations along a 100 ps trajectory. (a) Minimum energy profile. (b) Important geometric parameters. (c) log($k_H^{CVT-SCT}$). (d) SCT correction factor $\kappa_H^{CVT-SCT}$. (e) Potential of mean force using the antisymmetric stretch involving the donor, the proton, and the acceptor as the reaction coordinate.

Table 5. Rate Constants and Tunneling Factors for the Intramolecular Proton-Transfer Reaction in Solution Starting from Different Reactant Configurations[a]

set	ω (cm^{-1})	$V^{\ddagger}$ (kcal/mol)	E_x (kcal/mol)	s_*^{CVT}	log($k^{CVT-SCT}$)	$\kappa_H^{CVT-ZCT}$	$\kappa_H^{CVT-SCT}$
1	625	3.9	−5.8	−0.16	11.62	1.26	1.42
2	729	12.5	−4.4	−0.14	6.07	1.30	1.71
3	445	5.9	−13.2	0.61	10.44	1.15	1.31
4	878	12.2	−13.4	0.14	6.96	1.27	1.88
5	439	5.9	2.8	0.34	9.25	1.10	1.13
6	602	11.7	−1.1	0.10	5.75	1.11	1.22
7	486	2.6	−4.8	−0.23	11.89	1.11	1.15
8	586	6.9	−1.2	0.19	9.15	1.12	1.26
9	806	5.6	−13.3	−0.11	11.19	1.41	1.87
avg	622	7.5	−6.1	0.08	9.15	1.20	1.44
std	148	3.7	6.0	0.28	2.38	0.11	0.30
PMF[b]	769	10.0	3.6				

[a] The configurations were collected from a 100 ps (excluding equilibration) trajectory at 300 K. The definitions of quantities are the same as in Table 1. [b] Potential of mean force obtained using asymmetric stretch involving the donor, acceptor, and the transferred proton. All atoms in the model (2340) were allowed to move.

recrossing effect caused by the nonlinear coupling between the proton-transfer coordinate and the system (substrate and Glu 165) degrees of freedom.[66] The tunneling factor is similar to that found in the intramolecular proton transfer in TIM, which is 1.22 and 1.45 at the CVT−ZCT and CVT−SCT levels, respectively, at 300 K. The isotope effects are *overestimated* at the TST and CVT levels compared to CVT−SCT results, which is in accord with the previous study of enolase.[19] The H/D

(66) (a) Schenter, G. K.; McRae, R. P.; Garrett, B. C. *J. Chem. Phys.* **1992**, *97*, 9116. (b) McRae, R. P.; Schenter, G. K.; Garrett, B. C. *J. Chem. Soc., Faraday Trans.* **1997**, *93*, 997.

isotope effect at 300 K is 5.25, 3.60, and 3.48 at the TST, CVT, and CVT−SCT levels, respectively; the H/T isotope effect is 10.9, 7.46 and 6.86, respectively. The Swain−Schaad exponent is 3.28 at the CVT level and 2.84 with CVT−SCT, and there is very little temperature dependence at both levels.

Since the Cα atom in DHAP has two hydrogen atoms, there is the possibility of a significant secondary isotope effect. The H/T secondary isotope effect at 300 K is calculated to be 1.15 with the CVT−SCT method, slightly larger than the value of 1.05 at the CVT level and qualitatively different from the TST value of 0.91. The secondary Swain−Schaad exponent (α_{SS}^S) at the TST level is 4.15, and it decreases to 0.82 at the CVT level. The tunneling effect increases α_{SS}^S to 1.79 at the CVT−SCT level. To compare the quantities with those measured experimentally, we have to convert the isotope effects to the direction DHAP → EDT1 based on detailed balance. Numerically this requires the equilibrium isotope effects, which are readily calculated using the vibrational frequencies and energies for DHAP and EDT1; the secondary H/T equilibrium effect is calculated to be 1.14, which is close to the experimental value of 1.12.[9] With this conversion, the H/T secondary isotope effect for the forward reaction at the CVT−SCT level is 1.31, and the Swain−Schaad exponent is 2.44. The former is in good agreement with the value of 1.27 from the experimental estimate of Alston and co-workers,[9] while the calculated Swain−Schaad exponent (2.44) is significantly smaller than that measured experimentally, which is 4.4 ± 1.3. It should be noted that the α_{SS}^S is particularly sensitive to the exact values of the H/T and D/T isotope effects when the isotope effects are small; e.g.,
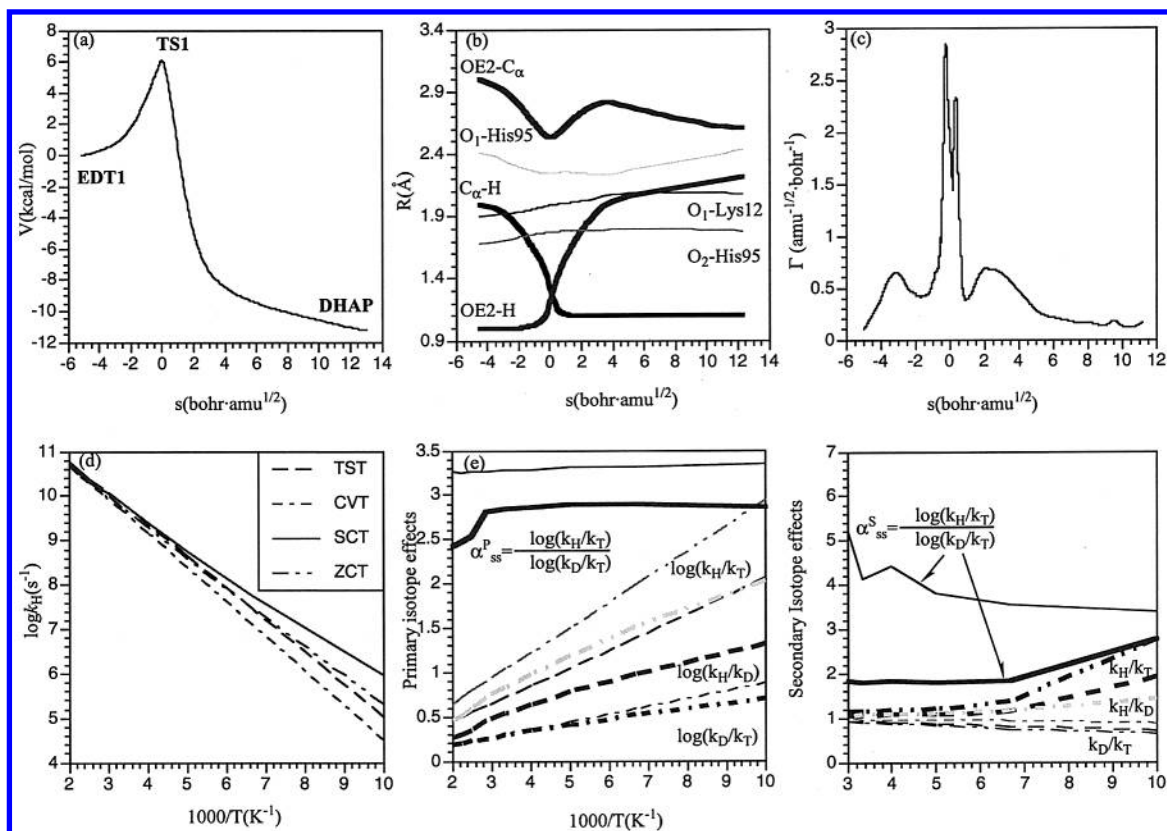
Figure 11. Reaction path properties along reaction coordinate s and rate constants for the intermolecular proton transfer in TIM with the "large" model as a function of temperature. (a) Minimum energy profile. (b) Important geometric parameters: donor−proton ($C\alpha\cdots H$), acceptor−proton ($OE2\cdots H$), and donor−acceptor ($C\alpha\cdots OE2$) distances; see Figure 1 for atomic labels. (c) Reaction path curvature. (d) Rate constants obtained with TST (dash), CVT (dash−dot), CVT−ZCT (dash−dot−dot), and CVT−SCT (solid). (e) Primary kinetic isotope effects. (f) Secondary kinetic isotope effects. See Figure 4 for symbols used for isotope effects. Note that no logarithm was taken for the secondary kinetic isotope effects for clarity.

Table 6. Rate Constants, Kinetic Isotope Effects (KIE), and Tunneling Factors for the Intermolecular Proton-Transfer Reactions in TIM at 300 K with the Large Models[a]

	TST	CVT	CVT–ZCT	CVT–SCT
$V^{\ddagger}/\omega$	6.1/925			
s_{*}^{CVT}		−0.31		
$\log(k_H)$	9.74	9.5	9.67	9.74
$\kappa_{H}^{CVT-SCT}$			1.22	1.45
KIE (H/D)	5.25	3.60	3.65	3.48
KIE (H/T)	10.90	7.46	7.35	6.86
α_{SS}^{P} [b]	3.28	2.76	2.85	2.84
$\Delta E_a(H,T)$	1.30	1.05	1.02	0.95
A_H/A_T	1.23	1.29	1.32	1.40
secondary KIE (H/D)	0.93	0.99	1.05	1.06
secondary KIE (H/T)	0.91	1.05	1.09	1.15
α_{SS}^{S} [b]	4.15	0.82	2.17	1.79

[a] The definitions for other quantities are the same as in Table 1. [b] The quantity α_{SS}^{P} is the primary Swain−Schaad exponent, and α_{SS}^{S} is the secondary Swain−Schaad exponent.

assuming that H/T is 1.31, the calculated value, D/T would have to be 1.063, versus the calculated value of 1.12, for α_{SS}^{S} to equal 4.4. It was argued in ref 9 that such a value for α_{SS}^{S} is larger than the classical limit of 3.3 and therefore suggests tunneling. However, as discussed in section IV, unlike the primary isotope effect, there is no clear "classical limit" for the secondary Swain−Schaad exponent. Furthermore, from the calculations there is no simple correlation between the value of α_{SS}^{S} and the magnitude of tunneling. No primary isotope effects were measured in ref 9.

The fact that the secondary H/T *kinetic* isotope effect (1.31) is larger than the corresponding secondary *equilibrium* isotope effect (1.14) suggests that the secondary hydrogen plays an important role in determining the structure and vibrational frequencies of the transition state ("coupled motion"), which in turn influence the magnitude of tunneling at the primary position. Moreover, the calculations show that the secondary KIE is larger at the CVT level (1.20) but smaller at the TST level (0.93) than the equilibrium isotope effect (1.14), indicating that tunneling is not necessarily the dominant factor. It is interesting to note that the trend that secondary kinetic isotope effect is larger than the corresponding equilibrium isotope effect seems to be a general trend in enzyme-catalyzed enolization, in contrast to the uncatalyzed reactions in solution.[9] Since the enolization in the enzyme tends to be less endothermic (e.g., due to the stabilization of charge formation by charged residues[67]), the transition state is expected to be "earlier", which would result in a smaller secondary KIE according to TST. The observation of a larger KIE in both experiments[9] and calculations suggests that variation in tunneling and the structure of the transition state upon secondary isotopic substitution is more significant in the enzyme than in solution, presumably because the transition state in solution is sufficiently "late", and that the coupling between the primary and secondary hydrogen atoms is small.

Effect of Donor−Acceptor Stretch. In both the intramolecular and intermolecular proton-transfer reactions, it is seen

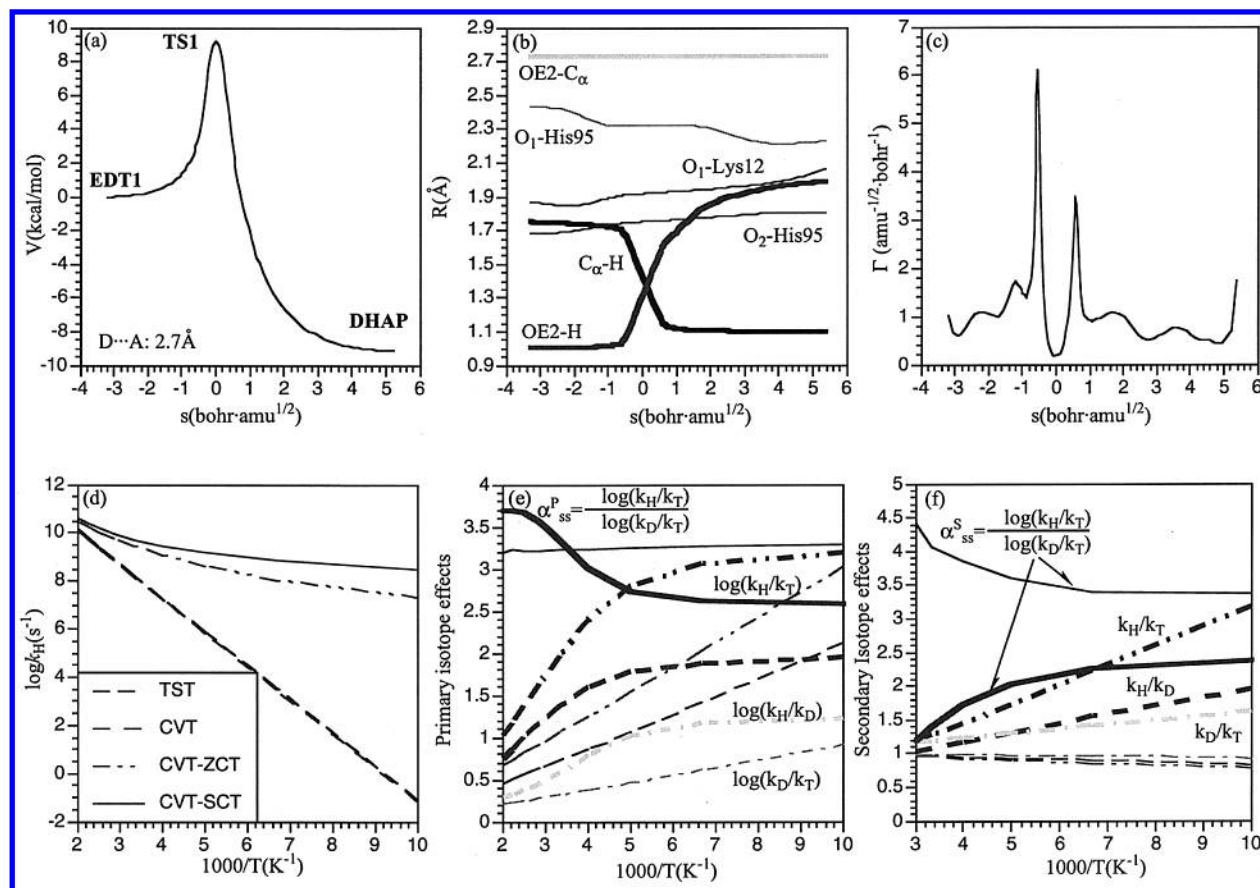(67) Bernasconi, C. F. *Acc. Chem. Res.* **1987**, *20*, 301.

Figure 12. Reaction path properties along reaction coordinate *s* and rate constants for the intermolecular proton transfer in TIM as a function of temperature with the distance between the proton donor (OE2 in Glu165) and acceptor (C3 in substrate) fixed at 2.7 Å. (a) Minimum energy profile. (b) Important geometric parameters: donor−proton (Cα···H), acceptor−proton (OE2···H), and donor−acceptor (Cα···OE2) distances; see Figure 1 for atomic labels. (c) Reaction path curvature. (d) Rate constants obtained with TST (dash), CVT (dash−dot), CVT−ZCT (dash−dot−dot), and CVT−SCT (solid). (e) Primary kinetic isotope effects. (f) Secondary kinetic isotope effects. See Figure 4 for symbols used for isotope effects. Note that no logarithm was taken for the secondary kinetic isotope effects for clarity.

that the donor−acceptor distance varies significantly along the reaction path. It is of interest, therefore, to determine how proton tunneling and the isotope effects are affected if no such donor−acceptor vibration is allowed. The result is clearly relevant to the question of whether there are specific vibrational motions (dynamics) that significantly influence the proton transfer/ tunneling (also see section IV). The donor−acceptor distance was fixed at 3.0 (equilibrium value in EDT1), 2.7, and 2.6 Å, and rate constants and secondary isotope effects were calculated; for the intermediate case of 2.7 Å, the primary isotope effect was also computed. The small model was used in the calculations.

The results for the intermediate case of 2.7 Å are shown in Figure 12. The IRP becomes shorter (∼9 vs ∼18 amu$^{1/2}$·bohr in the unconstrained case) when the donor and acceptor atoms are fixed. Both the donor−proton and the acceptor−proton distances start to vary rapidly closer to the saddle point than in the unconstrained reaction; this causes two peaks in the reaction path curvature profile. With the donor−acceptor fixed at a larger distance of 3.0 Å, the energy rises rapidly near the top of the barrier and makes both the barrier height and the barrier frequency larger than in the unconstrained case. The barriers are 24.5, 9.2, and 5.8 kcal/mol for the fixed donor−acceptor distances of 3.0 and 2.7 Å and the unconstrained case, respectively; the distance at the top of the barrier is 2.54 Å in the latter (see Figure 1; note that the donor−proton−acceptor

angle is 170.9°). The corresponding barrier frequencies are 2073*i*, 1778*i*, and 979*i* cm^{-1}, respectively. When the donor−acceptor distance is fixed at the short value of 2.6 Å, which is close to the unconstrained value, the barrier and barrier frequency are lower; they are 3.9 kcal/mol and 1361*i* cm^{-1}, respectively. We note that the unconstrained case has a larger barrier because there is an energetical cost in bringing the donor−acceptor to 2.54 Å; the proton-transfer barrier would be lower than 3.9 kcal/mol and the barrier frequency would be close to 979*i* cm^{-1} if the donor−acceptor distance were fixed at 2.54 Å.

In accord with the higher barrier frequency and barrier height for the larger distance, tunneling coefficients are larger compared to the case in which the relative donor−acceptor motion is allowed (see Table 7). For example, the value of $\kappa^{\text{CVT−SCT}}$ at 300 K is 3.0×10^4 and 36.5 with the donor−acceptor distance fixed at 3.0 and 2.7 Å, respectively; the value is 1.51 in the unconstrained case. Interestingly, the tunneling coefficient is very large even at the CVT−ZCT level; it is 4.9×10^3 and 18.5 at 300 K for the case of 3.0 and 2.7 Å, respectively. This suggests that the reaction path curvature is less important in this case, as compared to the width of the barrier (i.e., the barrier frequency). Tunneling has a large impact on the kinetic isotope effects and the Swain−Schaad exponents. For the intermediate case of 2.7 Å, the primary H/D isotope effect at 300 K is 6.59 and 24.5 at the CVT and CVT−SCT levels, respectively. The

Table 7. Rate Constants, Kinetic Isotope Effects (KIE), and Tunneling Factors for the Intermolecular Proton-Transfer Reactions in TIM at 300 K with the Proton Donor and Acceptor Atoms Fixed

	TST	CVT	CVT–ZCT	CVT–SCT
$V^\ddagger/\omega$	24.5/2073 (9.2/1778) [3.9/1361]			
s_*^{CVT}		−0.01 (−0.03) [+0.00]		
$\log(k_H)$	−2.45 (8.22) [11.9]	−2.45 (8.17) [11.9]	1.25 (9.44) [12.1]	2.03 (9.73) [12.2]
$\kappa_H^{CVT-SCT}$			4.9×10^3 (18.5) [1.88]	3.0×10^4 (36.5) [2.05]
KIE (H/D)	(5.42)	(6.59)	(18.8)	(24.5)
KIE (H/T)	(11.5)	(14.8)	(75.8)	(95.9)
α_{SS}^P	(3.24)	(3.34)	(3.10)	(3.34)
$\Delta E_a(H,T)$	(1.32)	(1.41)	(3.12)	(3.11)
A_H/A_T	(1.25)	(1.39)	(0.40)	(0.51)
secondary KIE (H/D)	0.97 (0.97) [0.95]	0.98 (0.97) [0.95]	1.14 (1.08) [1.05]	1.19 (1.07) [1.00]
secondary KIE (H/T)	0.96 (0.96)[0.94]	0.97 (0.95) [0.94]	1.20 (1.12) [1.10]	1.33 (1.28) [1.05]
α_{SS}^S	3.04 (4.07) [4.28]	2.78 (3.27) [4.28]	3.87 (2.89) [1.82]	2.57 (1.40) [1.00]

[a] The values were obtained with the small model including 106 movable atoms; the positions of the proton donor (OE2 in Glu 165) and acceptor (C3 in DHAP) were fixed at 3.0, 2.7, and 2.6 for the numbers without parentheses, in parentheses, and in brackets, respectively. The definitions for the quantities are the same as in Table 6.

primary Swain−Schaad exponent (α_{SS}^S) is 3.3 at the CVT level and depends little on temperature. At the CVT−SCT level, by contrast, α_{SS}^S has a significant temperature dependence; it is about 3.7 at 500 K and 2.6 at 100 K. The value is not much larger than the "classical limit" despite the large magnitude of tunneling (see Discussion, section IV). The Arrhenius parameters are also significantly influenced by tunneling. The A_H/A_T value is 1.25 and 0.51 at the TST and CVT−SCT levels, respectively; the quantity $E_a(T) - E_a(H)$ has a value of 1.32 and 3.11 kcal/mol at these levels, respectively. CVT−ZCT gives values even farther from the TST results (Table 7), despite the fact that the associated tunneling coefficients were smaller compared to those from CVT−SCT calculations. For the secondary Swain−Schaad exponent (α_{SS}^S), CVT gives a value close to 3.5 and has a small positive temperature dependence (Figure 12e). With tunneling at the CVT−SCT level, by contrast, α_{SS}^S is much *smaller* in magnitude (around 2) and has a negative temperature dependence (Figure 12f). The trend is similar to that found in the case where the donor−acceptor vibration is allowed, although the curvature of the temperature dependence of α_{SS}^S is somewhat different; i.e., α_{SS}^S approaches a constant value at high temperatures with unconstrained donor and acceptor atoms, while it does so at low temperatures with fixed donor and acceptor atoms. At a given temperature (e.g., 300 K), the trend in the secondary Swain−Schaad exponent for different fixed donor−acceptor distances depends on whether tunneling is included. At the TST level, α_{SS}^S is largest in the case of 2.6 Å; at the CVT−SCT level, however, α_{SS}^S is largest in the case of 3.0 Å, in which tunneling is the most important.

The results demonstrate that tunneling is likely to make a larger contribution to the rate constant when the donor and acceptor vibration is not allowed. As discussed in our earlier work,[30] this is due mainly to the fact that the potential energy barrier becomes very narrow near the transition state, as reflected by the high barrier frequency. In addition, the barrier becomes higher, and therefore the contribution of tunneling to the thermal rate constant, as defined in eq 5, becomes more pronounced. Similar effects were observed recently by Hammes-Schiffer and co-workers in a model for hydride transfer in ADH with a very different treatment of tunneling.[68]

(68) Webb, S. P.; Agarwal, P. K.; Hammes-Schiffer, S. *J. Phys. Chem. B* **2000**, *104*, 8884.

IV. Discussion

The primary purpose of this paper is to determine the importance of tunneling in TIM, relative to that in the gas phase and in solution, and to examine the factors that influence tunneling in the enzyme. In the discussion, we analyze the results and comment on certain features that may be of general interest for the understanding of proton (and hydride) transfer in enzymes. We focused on the dynamic factors that influence the rate constant and proton tunneling in the *intramolecular* proton transfer. We studied this step because we wish to determine whether the tunneling correction could significantly alter the results of the kinetics calculated from the relative barriers by TST, which indicated that it does not make a major contribution to the rate in wild-type TIM. In addition, the intramolecular proton transfer provides a well-defined model system for which it was possible to compare the importance of tunneling in the gas phase, in solution, and in the enzyme. Finally, and perhaps most importantly, we examine the relationship between the calculated magnitude of the tunneling and the values of the experimental observables that are often used to draw conclusions about its importance. We do this for both the first intermolecular transfer step (from DHAP to Glu 165), which is the rate-limiting chemical step in TIM, and the intramolecular step.

IV.1. Factors That Influence the Proton-Transfer Rate Constant and Tunneling in TIM. The results presented in section III demonstrate that tunneling contributes significantly to the proton-transfer rate constant in TIM even at room temperature and is crucial in determining the calculated isotope effects. The magnitude of tunneling differs for the two different processes studied; i.e., it is about a factor of 10 for the intramolecular proton transfer and 3.5 for the intermolecular proton transfer. This appears to support the conclusion of Klinman and co-workers, among others, that tunneling is important in enzymes, based on the analysis of experimental data for a variety of enzymes.[3−7] However, it should be noted that the factor of 10 in the increase of the rate found for TIM is a small contribution to the overall rate acceleration. Also, that tunneling exists in TIM does not by itself show that it has a role in catalysis. For that one has to compare the tunneling in the enzyme with that in solution.[23] As far as we are aware, this type of comparison has rarely been made either experimentally or theoretically for the reactions that appear to have a tunneling contribution in the enzyme. For TIM, a smaller secondary H/T
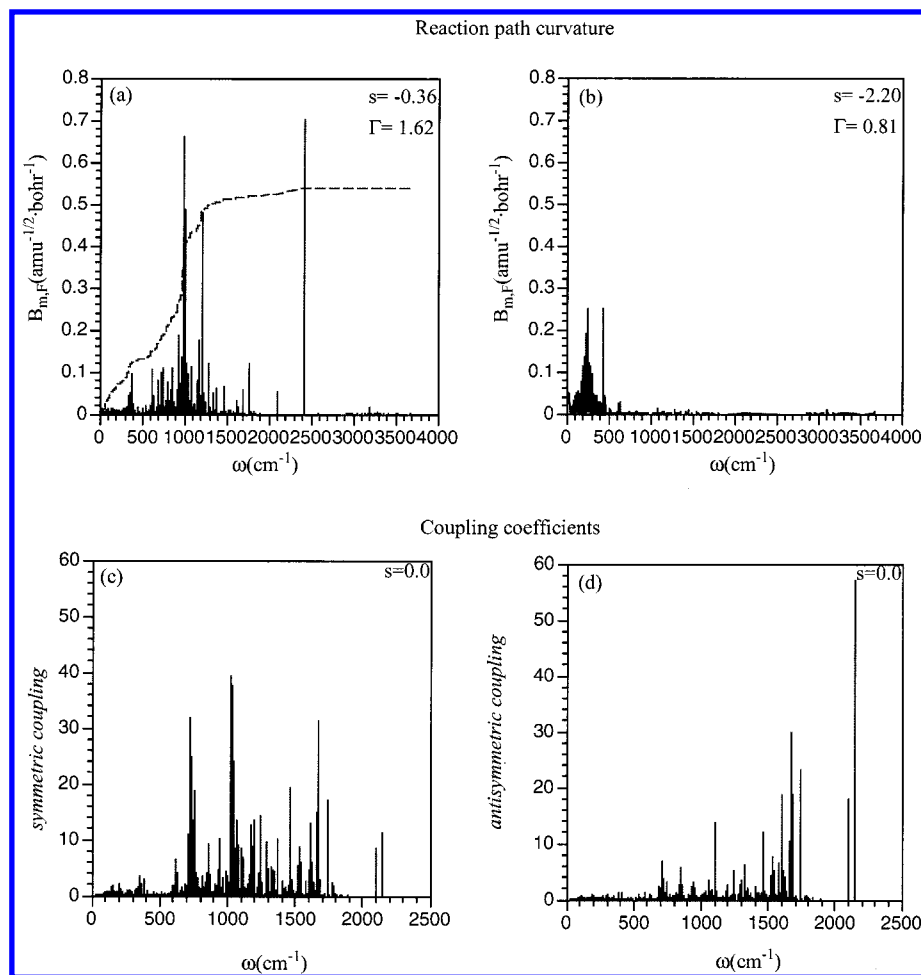
Figure 13. (a,b) Decomposition of the peaks of the reaction path curvature Γ for the intramolecular proton transfer in TIM into normal modes (see Figure 5 for the behavior of reaction path curvature along the reaction path) at $s = -0.36$ and $s = -2.20$ amu$^{1/2} \cdot$bohr. The dashed line is the cumulative contribution from path curvature components to the reduction of the effective mass along the reaction coordinate. The results were derived with the "large" model. (c,d) The approximate coupling coefficients to the proton-transfer coordinate of normal modes at the saddle point; each mode has both symmetric and antisymmetric components.

kinetic isotope effect was measured for the reaction between OH^- and $CH_3-(C=O)-Ph$ in solution compared to that in the enzyme in ref 9; however, as discussed below (section IV.3), the secondary kinetic isotope effect does not necessarily correlate with the magnitude of tunneling.

IV.1a. Analysis Based on Reaction Path Curvature and Its Generalized Normal-Mode Decomposition. It is well known that the flexibility of proteins is essential to their function.[69] Recently, a number of experiments have been interpreted as evidence for the importance of "dynamics" in enzyme catalysis. This includes the kinetic studies of alcohol dehydrogenases from different species at different temperature and glucose oxidase with different glycosylation,[3-7] as well as the pressure dependence of isotope effects found in yeast alcohol dehydrogenase.[70] In this subsection, we analyze the contribution of various modes to the reaction path curvature, an important factor in proton tunneling. In a separate paper,[30a] we describe some two-dimensional models to focus on the role of "promoting" and "demoting" modes in proton tunneling, a subject which has been discussed by a number of other workers,[13,14,16] and analyze the intermolecular and intramolecular proton-transfer

calculated for TIM to explore the promoting and demoting modes via more realistic systems.

As mentioned in section III, the reaction path curvature in TIM has two sets of peaks (see, for example, Figure 5). One set is larger in magnitude and occurs close to the saddle point ($s \approx \pm 0.3$). This has its origin in a rather sudden change in the components making up the reaction coordinate. The coordinate initially consists mainly of the donor–acceptor stretch, but near the saddle point it is composed of acceptor–proton and donor–proton stretches. The other set of peaks is smaller in magnitude and occurs farther from the saddle point. These peaks are caused by the structural reorganization of the active site in the initial stage ($s \approx \pm 2.0$) of the reaction, e.g., reorganization of the active site residues to allow the subsequent movement of Lys 12 and His 95 during the reaction (see Figure 11b). To make the description more quantitative, we use the generalized normal-mode decomposition of the path curvature (Γ) at the peak positions (Figure 13). Close to the saddle point ($s \approx -0.3$), Γ has large contributions from modes that are relatively high in frequency, typically between 1000 and 2000 cm^{-1}; their character is described below. For the second set of peaks, by contrast, most modes with relatively large contribution are low in frequency, typically around 300 cm^{-1}. As shown in section

(69) Brooks, C. L., III; Karplus, M.; Pettitt, B. M. *Advances in Chemical Physics 71*; John Wiley & Sons: New York, 1988.
(70) Northrop, D. B.; Cho, Y. K. *Biophys. J.* **2000**, *39*, 2406.

III, this set of peaks do not have a direct influence on the tunneling probability because they are in the region far from the saddle points, where the proton−donor bond is hardly affected; e.g., zeroing the reaction path curvature beyond ±1.5 amu$^{1/2}\cdot$bohr (which eliminates the contribution of the second set of peaks) gave essentially the same tunneling coefficient. Consequently, the main effect is to modulate the structure of the active site to allow the subsequent movement of the residues (e.g., Lys 12 and His 95 here) that are more directly involved in the proton transfer. In an earlier study of activated dynamics by classical trajectories,[33] it was found that vibrations in the 300 cm^{-1} range modulated the barrier height.

To analyze the direct contribution to tunneling, therefore, we focus on the inner set of curvature peaks. Modes with large contributions to the reaction path curvature in this region increase the tunneling probability by reducing the effective mass of the tunneling particle.[18] Figure 13 shows the cumulative contribution from the generalized normal modes to the decrease of the effective mass. The contributions are mainly from modes between 500 and 1500 cm^{-1}. Modes at higher frequencies make a relatively small contribution because the contribution is inversely proportional to the square root of the frequency, as is the displacement.

To clarify the character of the important vibrational motions, a projection procedure was followed; see ref 30 for a more detailed formulation. The generalized normal modes with a large curvature component at the peak position ($s \approx -0.5$), referred to as "path modes", were projected onto the eigenvectors at the saddle point. This was necessary because the "intrinsic" character of the modes may be masked due to the mixing with the proton-transfer coordinate in regions where the nature of the reaction coordinate varies rapidly.[30] The modes at the saddle point with large overlaps are referred to as "essential modes". A similar projection could be done with the normal modes in the reactant geometry, but the saddle point was chosen here because the peaks in the reaction path curvature occur close to the saddle point. For each essential mode, the displacement vectors of the reactant and the product relative to the saddle point were projected onto the corresponding eigenvector. The results were then combined to give the symmetric and antisymmetric displacements, which in turn gave the approximate coupling coefficient of the mode to the proton-transfer coordinate.[30] In general, each mode can have both symmetric and antisymmetric components; modes with large symmetric components have a promoting effect on the rate constant. This is due to the fact that the vibrational excitation of a symmetric mode decreases the effective barrier along the proton-transfer coordinate.

As shown in Table 8, the "path modes" typically have substantial overlap with many modes at the saddle point. The imaginary barrier mode (798i) has large overlaps with many "path modes" of relatively high frequency, corresponding to the fact that the character of the reaction coordinate is changing rapidly at the curvature peak position ($s = -0.3$). Most essential modes have large coupling coefficients. Since the intramolecular proton-transfer reaction is quite symmetric, a mode is usually dominated by only one component (symmetric or antisymmetric); this contrasts with the intermolecular proton-transfer reaction,[30] in which each mode can be associated with two components of similar magnitude. The participation ratios (see

Table 9 and Figure 14) confirm that the "essential modes" are rather local in nature, and that they consist of only a few residues that are close to the substrate, mainly Glu 165, Lys 12, His 95, and Solv 26. The character of the essential modes is illustrated in Figure 14, which shows that the atoms involved are the transferred proton, its donor and acceptor, and their neighbors. The donor and acceptor atoms are involved in many modes, especially those at low frequencies (e.g., 716 cm^{-1} in Figure 14). Another important motion is the carbonyl (C=O) stretch of the substrate (e.g., 1674 cm^{-1} in Figure 14). The local vibrational motions of the substrate can couple with the vibrational motion of the environment, generating a set of generalized normal modes with similar frequencies; e.g., modes 710−756 cm^{-1} in Table 9 have similar coupling coefficients and characters, and they contribute in groups with similar weights ($\sim$0.1) to the "path modes".

The calculations clearly demonstrate that the proton transfer in TIM is coupled to a large number of vibrational motions (including both symmetric and antisymmetric modes) in the active site. In general, these vibrations are *localized* primarily on atoms in the reaction region. One of these modes is the donor−acceptor stretch; it is the symmetric mode which strongly modulates the effective barrier for the proton transfer and also the effect of tunneling. There are other modes that are also symmetrically or antisymmetrically coupled to the proton-transfer coordinate, involving nearby residues such as Glu 165 and Asn 10. This suggests that the reaction path curvature, and therefore the tunneling, should have only a weak dependence on the number of residues allowed to relax during the reaction, *provided* that the reaction energetics (especially the barrier height) are not significantly perturbed by the size constraint. This is what was observed in section III, where we found very similar tunneling coefficients for the large (445 movable atoms) and the small models (106 movable atoms) with the environment fixed at the saddle-point geometry optimized with the large model. A larger change in tunneling was observed with the other small model, in which the environment was fixed at the reactant geometry optimized with the large model. This was due to the rather different reaction energetics and essential geometry at the saddle point in the two small models, rather than to the restriction on the mobile atoms. Since the saddle-point region is most important, the results suggest that an efficient way to calculate the tunneling contribution is to obtain the saddle-point structure with a large set of movable atoms and then to compute tunneling, per se, with a smaller set of movable atoms.

IV.1b. Effect of Structural Fluctuations on the Barrier Height and Frequency. As shown in section III, reaction path properties such as the barrier height and barrier frequency exhibit significant variations as a function of the active site geometry (Tables 3 and A2 (Supporting Information)). For the intermolecular proton transfer, the proton motion is rather simple geometrically and slightly perturbs the active site geometry. As a result, the fluctuations of the reaction path properties are relatively small: both the barrier height and exothermicity fluctuate on the order of 1 kcal/mol, and the standard deviation of the barrier frequency is 36 cm^{-1}. Fluctuations of a similar magnitude were found for the barrier height in a previous study with an EVB potential.[33] For the intramolecular proton transfer, which is simple in the gas phase, the process is more complicated structurally in the enzyme. It involves the breaking

Table 8. Overlap among Frequencies with Large Curvature Components and Modes at the Saddle Point in the Intramolecular Proton Transfer in TIM[a]

path modes		saddle-point modes		
ω (cm^{-1})	$B_{k,F}$	overlap	ω (cm^{-1})	coupling strength[c]
0[b]		0.82	798i	
		0.17	710	10.5 (6.7)
		0.27	716	31.9 (0.4)
		0.14	722	23.8 (3.9)
		0.16	727	24.4 (1.1)
		0.17	728	24.9 (1.2)
		0.11	735	17.7 (0.6)
		0.14	756	18.8 (0.4)
		0.22	2141	11.3 (57.0)
2422	0.7	0.35	798i	
		0.18	1674	31.2 (29.8)
		0.24	1736	17.0 (23.3)
		0.26	2102	8.6 (17.9)
		0.83	2141	11.3 (57.0)
997	0.66	0.21	798i	
		0.19	716	31.9 (0.4)
		0.12	722	23.8 (3.9)
		0.13	727	24.4 (1.1)
		0.13	728	24.9 (1.2)
		0.18	756	18.8 (0.4)
		0.63	996	2.0 (0.1)
		0.48	999	3.5 (0.1)
		0.14	1002	0.9 (0.0)
		0.12	1177	12.6 (0.0)
		0.12	1195	13.5 (1.0)
995	0.65	0.19	798i	
		0.18	716	31.9 (0.4)
		0.12	722	23.8 (3.9)
		0.12	727	24.4 (1.1)
		0.12	728	24.9 (1.2)
		0.17	756	18.8 (0.4)
		0.77	996	2.0 (0.1)
		0.27	999	3.5 (0.1)
		0.11	1002	0.9 (0.0)
		0.11	1177	12.6 (0.0)
		0.11	1195	13.5 (1.0)
1000	0.49	0.15	798i	
		0.14	716	31.9 (0.4)
		0.13	756	18.8 (0.4)
		0.10	996	2.0 (0.1)
		0.80	999	3.5 (0.1)
		0.32	1002	0.9 (0.0)
		0.12	1004	0.2 (0.1)
1213	0.48	0.15	798i	
		0.31	1177	12.6 (0.0)
		0.13	1195	3.9 (0.4)
		0.64	1195	13.5 (1.0)
		0.17	1199	2.5 (0.4)
		0.26	1200	4.7 (0.2)
		0.10	1215	0.2 (0.1)
		0.46	1215	1.5 (0.3)
		0.22	1218	1.4 (0.3)
1003	0.31	0.17	999	3.5 (0.1)
		0.90	1002	0.9 (0.0)
		0.24	1004	0.2 (0.1)
		0.11	1004	0.9 (0.0)
1216	0.24	0.15	1177	12.6 (0.0)
		0.29	1195	13.5 (1.0)
		0.12	1200	4.7 (0.2)
		0.86	1215	1.5 (0.3)
		0.30	1218	1.4 (0.3)
1218	0.22	0.13	1177	12.6 (0.0)
		0.23	1195	13.5 (1.0)
		0.17	1215	1.5 (0.3)
		0.93	1218	1.4 (0.3)
939	0.19	0.14	931	4.7 (0.3)
		0.17	935	3.9 (2.3)
		0.29	939	0.9 (2.6)
		0.14	940	0.4 (0.9)
		0.8	942	10.3 (3.2)
		0.21	943	4.7 (1.5)
		0.11	946	2.1 (0.4)
		0.15	1027	39.4 (0.8)
		0.11	1028	29.3 (1.4)
		0.14	1029	37.6 (1.5)

[a] The frequencies orthogonal to the reaction path were computed at $s = -0.32$amu$^{1/2}\cdot$bohr, where the reaction path curvature has the peak value (see Figure 5). The reaction path curvature components, $B_{k,F}$, are given in amu$^{-1/2}\cdot$bohr^{-1}. [b] The eigenvector associated with the reaction path motion at this configuration. [c] The approximate coupling strengths between the essential modes and the proton-transfer coordinate are given in the units of kcal/mol$\cdot$Å^{-1}. The values without parentheses are the approximate symmetric components, and the values in parentheses are the approximate antisymmetric components. See ref 30a for more discussions.

Table 9. Characters of Normal Modes That Have a Large Contribution to the Reaction Path Curvature (Γ) in Selected Configurations along the Reaction Path for the Intramolecular Proton Transfer in TIM[a]

ω, $R_i^\downarrow$, $R_i^\parallel$, C	residue[b]	dist[c]	contrib[d]	ω, $R_i^\downarrow$, $R_i^\parallel$, C	residue	dist[c]	contrib[d]
798i	Subs		0.98	**1674**	Subs		0.73
3.1	H95	7.56	0.01	8.6	K12	5.81	0.12
1.0	K12	5.81	0.01	1.8	E165	5.76	0.11
	E165	5.75	0.01	31.2 (29.8)	N10	5.57	0.01
	N10	5.57	0.01		V231	5.89	0.01
2141	Subs	- - - - -	0.86	**1027**	Subs		0.29
2.8	E165	5.76	0.13	34.8	G209	5.75	0.18
1.3	H95	7.56	0.01	6.2	G210	4.83	0.15
11.3 (57.0)	N10	5.56	0.01	39.4 (0.8)	I170	4.92	0.12
	W26	6.70	0.01		K12	5.81	0.06
1736	Subs	- - - - -	0.98	**1029**	G9	8.33	0.28
8.3	E165	5.76	0.01	31.3	Subs		0.25
1.0	N10	5.57	0.01	5.6	G8	8.90	0.14
17.0 (23.3)	K12	5.81	0.01	37.6 (1.5)	N10	5.56	0.08
	H95	7.56	0.01		K12	5.81	0.07
716	Subs		0.35	**722**	N10	5.57	0.39
33.1	E165	5.76	0.27	30.8	H95	7.56	0.24
4.2	P166	9.05	0.20	4.2	P166	9.05	0.13
31.9 (0.4)	N10	5.57	0.05	23.8 (3.9)	Subs		0.11
	F229	9.95	0.05		E165	5.76	0.07
727	K12	5.81	0.24	**728**	K12	5.81	0.32
55.2	N10	5.57	0.21	49.4	N10	5.57	0.20
7.1	Subs		0.14	5.4	Subs		0.14
24.4 (1.1)	W75	5.99	0.08	24.9 (1.2)	W75	5.99	0.05
	P166	9.05	0.08		P166	9.05	0.07

[a] The values were obtained with the "large" set of models. [b] "Subs" indicates the substrate in the enzyme. [c] Distances are defined as the center of geometry distances between the residues (*including* the main chain atoms) and the substrate. The R_i's are the participation ratios (see eq 7) for the ith mode; for the format of the coupling coefficients (C), see the footnote of Table 8. [d] The contribution of each residue is defined as the term after the first summation in eq 7b.

and forming of hydrogen bonds between the substrate and the nearby residues (Glu 165, His 95, and Lys 12). Therefore, as described in section III, the orientations of those residues have a significant effect on the reaction, which is manifested in terms of large fluctuations in the reaction path properties. The barrier height varies by nearly 2 kcal/mol, and the exothermicity by 4.6 kcal/mol. The fluctuation in the barrier frequency is also substantial; it ranges from 855 to 1171 cm^{-1}. However, it should be noted that the magnitudes of the variation may be exaggerated somewhat by the limited number of atoms that were allowed to relax in the intrinsic reaction path calculations.

Corresponding to the variation in reaction path properties, the tunneling coefficient also shows a significant geometry dependence. As shown in Figure 15, the tunneling coefficient exhibits a positive correlation with the barrier frequency and the barrier height; i.e., the tunneling coefficient is large for high barriers and high barrier frequencies, as expected. The reaction asymmetry (i.e., deviation of the reaction from being thermoneutral) does not have a strong correlation with the tunneling coefficient. This is due to the fact that the exothermic part of the potential energy surface does not enter the tunneling calculations explicitly in the CVT−SCT approach (eq 1); i.e., at a given total energy, the tunneling transmission coefficient, $P^{1d}(E)$, depends only on the potential energy surface between the corresponding turning points along the reaction path. The reaction asymmetry influences the reaction rate implicitly by affecting the barrier height and position, in a manner mostly consistent with the Hammond postulate; e.g., the proton-transfer barrier in TIM is generally lower for smaller endothermicity (see Tables 3 and A2).
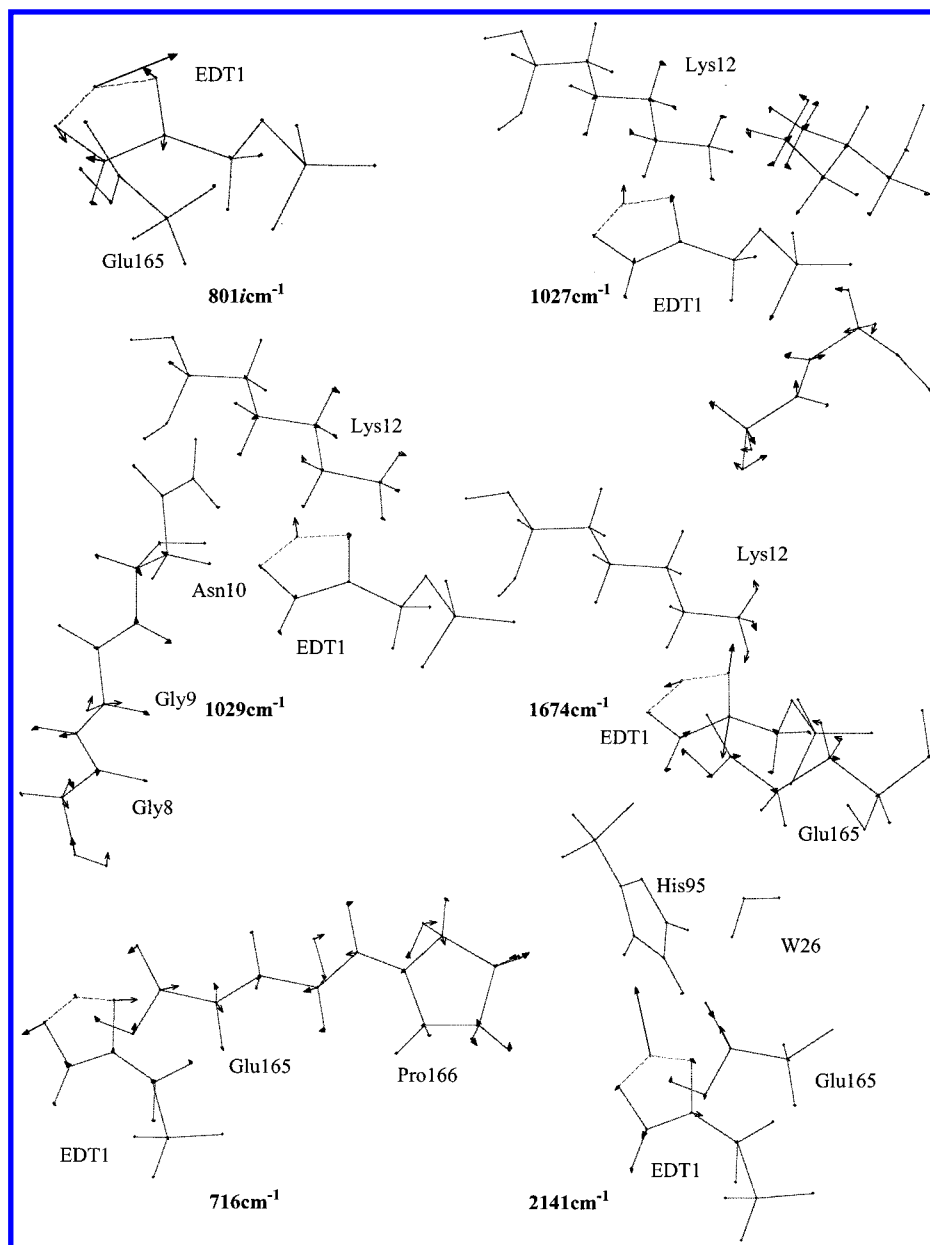
Figure 14. Plot of the barrier mode and the essential modes (the modes at the saddle point that have large overlap with modes having a large reaction path curvature component at the path curvature peak position, see also Tables 8 and 9) for the intramolecular proton transfer in TIM. The results were derived with the "large" model. The length of the arrow is proportional to the displacement of the atom in the normal mode.

The above discussion suggests that reliable rate constant calculations for proton-transfer reactions with a substantial barrier in an enzyme (or solution) can be done in several steps. First, one determines the transition state based on an equilibrium simulation with a QM/MM potential. The latter could be either a potential-of-mean-force calculation or a reaction-path-based calculation with large number of movable atoms, in which the environment adiabatically follows the reaction. Next, corrections to the transition-state calculation of the rate constant, such as classical nonequilibrium effects or tunneling, have to be determined. At room temperature, if both effects are characterized by time scales faster than the large-scale motions of the enzyme, it is appropriate to obtain a mean classical or quantum (tunneling) transmission coefficient by averaging over a number of enzyme configurations. Since tunneling has been shown to be controlled by the atoms close to site of the reaction, only a small number of atoms have to be allowed to move in the

calculation of the tunneling coefficient in a given enzyme configuration, after the saddle-point environment has been optimized with a larger set of movable atoms.

IV.2. Comparison of Proton Transfer in the Gas Phase, Solution, and Enzyme without and with Tunneling. In any estimate of the role of tunneling, or other factors, in enzyme catalysis, it is important to have a comparison with gas-phase and solution results to determine the effect of the enzyme on the reaction.[23] However, it is often more difficult to obtain accurate tunneling estimates in solution because the system is less constrained. Consequently, most calculations concerned with enzymatic reactions do not include solution results; exceptions are the calculations of Warshel and co-workers,[71] who often evaluate the parameters of the empirical potential functions used for the enzyme by fitting the data for the reactions in solution.

(71) Warshel, A. *Computer Modeling of Chemical Reactions in Enzymes and Solution*; John Wiley & Sons: New York, 1991.
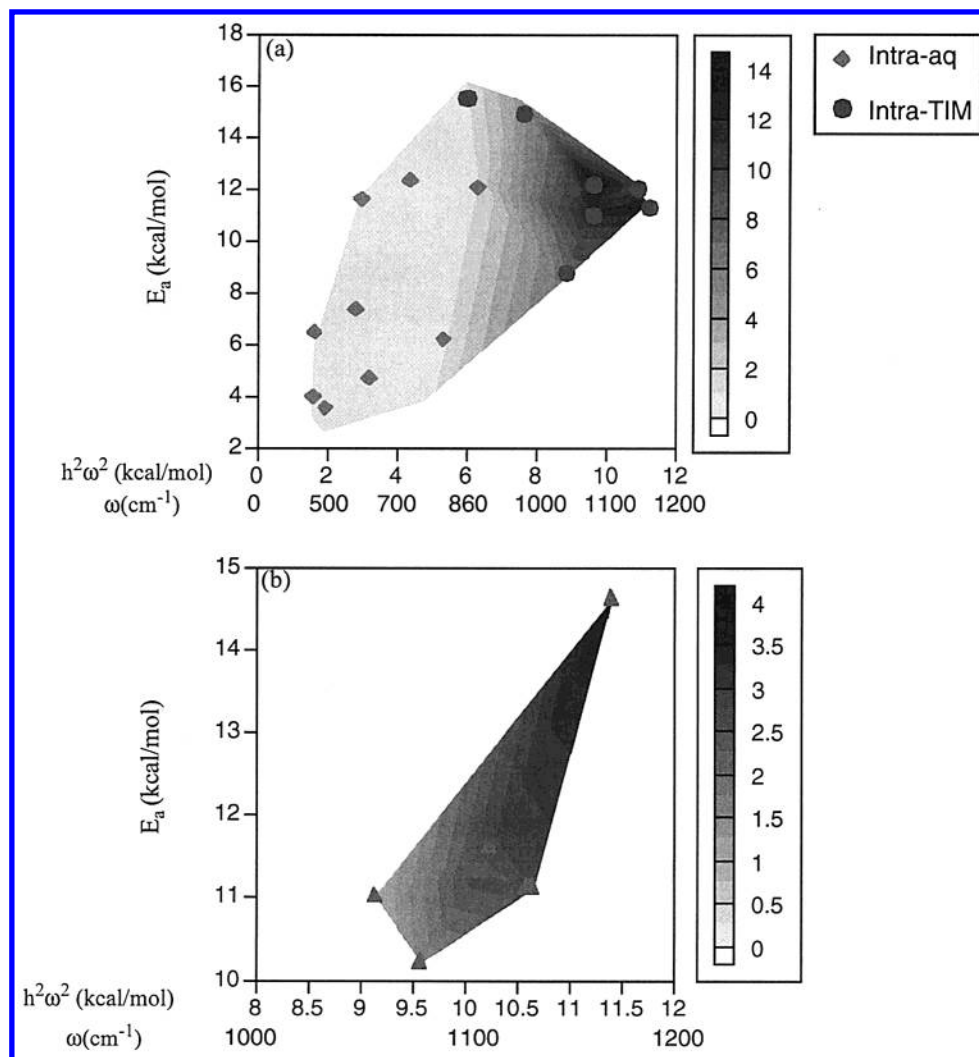
Figure 15. (a) Correlation of tunneling factor minus 1 (the z-axis), $\kappa^{CVT-SCT} - 1$, with the imaginary frequencies at the saddle points and the lower value of the forward and backward barrier heights (see text) for the intramolecular proton-transfer reactions. (b) Correlation for the intermolecular proton transfer.

In this section, we discuss the results for the intramolecular proton-transfer step of the TIM reactions, which is relatively easy to treat in solution, as well as in the enzyme. The intramolecular reaction avoids questions such as whether the proximity of the reacting groups plays a role in the enzyme reaction relative to the caging effect in solution.

The results from the calculations at 300 K for the intramolecular proton transfer in different media (section III) indicate that tunneling is significant in the gas phase and in the enzyme, but less so in solution. The average $\kappa^{CVT-SCT}$ value is about 8.0, 10.0, and <2.0 in the gas phase, enzyme, and solution, respectively. Thus, relative to solution, the tunneling is increased by a factor of 5 in the enzyme. However, it should be noted that TIM has an "anticatalytic" effect on the intramolecular proton transfer; i.e., the barrier is higher in the enzyme compare to that in solution and in the gas phase due to the presence of the conserved His 95 residue which plays essential roles in other steps of the catalytic cycle.[24]

Since the tunneling factor at 300 K is strongly correlated with the barrier frequency (i.e., the width of the barrier), the significantly lower barrier frequency calculated in solution relative to the gas phase and in the enzyme is the major source of this difference. Several factors could contribute to this result. The reaction energetics are altered by the solvent for this step,

as discussed above, such that the average barrier is *lower* in solution than it is in the gas phase and in the enzyme; a lower barrier often correlates with a lower barrier frequency. However, even for structures with barrier heights in solution similar to or even higher than that in the gas phase (e.g. sets 2, 4, and 6 in Table 5), the barrier frequency is still lower in solution by the same amount, so that this is not the only essential factor. The barrier frequency for the potential of mean force ($769i$ cm^{-1}) is also much lower than the gas-phase value ($1365i$ cm^{-1}), although the barriers are similar in magnitude (~10 kcal/mol). Another *possible* explanation is that there is strong coupling (friction) of the proton motion with that of the environment; i.e., the proton motion is "slowed" by the solvent, resulting in a lower barrier frequency.

To clarify if there is indeed a "slowing-down" effect due to the solvent, we analyze further the barrier frequency and the associated eigenvector by using the saddle-point structure optimized with the "large" model in solution and in TIM (see section II.2). The change in the imaginary barrier frequency is rather small if the entire environment (i.e., everything except the substrate) is fixed in the normal-mode analysis, although the effect is larger in solution; the values with frozen and flexible environments are $480i$ vs $591i$ cm^{-1} in solution, and $797i$ vs $798i$ cm^{-1} in the enzyme. The participation ratio for the barrier
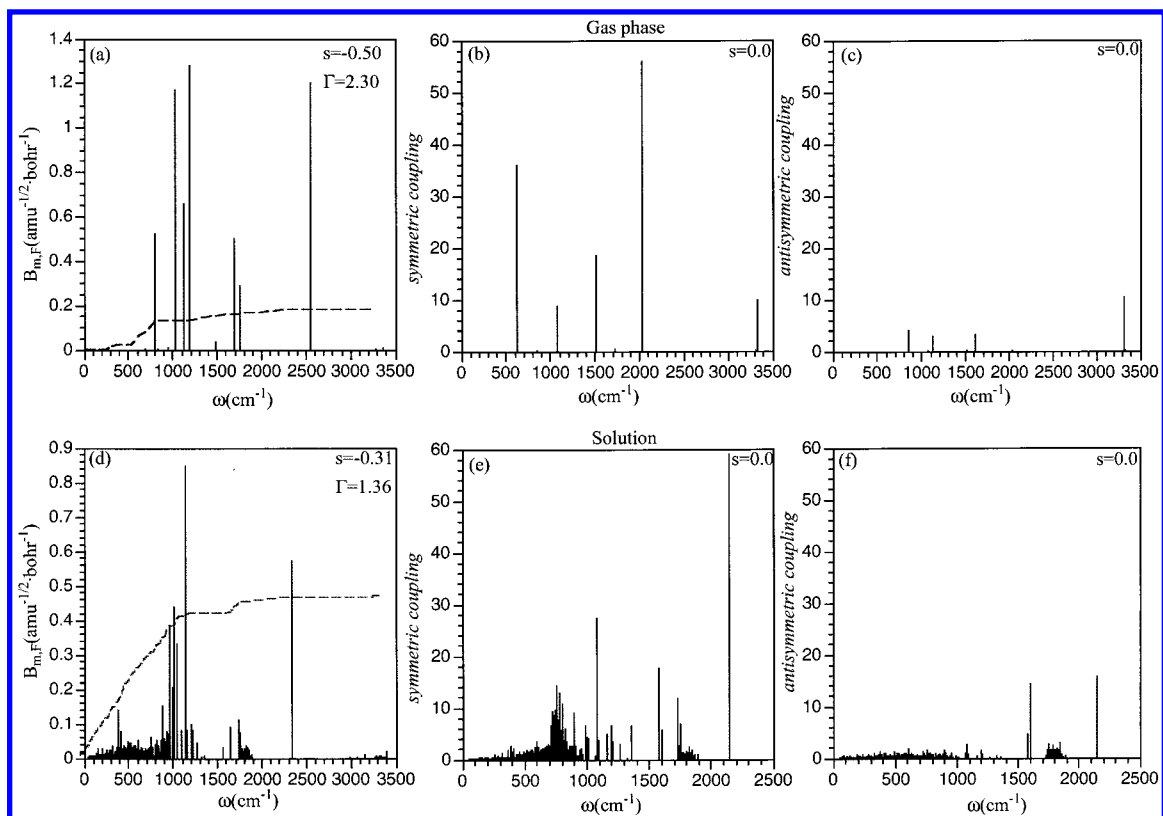
Figure 16. Intramolecular proton transfer in the gas phase and in solution. (a) Decomposition of reaction path curvature Γ into normal modes for the structure that exhibits large path curvature for the intramolecular proton transfer in the gas phase. (d) Same as (a), for the intramolecular proton transfer in solution (the plot was made for the peak close to the saddle point, see Figure 9 for the behavior of reaction path curvature along the reaction path); the "large" model was used. The dashed line is the cumulative contribution from path curvature components to the reduction of the effective mass along the reaction coordinate. (b,c and e,f) The approximate coupling coefficients to the proton-transfer coordinate of normal modes at the saddle point for the gas-phase and solution reactions, respectively; each mode has both symmetric and antisymmetric components.

mode is also slightly larger in solution ($R^I \approx 4.1$) than in enzyme ($R^I \approx 3.1$). However, both values are small, indicating that the barrier mode is highly localized in both media. Therefore, the change in the barrier frequency in the presence of the environment relative to the gas phase is *not* due to the inertial mixing (i.e., a "slowing-down" effect) of substrate motion and solvent motion (i.e., the substrate−solvent/enzyme block of the Hessian matrix in the analysis of Pollak[72] on the Grote−Hynes theory[73] of solvation). Instead, it is the force constant of the imaginary mode itself that is modified substantially in the solution. Indeed, if the electrostatic interaction between the substrate and solvent is turned off, the barrier frequency in solution becomes much higher, $896i$ cm^{-1}, compared to the value of $480i$ cm^{-1} in the frozen environment. A similar trend is observed in the enzyme, although the effect is much smaller; the barrier frequency is $797i$ and $856i$ cm^{-1} before and after zeroing out the partial charges of the environment. In other words, the electrostatic interactions with the enzyme reduce the force constant associated with the barrier mode less than the solution environment. Thus, the reduction of the barrier frequency in solution is due to the fact that electrostatic and polarization effects from the solvent molecules can substantially modify the shape of the potential energy surface for the proton transfer, and not due to any inertial effect (i.e., the substrate−solvent block of the Hessian, which is the origin of "solvent friction" in the analysis of Pollak[72]).

The barrier height and exothermicity of the reaction show larger fluctuations in solution than in the enzyme (compare Tables 4 and 6). This is in accord with previous studies[74] and reflects the fact that the enzyme active site is more organized and constrained structurally compared with solution. For example, in the case of the hydrophobic binding site in human serum albumin (HSA), the motion of the ligand (2-(2′-hydroxyphenyl)-4-methyloxazole) was found to be much more restricted in the protein compared to that in *p*-dioxane solution and in micelles of 1-*O*-octyl β-D-glucopyranoside;[75] time-resolved fluorescence measurements showed that the orientational anisotropy relaxation of the ligand had a time constant of 45, 97, and >500 ps in *p*-dioxane, micelle, and HSA, respectively.

The reaction path curvature and essential modes (see section IV.1a) that influence tunneling were found to be rather similar in the gas phase, in solution, and in enzyme. For the gas-phase reaction, which is the simplest structurally, only one set of peaks near the saddle point exists in the path curvature (Γ) (Figure 3). The generalized normal-mode decomposition of Γ (Figure 16) suggests that the essential modes are mostly high in frequency, similar to these in the enzyme.[30] The contribution of path curvature to the effective mass, $B_{k,F} t_k$, converged around 1500 cm^{-1} in both cases. It is interesting to note that the cumulative value, $\sum_k B_{k,F} t_k$, is much smaller ($\sim$0.2) in the gas

(72) Pollak, E. *J. Chem. Phys.* **1986**, *85*, 865.
(73) Grote, R. F.; Hynes, J. T. *J. Chem. Phys.* **1980**, *73*, 2715.

(74) Warshel, A. *Proc. Natl. Acad. Sci. U.S.A.* **1984**, *81*, 444.
(75) Zhong, D.; Douhal, A.; Zewail, A. H. *Proc. Natl. Acad. Sci. U.S.A.* **2000**, *97*, 14056.

phase than in solution (~0.5) and in the enzyme (~0.6). This is due to the fact that there are many more modes with non-negligible contribution to the value of $\sum_k B_{k,F} t_k$ in the latters. All the essential modes were found to have large symmetric coupling coefficients in the gas phase and in solution (see Figure 16).[30]

For the reaction in solution, two sets of peaks in Γ are found in the path curvature (Figure 8). For the peak close to the saddle point, the essential modes have frequencies around 1000 and 1200 cm⁻¹, and a few around 2000 cm⁻¹. For the set of peaks farther from the saddle point, most contributions to the path curvature arise from modes lower in frequency than 500 cm⁻¹ (not shown), although a few high-frequency modes (in the range of 3200−3500 cm⁻¹) also make contributions. The latter corresponds to the O−H vibrations of the water molecules that are directly hydrogen-bonded to the substrate (Figure 2). Therefore, although these modes do not influence tunneling in the substrate directly, they might transfer energy to the substrate if they were vibrationally excited (e.g., by lasers). This observation is of interest in relation to a recent pump−probe experiment that demonstrates that hydrogen bond networks provide an efficient energy-transfer pathway in the condensed phase.[76]

Similar to the intramolecular proton transfer in TIM, the modes in solution with large curvature components have substantial overlaps with many modes at the saddle point (Table 10). The participation ratio analysis (Table 11) indicates that some essential modes are very localized substrate vibrations (>1000 cm⁻¹), and that the others (~700 cm⁻¹) involve a substantial number (about 20) of water molecules. The solution modes seem to be more delocalized than the essential modes in TIM with similar frequency; e.g., the associated R^I value in solution is close to 100 (Table 11), and that in the enzyme is near 50 (Table 9). This might be due to the more homogeneous character of the solution despite the presence of the substrate. A typical motion in the high-frequency set involves the C−O or C−C stretch (e.g., 1574, 1734 cm⁻¹ in Figure 17), and the donor−acceptor stretch is commonly involved in the low-frequency set (e.g., 760 cm⁻¹ in Figure 17).

Thus, the results suggest that there is a significant solvation effect on the tunneling. The origin of this effect is the strong electrostatic interaction between the charged solute and the solvents, which, in principle, can affect both the substrate−substrate and substrate−solvent blocks of the Hessian; the effect on the former seems to be much more significant in the present case. By contrast, the inertial coupling (which is related only to the substrate−solvent block of the Hessian) was found to be small; i.e., the motions of the solvent molecules are not significantly coupled to the barrier mode. The strong solvation results in a large "renormalization" of the barrier frequency and the fluctuations of the reaction energetics in water, all of which reduces the proton tunneling. The general features of reaction path curvature and its generalized normal-mode decomposition are rather similar in all media (gas phase, solution, and enzyme) for regions close to the saddle point. The essential modes in solution, similar to those in the enzyme, are localized on atoms close to the solute, and the tunneling coefficient is directly influenced by a small number of solvent molecules.

IV.3. Analysis of the Use of Experimental Observables To Determine the Magnitude of Tunneling. One use of kinetic

Table 10. Overlap among Frequencies with Large Curvature Components and Modes at the Saddle Point in the Intramolecular Proton Transfer in Solution[a]

path modes		saddle-point modes		
ω (cm⁻¹)	$B_{k,F}$	overlap	ω (cm⁻¹)	coupling strength
0			591i	
		0.11	725	9.4 (0.0)
		0.10	737	8.5 (0.3)
		0.12	740	9.6 (0.2)
		0.11	747	9.4 (0.0)
		0.12	753	11.4 (1.0)
		0.15	760	14.2 (1.6)
		0.14	778	13.0 (1.0)
		0.11	799	10.7 (0.2)
		0.17	2146	59.0 (15.7)
1156	0.85	0.99	1156	4.7 (0.3)
2402	0.56	0.31	591i	
		0.13	1584	17.7 (4.6)
		0.23	1605	5.6 (14.2)
		0.88	2146	59.0 (15.7)
1008.4	0.44	0.27	983	6.5 (0.4)
		0.95	1009	4.1 (0.2)
		0.11	1078	27.4 (2.6)
956	0.39	0.11	591i	
		0.12	778	13.0 (1.0)
		0.30	901	9.0 (1.6)
		0.12	909	2.8 (0.2)
		0.10	940	1.8 (0.0)
		0.13	950	2.0 (1.0)
		0.65	983	6.5 (0.4)
		0.12	996	4.4 (0.2)
		0.11	1009	4.1 (0.2)
		0.50	1078	27.4 (2.6)
1035	0.33	0.15	591i	
		0.14	1009	4.1 (0.2)
		0.81	1072	0.6 (1.0)
		0.41	1078	27.4 (2.6)
		0.17	1094	3.9 (0.7)
997	0.20	0.98	996	4.4 (0.2)
		0.12	1078	27.4 (2.6)
887	0.15	0.25	880	2.7 (0.2)
		0.33	885	0.3 (0.6)
		0.49	891	1.9 (0.8)
		0.28	894	2.1 (0.6)
		0.58	901	9.0 (1.6)
		0.12	906	1.5 (1.1)
		0.12	909	2.8 (0.2)
		0.14	1078	27.4 (2.6)
1737	0.11	0.11	1605	5.6 (14.2)
		0.63	1734	11.9 (0.5)
		0.75	1740	2.7 (1.5)
1744	0.10	0.12	1605	5.6 (14.2)
		0.63	1734	11.9 (0.5)
		0.61	1740	2.7 (1.5)
		0.35	1746	2.0 (0.1)
		0.11	1752	1.3 (1.3)
		0.13	1755	6.9 (2.8)
		0.13	1756	2.3 (0.5)
		0.10	2146	59.0 (15.7)

[a] For notations, see the footnote of Table 8.

isotope effect experiments, in addition to their important role in analyzing enzyme mechanisms,[77] is to determine the contribution of proton tunneling to the reaction rate.[3] For this purpose, it is essential to have a full understanding of the connection between the magnitude of tunneling and the experimental observables. In this section, we use the results obtained for TIM to approach this question. We start by commenting on the Swain−Schaad exponents, which have been emphasized in recent experimental analyses, and then discuss briefly more

(76) Woutersen, S.; Baker, H. J. *Nature* **1999**, *402*, 507.

(77) See, for example: Cleland, W. W. *Methods Enzymol.* **1995**, *249*, 341.

Table 11. Characters of Normal Modes That Have Large Contribution to the Reaction Path Curvature (Γ) in Selected Configurations along the Reaction Path for the Intramolecular Proton Transfer in Solution[a]

ω, $R_i^{\dagger}$, $R_i^{\parallel}$, C	residue	dist	contrib	ω, $R_i^{\dagger}$, $R_i^{\parallel}$, C	residue	dist	contrib
591i	Subs		0.90	**1734**	Subs		0.54
4.1	W277	4.54	0.04	15.1	W70	4.68	0.24
1.2	W74	4.83	0.02	2.8	W90	4.47	0.06
	W62	4.07	0.01	11.9 (0.5)	W109	4.74	0.02
	W17	3.95	0.01		W74	4.82	0.02
2146	Subs		0.96	**1605**	Subs		0.94
1.3	W74	4.83	0.02	5.9	W17	3.95	0.01
1.1	W62	4.07	0.01	1.1	W70	4.68	0.01
59.0 (15.7)	W277	4.54	0.01	5.6 (14.2)	W3	2.90	0.01
	W29	2.65	0.01		W74	4.83	0.01
1584	Subs		0.96	**1078**	Subs		0.75
5.7	W70	4.68	0.01	5.4	W11	3.03	0.04
1.1	W74	4.83	0.01	1.8	W17	3.95	0.04
17.7 (4.6)	W62	4.07	0.01	27.4 (2.6)	W74	4.83	0.03
	W3	2.90	0.01		W277	4.54	0.03
799	Subs		0.11	**753**	Subs		0.13
117.6	W84	3.51	0.08	137.3	W84	3.51	0.04
25.1	W150	5.24	0.08	30.2	W87	5.51	0.04
10.7 (0.2)	W7	4.02	0.05	11.4 (1.0)	W423	7.88	0.04
	W124	7.99	0.05		W289	9.92	0.04
760	Subs		0.18	**778**	Subs		0.13
92.3	W37	7.2	0.07	98.9	W344	8.41	0.07
18.9	W127	11.0	0.06	22.6	W273	8.01	0.06
14.2 (1.6)	W288	6.3	0.04	13.0 (1.0)	W184	5.83	0.05
	W100	5.7	0.03		W32	7.58	0.05

[a] See footnotes of Table 9 for the definitions of quantities.

"conventional" small-molecule observables, such as the deviation from Arrhenius behavior and the temperature dependence of the kinetic isotope effects.

Isotope effects and the Swain−Schaad exponents were computed for two sets of geometries that have large tunneling coefficients, i.e., set 4 for the intramolecular and set 6 for the intermolecular proton transfer (Table 12 and Figure 18). We note that the temperature dependence calculated in the current work corresponds to a reaction path calculation at 0 K, so that the effective potential surface is independent of temperature and the only variation as a function of temperature arises from the motion on that surface due to changes in the vibrational contribution. For a more complete estimate of the temperature dependence, the reaction path itself would have to be determined at different temperatures.[65] This is very demanding computationally, and we restrict the analysis to the "fixed barrier" case, for the present purpose of making connection with the behavior of kinetic quantities; calculations with more extensive configuration sampling are left for the future. However, it must be noted that the donor−acceptor distance is allowed to relax and is an important part of the reaction coordinate in the current calculations. Therefore, the "fixed" barrier potential used here is not the same as that referred to in some discussions (e.g., Klinman and co-workers), where a "rigid" system is one in which no donor−acceptor distance change or vibrational excitation is present.[4]

IV.3a. Swain−Schaad Exponents. Primary Swain−Schaad Exponent, α_{SS}^{P}. In the experimental literature, it is generally assumed that for the primary isotope effect, TST at room temperature gives a Swain−Schaad exponent, α_{SS}^{P} (eq 8b), equal to 3.3 due to the difference in the zero-point energies of the different isotopes. In principle, TST includes all the excited states, but the zero-point effect dominates at room temperature. The value of 3.3 is based on an assumed frequency

for the X−H stretch in the reactant state and no contribution at the transition state (see below). A value larger than 3.3 is interpreted to mean that tunneling plays a role.[4] In cases where other evidence points to tunneling, while a "normal" primary Swain−Schaad exponent is observed, "kinetic complexity" is usually invoked; i.e., this assumes that the proton-transfer step is not fully rate-limiting and therefore the intrinsic effects of the isotope substitution are partially or fully masked by other isotope-insensitive processes.[4,5] However, it has already been remarked that α_{SS}^{P} does not have to be larger than 3.3 in the presence of tunneling.[78] According to the present calculations in the gas phase and in TIM, α_{SS}^{P} rarely exceeds the TST limit of 3.3, even when tunneling is significant. For example, in the model system for the intermolecular proton transfer with a fixed donor−acceptor distance where tunneling is large ($\kappa^{CVT-SCT} = 36.5$ at 300 K), α_{SS}^{P} is 3.34 at 300 K; in the absence of tunneling it is 3.24. In set 6 intermolecular proton transfer in the enzyme environment (Table 12), the CVT−SCT method gives a lower Swain−Schaad exponent (2.65) than TST (3.38) and CVT (3.36). Kim and Kreevoy[79] used the VTST approach to study the effect of tunneling on the Swain−Schaad exponent in solution with empirical potential functions and a bilinearly coupled oscillator model for the solvent. They found that variational transition-state theory without tunneling can yield very large α_{SS}^{P} (up to 4.13), and that tunneling actually tends to bring α_{SS} into the expected range ($2.8 < \alpha_{SS}^{P} < 4.0$). From these results, a value of α_{SS}^{P} significantly larger than 3.3 is neither a necessary nor a sufficient condition for the presence of proton tunneling. We note that mixed primary−secondary isotope substitution measurements, which are often carried out experimentally, tend to give a higher "secondary" Swain−Schaad exponent.[80,81]

The relationship between the Swain−Schaad exponent and tunneling can be made clear by writing the former in the following form,

$$\alpha_{SS} \equiv \frac{\ln(k_H/k_T)}{\ln(k_D/k_T)} = \frac{\ln(\kappa_H^{Tun} k_H^{TST}/\kappa_T^{Tun} k_T^{TST})}{\ln(\kappa_D^{Tun} k_D^{TST}/\kappa_T^{Tun} k_T^{TST})} =$$

$$\frac{\ln(\kappa_H^{Tun}/\kappa_T^{TST}) + \ln(\kappa_H^{TST} k_T^{TST})}{\ln(\kappa_D^{Tun}/\kappa_T^{TST}) + \ln(k_D^{TST} k_T^{TST})} \quad (8a)$$

$$= \frac{\ln(\kappa_H^{Tun}/\kappa_T^{Tun})/\ln(k_D^{TST}/k_T^{TST}) + \alpha_{SS}^{TST}}{\ln(\kappa_D^{Tun}/\kappa_T^{Tun})/\ln(k_D^{TST}/k_T^{TST}) + 1} \quad (8b)$$

where κ_I^{Tun} is the tunneling coefficient (eq 5) for isotope I. For simplicity, we ignore the correction factor due to CVT, (i.e., κ^{CVT} in eq 5), although κ^{CVT} may also have an isotope dependence and therefore affect the Swain−Schaad exponent; e.g., α_{SS}^{P} is 3.34 and 3.27 at the TST and CVT levels, respectively, for the intramolecular proton transfer in the enzyme (see Table 2).

Assuming the typical vibrational frequency of 3000 cm^{-1} for the donor−proton vibration, one may use the mass-frequency

(78) (a) Stern, M. J.; Weston, R. E., Jr. *J. Chem. Phys.* **1974**, *60*, 2815. (b) Saunders, W. H. *J. Am. Chem. Soc.* **1985**, *107*, 164. (c) Grant, K. L.; Klinman, J. P. *Bioorg. Chem.* **1992**, *20*, 1.
(79) Kim, Y.; Kreevoy, M. M. *J. Am. Chem. Soc.* **1992**, *114*, 7116.
(80) Huskey, W. P. *J. Phys. Org. Chem.* **1991**, *4*, 361.
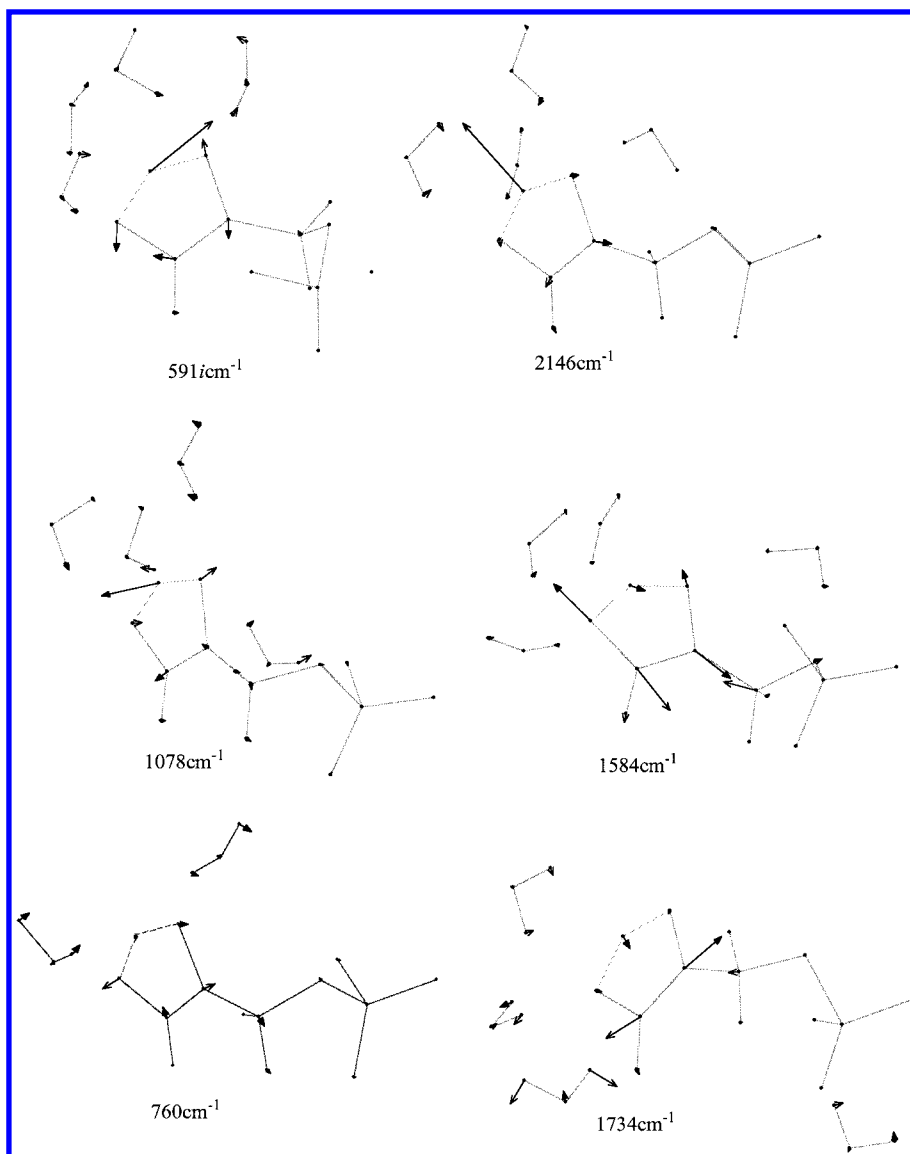(81) Cui, Q.; Elstner, M.; Karplus, M. *J. Phys. Chem. B*, submitted.

Figure 17. Plot of the barrier mode and the essential modes (the modes at the saddle point that have large overlap with modes having large reaction path curvature component at the path curvature peak position, see also Tables 10 and 11) for the intramolecular proton transfer in solution. The results in solution were derived with the "large" model.

Table 12. Kinetic Isotope Effects for Configurations with Large Tunneling Coefficient at 300 K[a]

	intramolecular set 4	intermolecular set 6
$V^{\ddagger}/\omega$	18.5/1083.9	11.3/1113.6
s_*^{CVT}	0.01	0.06
$\log(k_{\mathrm{H}}^{\mathrm{CVT-SCT}})$	1.89 (0.74) [0.73]	7.08 (6.56) [6.55]
$\kappa_{\mathrm{H}}^{\mathrm{CVT-SCT}}$	14.5	3.68
KIE (H/D)	10.8 (3.68) [5.93]	7.60 (5.89) [5.82]
KIE (H/T)	27.8 (6.87) [10.8]	25.9 (12.4) [12.3]
$\alpha_{\mathrm{SS}}^{\mathrm{P}}$	3.52 (3.09) [3.98]	2.65 (3.38) [3.36]
$\Delta E_{\mathrm{a}}(H,T)$	2.3 (0.9) [1.01]	1.82 (1.37) [1.29]
$A_{\mathrm{H}}/A_{\mathrm{T}}$	0.63 (1.49) [1.96]	1.22 (1.24) [1.42]
secondary KIE (H/D)		1.32 (0.94) [0.94]
secondary KIE (H/T)		1.41 (0.92) [0.91]
$\alpha_{\mathrm{SS}}^{\mathrm{S}}$		5.27 (3.67) [3.51]

[a] The values in parentheses and brackets were obtained at the TST and CVT levels, respectively. Numbers without parentheses or brackets were obtained at the CVT−SCT level. Definitions of other quantities are the same as in Table 1.

relation (with the reduced mass, $m_{\mathrm{H}}m_{\mathrm{D}}/(m_{\mathrm{H}} + m_{\mathrm{D}})$, where m_{D} is the mass of the donor atom, taken to be that of oxygen) to estimate the difference in the zero-point energy in the reactant

between different hydrogen isotopes; it is assumed that no contribution from this vibration is present in the transition state. The resulting value for the TST estimate of the Swain−Schaad exponent, $\alpha_{\mathrm{SS}}^{\mathrm{P,TST}}$, is 3.3 at 300 K. Since most of the TST results in the current work are close to this value, we substitute it into eq 8, to obtain the condition for $\alpha_{\mathrm{SS}}^{\mathrm{P}}$ to be larger than 3.3 (i.e., the condition for tunneling to *increase* $\alpha_{\mathrm{SS}}^{\mathrm{P}}$ beyond the TST limit),

$$\frac{\ln(\kappa_{\mathrm{H}}^{\mathrm{Tun}}/\kappa_{\mathrm{T}}^{\mathrm{Tun}})}{\ln(\kappa_{\mathrm{D}}^{\mathrm{Tun}}/\kappa_{\mathrm{T}}^{\mathrm{Tun}})} > 3.3 \qquad (9)$$

This relation is not true in general. In fact, it is violated in the simple case of tunneling through a square barrier, where the transmission coefficient is proportional to $\exp[-(m_{\mathrm{l}})^{1/2}]$. For this case, the left-hand side of eq 9 has a value of 2.30, *independent of temperature* and the width or height of the barrier. With the Wigner expression for tunneling through a parabolic barrier, eq 9 is roughly satisfied for a sufficiently high barrier frequency
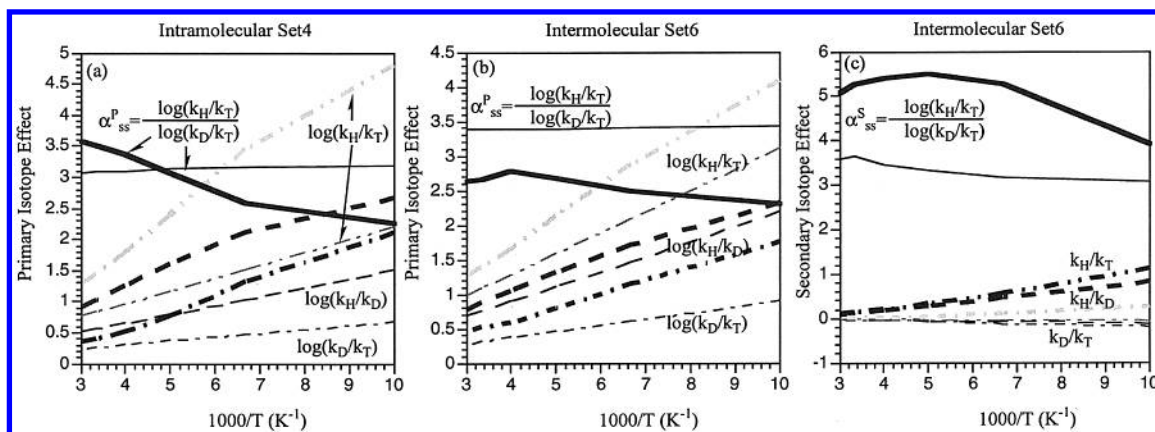
Figure 18. Kinetic isotope effects (log k_H/k_T, log k_H/k_D, log k_D/k_T) and the Swain−Schaad exponent as a function of temperature for the sets of (a) intramolecular and (b,c) intermolecular proton-transfer reaction in TIM that exhibit the largest tunneling. They correspond to set 4 in Table 3 and set 6 in Table A2 (Supporting Information), respectively. The results were derived with the "small" model. See Figure 4 for symbols used for isotope effects. Note that no logarithm was taken for the secondary kinetic isotope effects for clarity. See also Table 12 for values at 300 K.

ω. Assuming an ω of $1300i$ cm^{-1}, the left-hand side of eq 9 is 3.07. A more elaborate tunneling formula for a truncated parabola[82] with a barrier of 10 kcal/mol gives a higher value (4.71) for the left-hand side of eq 9; this would imply a larger (3.72) Swain−Schaad exponent. However, it should be noted that such a value is likely to be too large because one-dimensional models tend to substantially overestimate the magnitude of tunneling compared to multidimensional calculations.[18] For the reactions in TIM studied here, the left-hand side of eq 9 is typically found to be close to or less than 3.3 at 300 K; e.g., the value for the intramolecular proton transfer with the large model is 2.87.

Although it is clear from the above that the value of α_{SS}^P cannot be used to *prove* that tunneling makes a significant contribution to the reaction rate, it is interesting to use the TIM calculations to examine whether larger values of the Swain−Schaad exponent correlate with larger tunneling. Among the results for TIM, there are several examples that support this possibility. For example, systems with large tunneling coefficients (set 4 intramolecular proton transfer in Table 13) have primary Swain−Schaad exponents larger than those with smaller tunneling coefficients (Table 2 for intramolecular proton transfer with the environment close to the X-ray data). However, such a trend is not universal; e.g., set 6 intermolecular proton transfer (Table 12), with greater tunneling, has a smaller primary Swain−Schaad exponent than the set with the environment close to the X-ray (Table 5). This is due to the form of the Swain−Schaad exponent; i.e., it is highly sensitive to the value of D/T KIE. As illustrated in Figure A6 in the Supporting Information, a large Swain−Schaad exponent may occur at small KIE values, which usually correlate with a small tunneling coefficient.

Another issue is the temperature dependence of α_{SS}^P, which has been used to infer the temperature dependence of tunneling, based on the assumption that α_{SS}^P correlates with the magnitude of tunneling.[3−7] Because the value of the Swain−Schaad exponent in TST is due mostly to the difference in zero-point energies among different isotopes, it would be expected to be insensitive to temperature in the usual simplified treatment in which the transition-state contribution is neglected. However, the vibrational activation entropy, which arises from generalized normal modes orthogonal to the reaction coordinate that involve

the transferring proton (e.g., bending modes involving the proton), can be isotope sensitive. For all the reactions considered here, the isotope dependence for the vibrational entropy is very small and the primary Swain−Schaad exponents at the TST level has very little temperature dependence. At the CVT−SCT level, α_{SS}^P has a substantial temperature dependence in many cases, especially when the tunneling coefficient is large (Figures 4 and 18). Therefore, a strong variation of α_{SS}^P with temperature is suggestive of tunneling. However, it should be noted that α_{SS}^P does not necessarily become *larger* in magnitude as tunneling becomes more important. In many cases (Figures 4 and 5), α_{SS}^P actually decreases as the temperature decreases and tunneling becomes more significant. See Supporting Information for a more detailed analysis.

Secondary Swain−Schaad Exponent, α_{SS}^S. Since the secondary Swain−Schaad exponent is determined by the kinetic isotope effect obtained for a hydrogen atom that is not the one transferred in the reaction, it is usually interpreted as reflecting the magnitude of "coupled motion", i.e., the involvement of the secondary hydrogen in determining the transition-state structure, or stated another way, the contribution of the displacement of that hydrogen to the reaction coordinate. In several recent experiments,[3] large α_{SS}^S values (>10) were observed, and it was suggested that α_{SS}^S also reflects the magnitude of tunneling. It is not clear that this interpretation is generally valid because the secondary Swain−Schaad exponent is a very sensitive function of the measured secondary kinetic isotope effects (KIEs), which are generally small in magnitude. As shown in Figure A6 in the Supporting Information, for example, a small variation in the secondary KIEs can result in a large change in α_{SS}^S.

The calculations reported for TIM indicate that the magnitude of the secondary Swain−Schaad exponent is not correlated with the magnitude of tunneling. First, TST can give secondary Swain−Schaad exponents as large as 4.0 (Figure 18). Indeed, unlike the primary isotope effect, where the "classical limit" is 3.3, there is no clear limit for the secondary Swain−Schaad exponents. This results from the fact that the zero-point energy difference caused by secondary isotope substitution is not lost completely at the saddle point, since the vibrations involving the secondary proton (e.g., the donor−*secondary* proton stretch) are not the major reaction path motions (e.g., the donor−*primary*

---

(82) Skodie, R. T.; Truhlar, D. G. *J. Phys. Chem.* **1981**, *85*, 624.

proton stretch) at the saddle point. Second, tunneling does not necessarily increase the value of α_{SS}^S. A striking example is the behavior found for the model intermolecular proton transfer with the donor and acceptor atoms held fixed. In that case, the magnitude of the tunneling coefficient is 36.5 at room temperature, but α_{SS}^S is only about 2 and is well below the values (4.07 at 300 K) predicted at the TST level. Finally, we notice that the temperature variation is generally larger for the secondary Swain−Schaad exponent than the primary exponent (e.g., compare Figure 11e and f; also see Figure 18b,c). Since TST predicts substantial temperature dependence for α_{SS}^S, the temperature dependence cannot be related to tunneling.

In summary, based on the calculations carried out for TIM, we conclude that values of the primary Swain−Schaad exponent (α_{SS}^P) larger than 3.3 are not a good signature for large contribution from tunneling. However, a significant temperature dependence of α_{SS}^P is likely to suggest that tunneling plays a role. As to the secondary Swain−Schaad exponent, we emphasize that it is a very sensitive function of the kinetic isotope effects and therefore does not necessarily correlate with the magnitude of tunneling. As matter of fact, the model reaction in TIM with the largest tunneling (intermolecular proton transfer with fixed donor and acceptor) yields a very small secondary Swain−Schaad exponent.

IV.3b. Kinetic Isotope Effects on Arrhenius Parameters.
A more conventional signature of tunneling, used generally for small-molecule reactions for which a wide range of temperatures are accessible, is the deviation of the rate from simple Arrhenius behavior at low temperatures.[83] Two parameters of interest are the isotope effect on the Arrhenius prefactor, A_H/A_T or A_D/A_T, and the isotope effect on the apparent activation energy (E_a) obtained from an Arrhenius plot, $E_a(T) − E_a(H)$ or $E_a(D) − E_a(H)$. Here, A_I is the Arrhenius pre-exponential factor around room temperature for isotope I. The criteria proposed for the existence of tunneling are the following: (i) A_H/A_T or A_D/A_T deviates significantly from unity (either above or below, depending on whether only one or both isotopes have large tunneling contributions)[3] and (ii) $E_a(T) − E_a(H) > 1.8$ kcal/mol or $E_a(D) − E_a(H) > 1.2$ kcal/mol (i.e., the isotopic substitution leads to larger effects on the activation energy than the typical zero-point energy difference). In what follows we refer primarily to the primary isotope effect.

The results obtained from the current calculations are used to determine if these conditions are robust criteria for tunneling. We have selected the four sets of systems with the largest tunneling coefficients and plotted A_H/A_T and $E_a(T) − E_a(H)$ as functions of temperature in Figure 19. The qualitative behavior of A_H/A_T is similar to that described in ref 3. At high temperature (e.g., 500 K), A_H/A_T is fairly close to unity at all levels of theory. As the temperature drops to room temperature, the proton tunnels more significantly than tritium, which results in a value of A_H/A_T smaller than 1. The more important the tunneling, the smaller A_H/A_T is found to be. For example, A_H/A_T at 300 K equals 0.51 at the CVT−SCT level for the intermolecular proton transfer with the donor and acceptor fixed, which is the system that exhibits the largest tunneling coefficient (36.5 at 300 K when the donor−acceptor distance was fixed at 2.7 Å) in the current work. For the intermolecular proton transfer set 6, which

has the smallest tunneling coefficient among the four selected sets, A_H/A_T is 1.22 at 300 K, slightly larger than unity. At the temperature drops further, both isotopes tunnel significantly, and A_H/A_T becomes much larger than unity. An extreme case is the intermolecular proton transfer with the donor and acceptor fixed (at 2.7 Å), for which A_H/A_T has a value of 614.6 at 100 K with CVT−SCT. Without tunneling contributions (TST and CVT), the A_H/A_T remains close to unity at all temperatures. Except for the extreme case of intermolecular proton transfer with fixed donor and acceptor, there is a substantial difference between the CVT−ZCT and CVT−SCT results, which once more highlights the importance of including reaction path curvature. As to the value of $E_a(T) − E_a(H)$, tunneling makes a significant difference, and this difference is correlated with the magnitude of tunneling and temperature. At room temperature, where the tunneling contribution is significant only for the proton, the value of $E_a(T) − E_a(H)$ is larger than 1.8 kcal/mol at the level of CVT−SCT, and the value is greater for large tunneling cases. At low temperature, both isotopes have a significant contribution from tunneling, and $E_a(T) − E_a(H)$ decreases.

The behavior of Arrhenius parameters correlates rather well with the magnitude of tunneling at room temperature. A value of A_H/A_T significantly smaller than unity and/or $E_a(T) − E_a(H)$ much larger than 1.8 kcal/mol appears to be a reliable signature of large-scale tunneling at room temperature, better behaved at least for this enzyme than the Swain−Schaad exponent. For more moderate tunneling, however, the Arrhenius criteria are also not very robust.

V. Conclusion

Proton-transfer rate constants in complex systems such as enzymes are of great interest. One possibility for protons, but not for other atoms except at very low temperatures (e.g., CO in myoglobin[84]), is that quantum mechanical effects, particularly tunneling, may play an important role even at room temperature. Since the tunneling contribution depends sensitively on the height and shape of the potential energy barrier, which are both modulated by the environment, the potential energy surface and the dynamics have to be studied carefully to obtain meaningful result. In this paper, several issues concerned with proton tunneling in enzymes have been studied using triosephosphate isomerase (TIM) as an example. Specifically, the rate constants for two proton-transfer steps catalyzed by TIM have been calculated with the VTST−SAG approach as a function of temperature; they are the rate-limiting chemical step involving intermolecular proton transfer from the dihydroxyacetone phosphate (DHAP) to the catalytic residue Glu 165, and a possible intramolecular proton-transfer step within an enediolate intermediate. The rate constants for the intramolecular proton transfer have also been computed in the gas phase and solution for comparison. The latter reaction was chosen because its intramolecular nature avoids the need to correct for concentration effects in the gas phase or solution. Since we determined the activation barriers in earlier papers,[24] we focused in this work on the effect of tunneling; specifically, we determined the dynamic factors that influence the rate constant and proton tunneling in an enzyme. We also used the TIM results to examine the relationship between the calculated tunneling

(83) See, for example: Steinfeld, J. I.; Francisco, J. S.; Hase, W. L. *Chemical Kinetics and Dynamics*; Prentice Hall: Englewood Cliffs, NJ, 1995.

(84) Vitkup, D.; Petsko, P. A.; Karplus, M. *Nature Struct. Biol.* **1997**, *4*, 202.
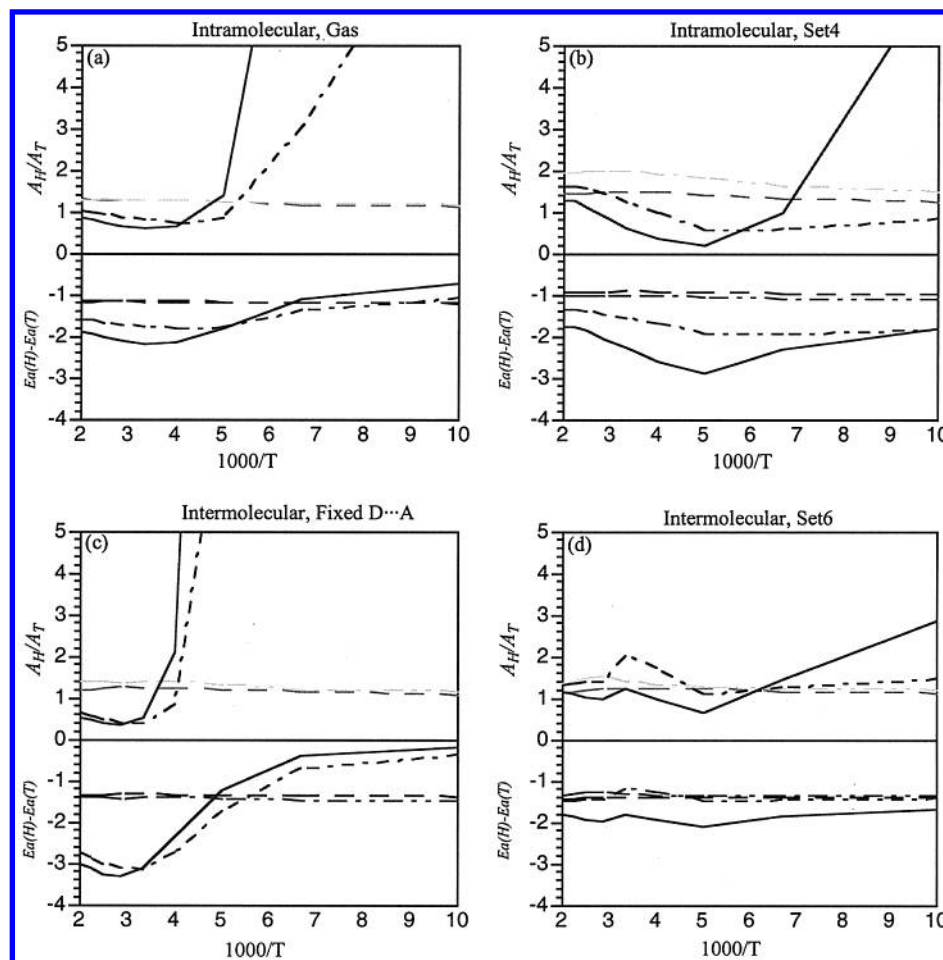
Figure 19. Arrehenius parameters (see eq 6 for definitions) for four sets of reactions that exhibit large tunneling contributions (see text) as a function of temperature. (a) Gas-phase intramolecular proton transfer. (b) Set 4 intramolecular proton transfer in TIM. (c) Intermolecular proton transfer in TIM with the donor and acceptor atoms fixed. (d) Set 6 intermolecular proton transfer in TIM. The results were derived with the "small" model. The dashed lines represent TST results; the dash−dot−dot lines represent CVT results; the dash−dot lines represent CVT−ZCT results; and the solid lines represent CVT−SCT results.

contribution and the experimental observables that are often used to draw conclusions about its magnitude.

The effect of tunneling was found to be less than a factor of 10 at room temperature for both proton-transfer reactions. This means that, although tunneling is significant for the rate of proton transfer, it is of minor importance for catalysis, per se; a factor of 10 is "small" relative to the rate acceleration of 10^9 by TIM. However, there may be other enzyme reactions where tunneling is more critical, so that model studies, like the present one, are important. Tunneling was found to be about 5 times larger in the enzyme than in solution, with the difference arising mainly from the increase in the barrier width in the latter relative to the former. Interestingly, the barrier width in the enzyme was found to be very similar to that in the gas phase.

In the VTST−SAG framework used for the present calculations, the quantities that influence tunneling include the barrier frequency (width), the barrier height, and the reaction path curvature. A thin barrier (with a high imaginary frequency) leads to a large tunneling contribution; a high barrier makes the tunneling correction to thermal rate constant more pronounced; and a large reaction path curvature makes the corner-cutting effect more important and consequently induces a larger tunneling probability. All of these factors were illustrated by the analysis of the reactions in TIM. Participation ratios showed

that both the barrier mode (with the imaginary frequency) and modes that make large contributions to the reaction path curvature ("essential modes") were localized on the atoms in the active site, i.e., the substrate and nearby residues (such as Glu 165, His 95, and Lys 12). Therefore, only a small number of atoms that are close to the substrate and their motions (e.g., the donor−acceptor vibration) directly determine the magnitude of tunneling in this enzyme. Atoms that are farther from the active site influence the tunneling indirectly by modulating the barrier height and shape. This explains the dependence of tunneling on the structure of the active site and on the number of atoms that are allowed to move in the reaction path and tunneling calculations. The results suggest that the most efficient way to calculate the tunneling contribution is to obtain the saddle-point structure with a large set of movable atoms, and to compute the actual tunneling with a smaller set of movable atoms in the neighborhood of the substrate. This procedure should be carried out for a number of enzyme configurations to obtain an average tunneling correction. An alternative, when the overall time scale for the chemical step is slower than the enzyme motions, is to evaluate the quantum correction on the classical potential of mean force via techniques such as path-integral approaches.[23,30b]

In any estimate of the role of tunneling in enzyme catalysis, it is useful to have a comparison with the solution results. For the intramolecular proton transfer, it was found that tunneling is most important in the gas phase, less so in enzyme, and the least significant in water. One reason for this trend is that the barrier frequency is substantially lower in water, compared with the gas-phase and enzyme values. Analysis showed that this is caused by the strong electrostatic interaction between the charged solute and the polar water solvent molecules; i.e., the electrostatic interaction and polarization effect due to the solvent can substantially modify the shape of the potential energy surface for the proton transfer. Inertial coupling between the substrate and the solvent motions was found to play a small role. In terms of the normal-mode analysis of solvent friction by Pollak,[72] this corresponds to large effects on the substrate–substrate block and small values on substrate–solvent block of the Hessian. The effect of reaction path curvature on tunneling and the nature of the essential modes in solution were found to be rather similar to those in the enzyme. One difference is that the low-frequency essential modes are more delocalized in solution than in enzyme.

In the examination of the relationship between tunneling and experimentally measurable quantities, it was found that the conventionally used Arrhenius parameters (i.e., the ratio of Arrhenius preexponential factors and isotope effect on the apparent activation barriers) are likely to be more robust as criteria for tunneling than the Swain–Schaad exponents (SSE). For the primary SSE, although values larger than the TST limit (3.3) were observed in many cases when tunneling was included, no clear relationship between the magnitude of tunneling and the magnitude of the SSE was found; e.g., although the intermolecular proton transfer with fixed donor and acceptor distances has substantially larger tunneling than models without constraints (e.g., Table 12), the primary SSE is not particularly large (see Table 9). Furthermore, the temperature dependence of the primary SSE does not appear to be a reliable criterion. In many cases, the value of SSE decreases as the temperature is lowered (i.e., when tunneling becomes more significant). For the secondary SSE, two points should be emphasized. First, unlike the primary SSE, there is no classical limit value (3.3). This is a result of the fact that the zero-point energy due to the secondary hydrogen is not completely lost at the transition state. Indeed, a value around 4 was observed even with TST for the intermolecular proton-transfer reactions. Second, the secondary kinetic isotope effect is much smaller, which makes the value of secondary Swain–Schaad exponent much more sensitive to the D/T KIE (which mainly reflects "coupled motion") than to the magnitude of tunneling. For example, the intermolecular

proton transfer with fixed donor–acceptor distance does not have a large secondary Swain–Schaad exponent, despite the large tunneling factor.

Finally, we note that the effect of reaction path curvature was treated in the small-curvature (SCT) approximation. For the qualitative analysis made here, the VTST–SCT approach is likely to be satisfactory. For more quantitative calculations involving sampling of enzyme conformations and comparison with detailed experimental data, such as exists for the alcohol dehydrogenase, other treatments of tunneling (e.g., path-integral simulations) are useful to establish the reliability of the VTST–SCT approach. Such calculations are in progress.

Note Added after ASAP: There were errors in eq 4 and Tables 7, 9, and 11 in the version posted ASAP, February 23, 2002; the corrected version was posted February 26, 2002.

Supporting Information Available: Discussion of the environmental configurations on the intramolecular proton-transfer reaction in solution and in TIM, the effect of solvation on the position of transition state, the effect of environmental configurations on the intermolecular proton transfer in TIM, the temperature dependence of the Swain–Schaad exponent, and the sensitivity of the Swain–Schaad exponents; tables listing rate constants, kinetic isotope effects, and tunneling factors for the intermolecular proton-transfer reactions in TIM; and figures depicting selected active site structures, stereo diagrams of reactant and product structures, comparison of minimum energy profile and adiabatic vibrationsl ground-state profile, comparison of rate constants obtained with the "large" and "small" models, reaction path and kinetic properties for the intermolecular proton transfer in TIM, and the numerical dependence of the primary and secondary Swain–Schaad exponents on kinetic isotope effects (PDF). This material is available free of charge via the Internet at http://pubs.acs.org.

JA0118439